POWER SYSTEM STATE ESTIMATION

KAMINI KOUSALYA SEKARAN

POWER SYSTEM STATE ESTIMATION

BY

© KAMINI KOUSALYA SEKARAN, B.E.

A thesis submitted to the school of Graduate Studies in
partial fulfillment of the requirements for the
degree of Master of Engineering

Faculty of Engineering and Applied Science
Memorial University of Newfoundland
September 2008

St John's Newfoundland Canada

ABSTRACT

Monitoring and control of a complex interconnected power system requires the accurate estimate of its states. Different meters are placed at the various substations and the measurements are transmitted to the central control center. However, it is likely that there may be errors associated with the measurements and in some cases, some measurements may not be available. Power system state estimation is a technique by which the state of a power system (usually magnitude and angle of bus voltages) is determined using raw measurements. The results of the state estimation are used for real-time security analysis, optimal power flow, etc. These are also used in calculating the line power flows between buses, by which the system operators will be able to conclude if any line is overloaded, and then take necessary action to prevent any mishap from happening. In the initial part of this thesis, State Estimation (SE) based on Weighted Least Squares (WLS) technique and bad data detection, identification, and elimination are presented. The bad data detection and identification are facilitated by the chi-squared test and normal residual methods. The WLS, chi-Squared test and normal residual methods are implemented in Matlab and tested using different power system models.

Case studies demonstrate that the WLS technique is reliable in estimating state variables of a power system. Chi-squared and Normal residual methods detect and identify bad data efficiently.

In the second part of this thesis, the transmission line reactance parameter error estimation is formulated and implemented using the residual sensitivity analysis for various power system models. The estimation involves two steps: the error identification and estimation of the parameter implemented using Matlab. The identification of the parameter error is facilitated by the normalized residual technique, and the parameter error estimation is facilitated using the residual sensitivity analysis. The parameters estimated are reliable and close to the actual (true) value.

In the final part of this thesis the measurements considered to be available for state estimation are a few synchronized phasor measurements in addition to the conventional measurement data, to enhance the performance of the state estimator, for a very large power system. The phasor measurement, when present in sufficient numbers, with other measurements, improves the accuracy of the SE. Matlab is used to implement multi-area SE using various case studies.

ACKNOWLEDGEMENTS

I would like to thank my supervisor Dr. Benjamin Jeyasurya for his constant advice, guidance and encouragement during all stages of this research.

Special thanks and appreciation are given to the Natural Sciences and Engineering Research Council of Canada and to Memorial University of Newfoundland for the financial support that made this research possible. Thanks are also given to the Faculty of Engineering at Memorial University for providing the resources to carry out this research.

Finally, I would also like to express my deepest gratitude, to my mentor and my father Mr. K. Sekaran, my mother Mrs. Lalitha Sekaran and my husband Mr. Kathiravan Chenthilnathan for their constant encouragement, motivation, understanding and support.

LIST OF ABBREVIATIONS

SE	State Estimation
AGC	Automatic Generation Control
WLS	Weighted Least Square
EMS	Energy Management System
RMU	Remote Terminal Unit
PMU	Phasor Measurement Unit
GPS	Global Positioning System
SCDR	Symmetrical Component Distance Relay
CSE	Central State Estimator

CONTENTS

LIST OF FIGURES

LIST OF TABLES

CHAPTER 1

INTRODUCTION

1.1 OVERVIEW OF POWER SYSTEM STATE ESTIMATION

The importance of State Estimation (SE) in an electrical power system can be realized by considering the North-east blackout 2003 that took place in US and Canada, due to poor control-room procedures and failure of the power grid organization to keep it from spreading [1]. This shows that a better power system estimating tool is necessary for the safe operation of the power system and it can be established by the implementation of state estimation in power systems.

State estimation gained popularity in the 1950's and 1960's as it was used in the military industry to derive estimates of the trajectory of a missile, plane or spacecraft based on a redundant set of imperfect measurements usually based on radar tracking of its position and velocity vector [2]. The static state estimation for a power system network based on the power flow model was first proposed by Fred Schweppe [3].

State estimation is a technique developed to provide an estimate of an unknown system state variable and to quantitatively analyze the estimated state variable before it is used for real-time power-flow calculations or on-line system security assessment. A state estimator is a data processing algorithm for converting redundant meter readings and other available information into an estimate of the state of an electric power system. It plays an essential part in every energy management system and also is a basic tool in ensuring the secure operation of a power system

State estimation is the process of assigning a value to an unknown system state variable based on measurements from that system according to certain criteria. This process involves imperfect measurements that are redundant being used in estimating the system states, based on a statistical criterion that estimates the true value of the state variables to minimize or maximize the selected criterion [2]. The most widely used criterion is that of minimizing the sum of the squares of the differences between the estimated and "true" (i.e., measured) values of a function.

In a power system, measurements are required in order to estimate the system performance in real time for both system security control and constraints on economic dispatch. The estimator is designed to produce the "best estimate" of the system state variables, recognizing that there are errors in the measured quantities and that there may be redundant measurements. The output data are then used in system control centers in the implementation of the security-constrained dispatch and control of the power system [2].

Transducers for power system measurements, like any measurement device, will be subject to error. If the errors are small, they may go unnoticed or undetected and can cause misinterpretation by those reading the measured values. The instruments may have gross measurement errors that render their output useless. Finally, the telemetry equipment often experiences periods when communication channels are completely out, thus, depriving the system operator of any information about some parts of the power system network. Power system state estimation techniques have been developed for these reasons. A state estimator can "smooth out" small random errors in the meter's readings, detect and identify gross measurement errors, and "fill in" meter readings that have failed due to communications failures [2]. In general, state estimation is the art of estimating the exact system state given a set of imperfect measurements made on the power system.

Of the many criteria that have been examined and used in the literature , the Weighted Least-Square (WLS) technique, where the objective is to minimize the sum of

the squares of the weighted deviations of the estimated measurements from the actual measurements, is used in this thesis to implement state estimation for various case studies.

1.2 OBJECTIVES OF THE THESIS

For various power system models, power system state estimation, bad data processing technique, network parameter error processing technique and for a large power system addition of phasor measurements to the conventional measurement data are considered in this thesis. A reliable estimate of the system states of any electrical power system is vital for all post state estimation applications and for the effective operation of the power utility. The main goals of this research are as follows:

- To gain thorough understanding of power system state estimation and its features.
- To implement WLS technique, bad data elimination, and finally estimate the network parameter error.
- To enhance the performance of state estimation with the phasor measurements.
- To implement the studied methods for standard power system models

1.3 ORGANIZATION OF THE THESIS

A brief literature review and an overview of the research for the different chapters are discussed in the respective chapters. In Chapter 2, the power system state estimation for the static ac power system is discussed and illustrated using 6-bus and 39-bus systems. The modeling of the WLS (Weighted Least Square) technique, measurement and components are also briefly illustrated. The 6-bus system is solved with two different measurement data. The results of the estimate system states are compared with the actual value to illustrate the accuracy of the SE. The SE demonstrates its ability to give the best estimate of the system state variables.

Chapter 3 formulates and implements the bad measurement data processing techniques. Initially a few bad measurements are introduced into the measurement data. The bad measurement data are detected using the chi-squared test. They are identified using the normalized residual test and finally eliminated from the measurement data. The 6-bus and 39-bus systems are used to illustrate bad data processing techniques.

The network parameter error estimation is devised and implemented in Chapter 4. The line reactance parameter error is the focus of this chapter. Errors are introduced into the line reactance for 6-bus and 39-bus systems. The identification of the parameter errors

is facilitated by the normalized residual technique. The parameter errors are estimated and the correct line reactance is updated into the system model.

In addition to the conventional measurement data in a very large power system, the performance of SE in the presence of phasor measurements is studied in Chapter 5. In a multi-area power system, the two-level SE is formulated using 6-bus and illustrated using 39-bus and 118-bus power system models. The state variables of the individual area are estimated in the first level of the two-level SE. The measurement data for the Central State Estimator (CSE) comprises the estimated state variables of the individual area, a few boundary and external bus measurements and phasor measurements. The CSE estimates the overall state of the system (which is the second level of the two-level SE).

Chapter 6 provides the conclusion of the thesis and enumerates the contributions of this research. Finally, the possible future research in this area is discussed.

CHAPTER 2

POWER SYSTEM STATE ESTIMATION

2.1 INTRODUCTION

As discussed in Chapter 1, the technique that can provide an estimate of the unknown quantities with a few available measurements is known as state estimation. The purpose of this chapter is to briefly study the application of power system state estimation and to implement it using WLS techniques for various power system models. The power system models used are 6-bus and 39-bus system models. The estimated state variables are compared with the actual value, to prove that a state estimator can give the best estimate of the state of a power system.

2.2 APPLICATION OF POWER SYSTEM STATE ESTIMATION (SE)

Power system state estimation is the process of reading field measurements and deriving the best guess of the state of a power system. The power system states are the voltage magnitudes and relative phase angles of all buses in the system. The estimated state variables are used to calculate the estimates of the real and reactive power flow between the lines. With the estimated power flows, the operator in a power system utility will have access to the real time information and take necessary measures in case of overloading to avoid blackouts in a power system. In addition, the power system state variables are used in advanced applications, such as security analysis and optimal power flow, implemented in the control centre.

The energy control centre system security schematic in Figure 2.1 illustrates the information flows between the various functions to be executed in an operations control center. The remote terminal unit performs various functions such as updating the system regarding the current status of the power system and encoding measurement transducer outputs and opened/closed status information into digital signals, which are transmitted to the operations center over the communications circuit. The control center can also transmit control information, such as raise/lower commands to generators and open/close commands to circuit breakers/switches. The information approaching the state estimator

is broken down into the analog measurements and breaker/switch status indications. The state estimator will process all data before being used by other programs, except the analog measurements of generator outputs, which are used directly, by the Automatic Generation Control (AGC) program.

The next important information necessary for the state estimator is the network topology. This is the information that gives the mapping of the transmission lines to the buses and breaker/switch status (open/close). This information is significant since the breaker/switches status in any substation can cause the network topology to change. Hence, a program is provided to read the telemetered breaker/switch status indications and restructure the electrical model of the system. The updated electrical model of the power transmission system is sent to the state estimator program together with the analog measurements. The output of the state estimator consists of all bus voltage magnitudes, phase angles, power injections and power flows. The bad data is also identified, detected and, if possible, eliminated by the estimator. The output data together with the electrical model developed by the network topology program provides the basis for the economic dispatch program and contingency analysis program [2] and [4].

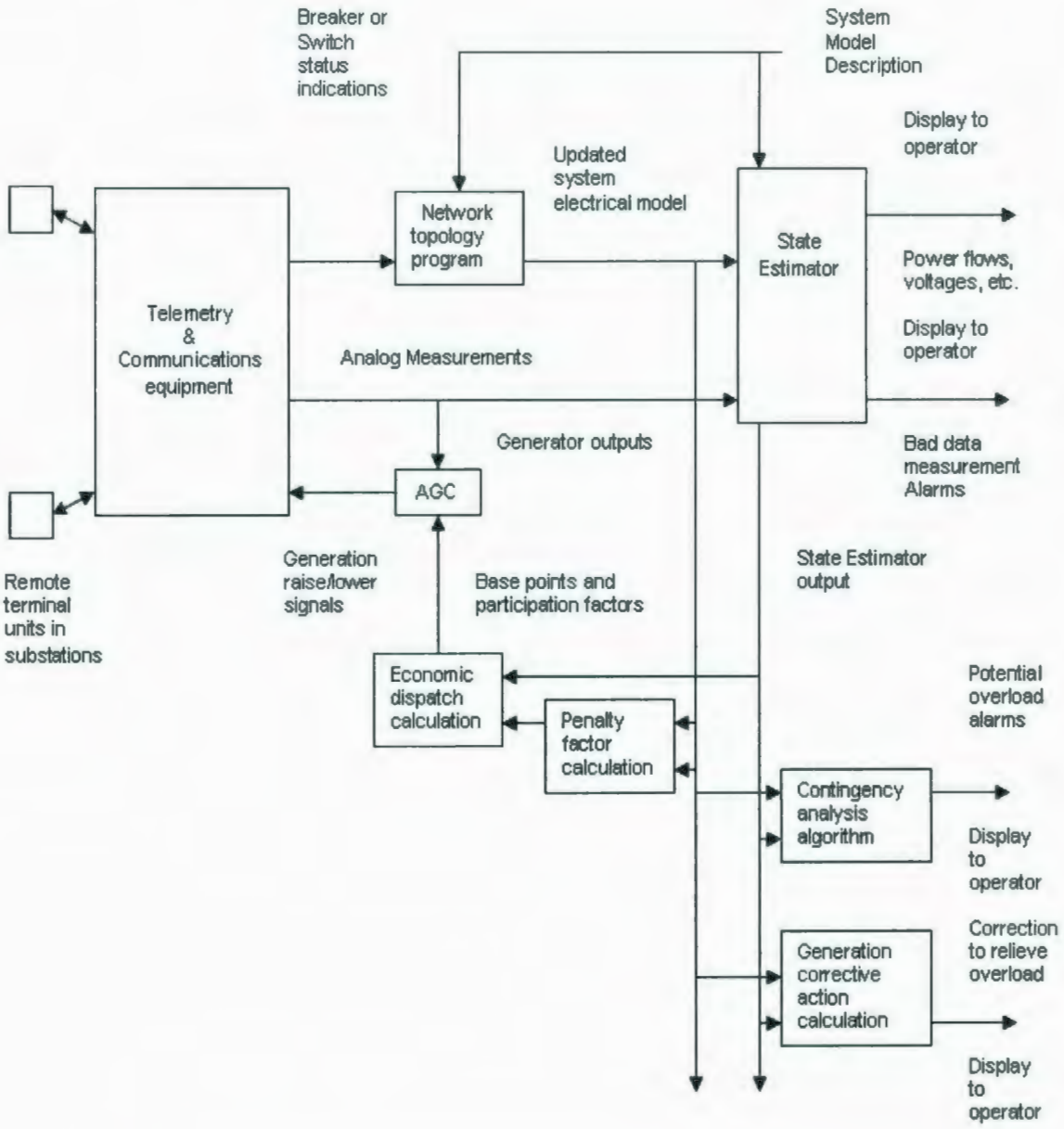

Figure 2.1: Energy control center system security schematic [2]

2.3 IMPLEMENATION OF STATE ESTIMATION

The electric power transmission system uses various meters to measure real power, reactive power, bus voltages and currents. The current and potential transformers installed in the transmission lines, transformers, buses of the power plant or a substation monitor these continuous or analog quantities. The analog quantities monitored using the transducers are passed on to the analog-to-digital converters. The digital outputs are then telemetered to the energy control center over various communication links. The data received at the energy control center are processed by computers, which inform the system operators of the present state of the power system.

The acquired data always contains inaccuracies, which are unavoidable as physical measurements cannot be entirely free of random error or noise. These errors can be quantified in a statistical sense and the estimated values of the quantities being measured are then either accepted or rejected if certain measures of accuracy are exceeded. Due to noise, the true values of the physical quantities are never known, so a technique must be used to calculate the best possible estimates of the unknown quantities.

There are various methods used to formulate the best estimate of the unknown parameter. A few of the most commonly used criteria are the maximum likelihood criterion, the weighted least-square and the minimum variance criterion. The one used in

the following case studies is the weighted least-square criterion, where the objective is to minimize the sum of the squares of the weighted deviations of the estimated measurement from the actual measurement.

2.3.1 Weighted Least Square

Due to noise or random error, the true value of any physical quantity is not known; hence, a suitable procedure has to be followed to calculate the best estimate of the unknown quantity [2]. The method of least squares is often used to "best fit" measured data relating to two or more quantities. The modeling and implementation of the weighted least-square method is explained using two case studies in the next section. The ac systems used in the case studies are 6-bus and 39-bus systems. These systems are solved with two different measurement data with error.

2.4 CASE STUDIES

In an ac power system, the measured quantities are power injections, line power flows, currents, transformer tap position and voltage magnitude. The function of the measurement equations and their partial derivatives (Jacobian matrix) are all nonlinear. Therefore, solving an ac system is complicated. The unknown state variables of an ac

power system are the bus voltage magnitudes and bus phase angles (except the reference bus). The two systems are solved with two measurement data. The 6-bus system is solved with 18 and 62 measurement data, and the 39-bus system with 131 and 277 measurement data. The state estimator's ability to estimate the state variables with a small number of measurements is tested.

2.4.1 Modeling of Weighted Least Square Technique

WLS state estimation minimizes the weighted sum of the squares of the residuals. Consider the measurement set vector z as in equation (2.1):

$$z = \begin{bmatrix} z_1 \\ z_2 \\ \vdots \\ z_m \end{bmatrix} = \begin{bmatrix} h_1(x_1, x_2, x_3 \cdots, x_n) \\ h_2(x_1, x_2, x_3 \cdots, x_n) \\ \vdots \\ h_m(x_1, x_2, x_3 \cdots, x_n) \end{bmatrix} + \begin{bmatrix} e_1 \\ e_2 \\ \vdots \\ e_m \end{bmatrix} = h(x) + e \qquad (2.1)$$

where: $z^T = [z_1, \quad z_2, \quad \cdots, \quad z_m]$ is the measurement vector.

$h^T = [h_1(x), \quad h_2(x), \quad \cdots, \quad h_m(x)]$

$h_i(x)$ is the nonlinear function relating measurement i to the state vector x

$x^T = [x_1, \quad x_2, \quad \cdots, \quad x_n]$ is the system state vector

$e^T = [e_1, \quad e_2, \quad \cdots, \quad e_m]$ is the vector of the measurement errors.

m is the number of measurements and n is the number of state variables to be estimated.

Let $E(e)$ denote the expected value of e with the following assumption:

$$E(e_i) = 0, \quad i = 1, \cdots, m \tag{2.2}$$

Measurement errors are independent, i.e. $E[e_i e_j] = 0 \quad \forall j \neq i$. Hence the covariance of the error is given as:

$$\text{cov}(e) = E[e.e^T] = R = diag\{\sigma_1^2, \sigma_2^2, \ldots \sigma_m^2\} \tag{2.3}$$

σ_i is the standard deviation of each measurement i, calculated to reflect the expected accuracy of the meter used [5].

The objective function to be minimized by weighted least square is given in equation (2.4). It is the square of the difference between each measured value and the true value divided by the covariance of the error.

$$J(x) = \sum_{i=1}^{m} \frac{[Z_i - h_i(x)]^2}{R_{ii}^2} \tag{2.4}$$

$$= [z - h(x)]^T R^{-1} [z - h(x)]$$

The gradient of the objective (residual vector) is taken and then equated to zero.

$$g(x)=\frac{\partial J(x)}{\partial x}=-H^{T}(x)R^{-1}[z-h(x)]=0 \quad \text{where, } H(x)=\left[\frac{\partial h(x)}{\partial x}\right] \tag{2.5}$$

Then, expanding the nonlinear function $g(x)$ into Taylor series and neglecting the higher order terms lead to an iterative scheme, as in the Gauss-Newton method shown in equation (2.6), which is used to solve equation (2.5)

$$x^{k+1} = x^{k} - \left[G\left(x^{k}\right)\right]^{-1} \cdot g\left(x^{k}\right) \tag{2.6}$$

where k is the iterative index and x^{k} is the solution vector at the iteration k . $G(x)$ is the gain matrix, which is expressed in equation (2.7):

$$G\left(x^{k}\right)=H^{T}\left(x^{k}\right)R^{-1}H\left(x^{k}\right) \tag{2.7}$$

$$g\left(x^{k}\right)=-H^{T}\left(x^{k}\right)R^{-1}\left(z-h\left(x^{k}\right)\right) \tag{2.8}$$

Usually, the gain matrix is sparse and is decomposed into triangular factors. The sparse linear set of equations is solved using forward or backward substitution at each iteration k , where $\Delta x^{k+1} = x^{k+1} - x^{k}$:

$$\left[G\left(x^{k}\right)\right]\Delta x^{k+1} = H^{T}\left(x^{k}\right)R^{-1}\left[z-h\left(x^{k}\right)\right] \tag{2.9}$$

The iteration is continued until $Max\left|\Delta x^{k}\right| < \varepsilon$ where ε is a very small value.

2.4.2 Weighted Least Square Algorithm

The iterative solution to equation (2.9) gives a reliable WLS estimate of the unknown state variable. The algorithm used for the technique is outlined in the flowchart, shown in Figure 2.2.

1. Begin the iteration by setting the iteration index $k = 0$ and defining k_{limit} to any desired value, so that when the solution does not converge, it will stop the iteration. Then, set flat start values 1 and 0 to bus voltage magnitudes and bus phase angles, respectively. Finally, ε is set to a very small value.
2. Terminate the iteration when $k > k_{limit}$.
3. Calculate the measurement function $h(x^k)$, the Jacobian matrix $H(x^k)$ and the gain matrix $G(x^k) = H^T(x^k)R^{-1}H(x^k)$.
4. Solve Δx^k using equation (2.9).
5. If $|\Delta x^k| > \varepsilon$, then go to step 2. Otherwise stop (algorithm converged).

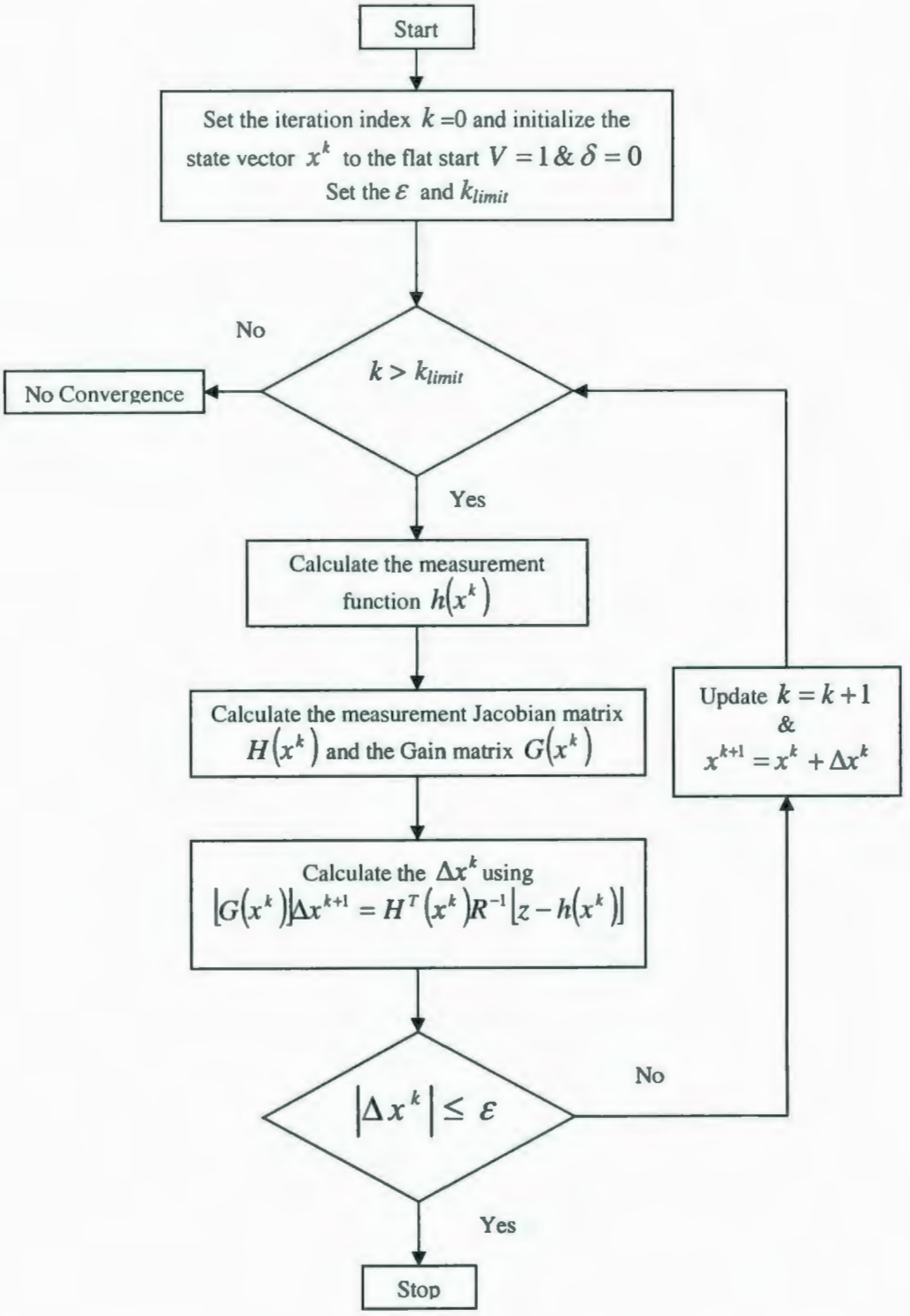

Figure 2.2: Flowchart for Weighted Least Square Technique

2.4.3 Measurement and Component Modeling

The measurements in an ac system are mainly of three types, bus power injection, line power flows and bus voltage magnitudes. These quantities can be expressed using the state variables. If there are N buses in a system then there will be (2N-1) state variables comprising N bus voltage magnitudes and N-1 bus phase angles, since at the reference bus, the bus phase angle is zero. Let i and j be the two buses as shown in Figure 2.3, which is an equivalent π model of a two bus system.

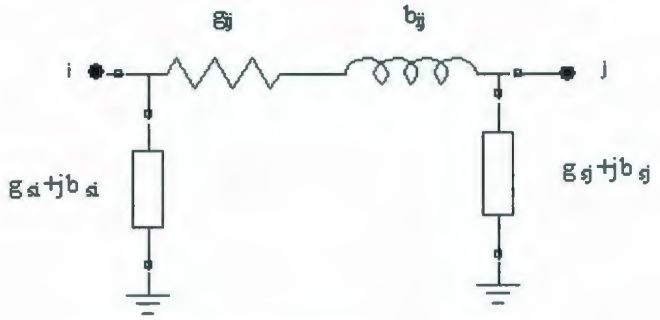

Figure 2.3: Two-port π-model of a network branch [5]

The real and reactive power injection at a bus can be expressed as in equations (2.10) and (2.11) respectively.

$$P_i = V_i \sum_{j \in N_i} V_j \left(G_{ij} \cos \theta_{ij} + B_{ij} \sin \theta_{ij} \right) \tag{2.10}$$

$$Q_i = V_i \sum_{j \in N_i} V_j \left(G_{ij} \sin \theta_{ij} - B_{ij} \cos \theta_{ij} \right) \tag{2.11}$$

where P_i and Q_i are respectively the real and reactive bus power injection at bus i.

V_i, θ_i is the voltage magnitude and phase angle at bus i and $\theta_{ij} = \theta_i - \theta_j$

$G_{ij} + jB_{ij}$ is the ij th element of the complex bus admittance matrix.

N_i are the buses that are connected to bus i directly.

The real and reactive power flow from bus i to bus j are expressed in equations (2.12) and (2.13) respectively.

$$P_{ij} = V_i^2 \left(g_{si} + g_{ij}\right) - V_i V_j \left(g_{ij} \cos \theta_{ij} + b_{ij} \sin \theta_{ij}\right) \qquad (2.12)$$

$$Q_{ij} = -V_i^2 \left(b_{si} + b_{ij}\right) - V_i V_j \left(g_{ij} \sin \theta_{ij} - b_{ij} \cos \theta_{ij}\right) \qquad (2.13)$$

where P_{ij} and Q_{ij} are the real and reactive line power flow from bus i to bus j.

$g_{ij} + jb_{ij}$ is the admittance of the series branch connecting buses i and j.

$g_{si} + jb_{si}$ is the admittance of the shunt branch connected at bus i.

The formulae for the Jacobian of the real power injection measurement are given in equations (214)-(2.17).

$$\frac{\partial P_i}{\partial \theta_i} = \sum_{j=1}^{N} V_i V_j \left(- G_{ij} \sin \theta_{ij} + B_{ij} \cos \theta_{ij}\right) - V_i^2 B_{ii} \qquad (2.14)$$

$$\frac{\partial P_i}{\partial \theta_j} = V_i V_j \left(G_{ij} \sin \theta_{ij} - B_{ij} \cos \theta_{ij} \right) \tag{2.15}$$

$$\frac{\partial P_i}{\partial V_i} = \sum_{j=1}^{N} V_j \left(G_{ij} \cos \theta_{ij} + B_{ij} \sin \theta_{ij} \right) + V_i G_{ii} \tag{2.16}$$

$$\frac{\partial P_i}{\partial V_j} = V_i \left(G_{ij} \cos \theta_{ij} + B_{ij} \sin \theta_{ij} \right) \tag{2.17}$$

The formulae for the Jacobian of the reactive power injection measurement are given in equations (2.18)-(2.21)

$$\frac{\partial Q_i}{\partial \theta_i} = \sum_{j=1}^{N} V_i V_j \left(G_{ij} \cos \theta_{ij} + B_{ij} \sin \theta_{ij} \right) - V_i^2 G_{ii} \tag{2.18}$$

$$\frac{\partial Q_i}{\partial \theta_j} = V_i V_j \left(- G_{ij} \cos \theta_{ij} - B_{ij} \sin \theta_{ij} \right) \tag{2.19}$$

$$\frac{\partial Q_i}{\partial V_i} = \sum_{j=1}^{N} V_j \left(G_{ij} \sin \theta_{ij} - B_{ij} \cos \theta_{ij} \right) - V_i B_{ii} \tag{2.20}$$

$$\frac{\partial Q_i}{\partial V_j} = V_i \left(G_{ij} \sin \theta_{ij} - B_{ij} \cos \theta_{ij} \right) \tag{2.21}$$

The formulae for the Jacobian of real line power flow measurement are given in equations (2.22)-(2.25).

$$\frac{\partial P_{ij}}{\partial \theta_i} = V_i V_j \left(g_{ij} \sin \theta_{ij} - b_{ij} \cos \theta_{ij} \right) \tag{2.22}$$

$$\frac{\partial P_{ij}}{\partial \theta_j} = -V_i V_j \left(g_{ij} \sin \theta_{ij} - b_{ij} \cos \theta_{ij} \right) \tag{2.23}$$

$$\frac{\partial P_{ij}}{\partial V_i} = -V_j \left(g_{ij} \cos \theta_{ij} - b_{ij} \sin \theta_{ij} \right) - 2 \left(g_{ij} + g_{si} \right) V_i \tag{2.24}$$

$$\frac{\partial P_{ij}}{\partial V_j} = -V_i \left(g_{ij} \cos \theta_{ij} + b_{ij} \sin \theta_{ij} \right) \tag{2.25}$$

The formulae for the Jacobian of the reactive line power flow measurement are given in equations (2.26)-(2.29).

$$\frac{\partial Q_{ij}}{\partial \theta_i} = -V_i V_j \left(g_{ij} \cos \theta_{ij} + b_{ij} \sin \theta_{ij} \right) \tag{2.26}$$

$$\frac{\partial Q_{ij}}{\partial \theta_j} = V_i V_j \left(g_{ij} \cos \theta_{ij} + b_{ij} \sin \theta_{ij} \right) \tag{2.27}$$

$$\frac{\partial Q_{ij}}{\partial V_i} = -V_j \left(g_{ij} \sin \theta_{ij} - b_{ij} \cos \theta_{ij} \right) - 2 \left(b_{ij} + b_{si} \right) V_i \tag{2.28}$$

$$\frac{\partial Q_{ij}}{\partial V_j} = -V_i \left(g_{ij} \sin \theta_{ij} - b_{ij} \cos \theta_{ij} \right) \tag{2.29}$$

The values of the Jacobian for the voltage magnitudes are:

$$\frac{\partial V_i}{\partial V_i} = 1 \,, \frac{\partial V_i}{\partial V_j} = 0 \,, \frac{\partial V_i}{\partial \theta_i} = 0 \,, \frac{\partial V_i}{\partial \theta_j} = 0 \tag{2.30}$$

The Jacobian matrix H has a number of rows and columns equal to the number of measurements and state variables, respectively.

2.4.4 6-Bus System

The six-bus ac network as in Figure 2.4 is the first system of this case study, which is used for the implementation of the state estimation using WLS. There are 6 buses in this system, i.e. N=6. Therefore, 2N-1=11 state variables are to be estimated, which comprises N=6 bus voltage magnitudes and N-1=5 bus phase angles. Bus 1 is the slack bus (the bus phase angle is zero). The buses 2 and 3 represent a bus connected to a generating station (PV buses). Buses 4, 5 and 6 represent a bus connected to the load centre (PQ buses). There are eleven transmission lines and hence there are 44 line power flows (11*2=22 real and 11*2=22 reactive). Details of the 6-bus system are given in Appendix A.

This system has a 62 measurement data set that consists of 6 real and 6 reactive bus power injections, 22 real and 22 reactive line power flows and 6 bus voltage

magnitudes. To compare the results and to check the performance of the state estimation with less number of measurements, the system is initially solved with only 18 measurement data and finally with 62 measurement data. The 18 measurement data consists of only the bus power injections and the bus voltage magnitudes.

Matlab [6] is used to formulate the iterative algorithm for the WLS due to its ability to solve matrices of higher order. Set $\varepsilon = 0.0001$ and $k = 0$. The matrices $h(x^k)$, the Jacobian matrix $H(x^k)$ and the gain matrix $G(x^k)$ are all calculated. The Jacobian H matrix for the 18 and 62 measurement data are calculated using the appropriate formulas. The order of the H matrix for 18 measurement data is 18X11 and for 62 measurement data it is 62X11. The iteration continues until the maximum estimated values Δx^k are less than or equal to the chosen value of the ε, i.e. $|\Delta x^k| \leq \varepsilon$. If the value is greater than ε, then x^k is updated and the iteration continues until the inequality is met. The algorithm converges at the fourth iteration, giving a reliable estimate to the system. Using the estimated state variables, the line power flows are calculated.

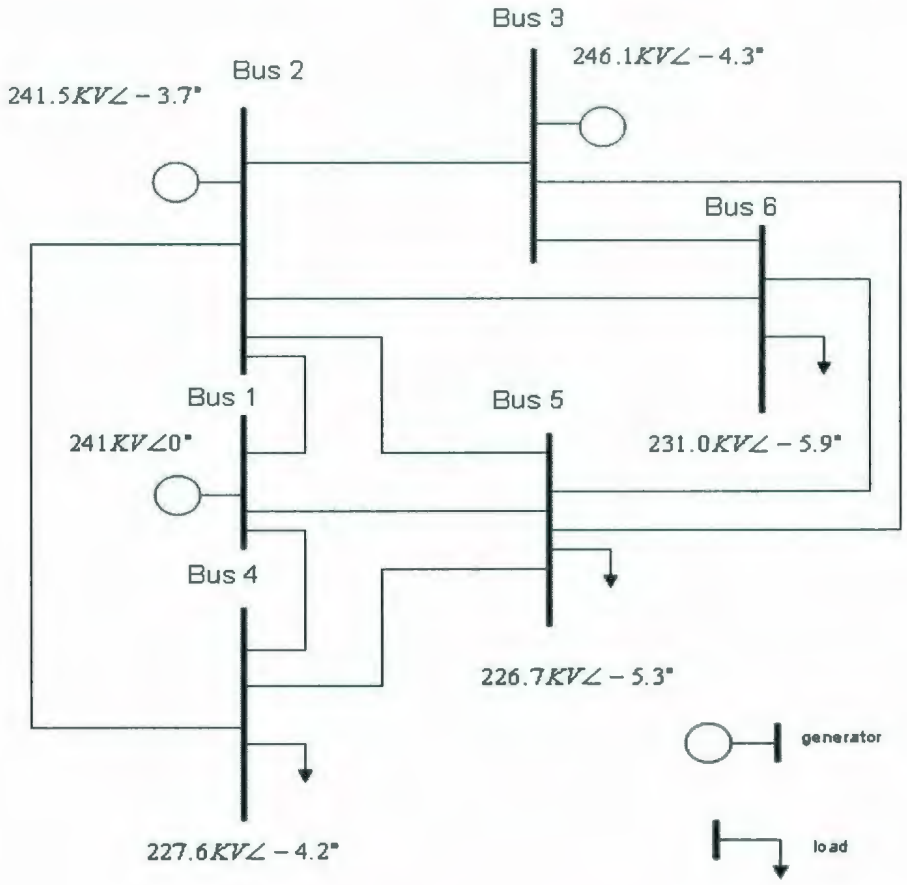

Figure 2.4: 6-bus network [2].

In order to evaluate the performance of the state estimator, a base case or a reference case of the system is required. Hence, the system is solved using the Power World Simulator [7] and the power flow list from the simulator is assumed to be the actual or true power flow values of this system. The estimated values are compared against the actual values using a bar chart. Different shades are used in the bar chart to represent each case (blank - for actual case, slightly shaded - for 18 measurement data and dark -for 62 measurement data).

The comparison between estimated state variables and the actual values for both 18 and 62 measurement data are given in Figure 2.5 and Figure 2.6. The estimated (both real and reactive) bus power injection and line power flows values are also plotted against the actual values, for both 18 and 62 measurement data, as shown in Figure 2.7 through Figure 2.10. In Figure 2.9 and Figure 2.10 only a few randomly chosen line power flows are compared.

In the case of the bus phase angle plot in Figure 2.6, the 62 measurement data provides a closer estimation to the actual value and in bus voltage magnitude plot in Figure 2.5, 18 measurement data provides a closer estimation to the actual value. In the power injection and line power flow plot, the 62 measurement data gives a close estimate to the actual case. By summarizing the results of the estimated values, it can be seen that they are very close to the actual case values and differ only by a few degrees in both cases. This also shows that even with smaller set of measurement data, the state estimation is able to perform well and provide a reliable estimate of state variables.

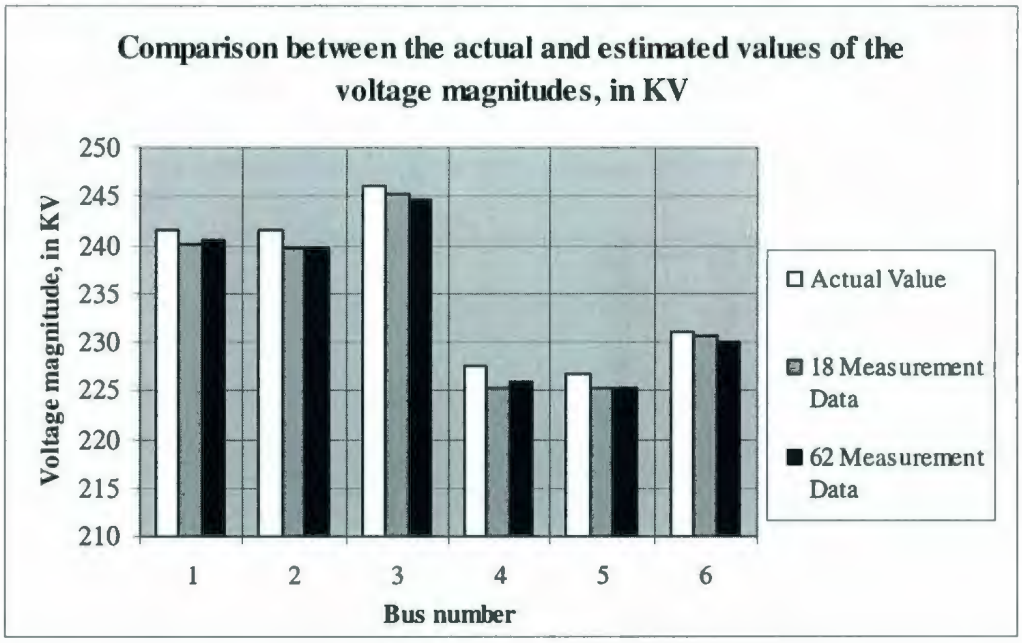

Figure 2.5: Comparison between actual and estimated values of the bus voltage magnitude, in KV

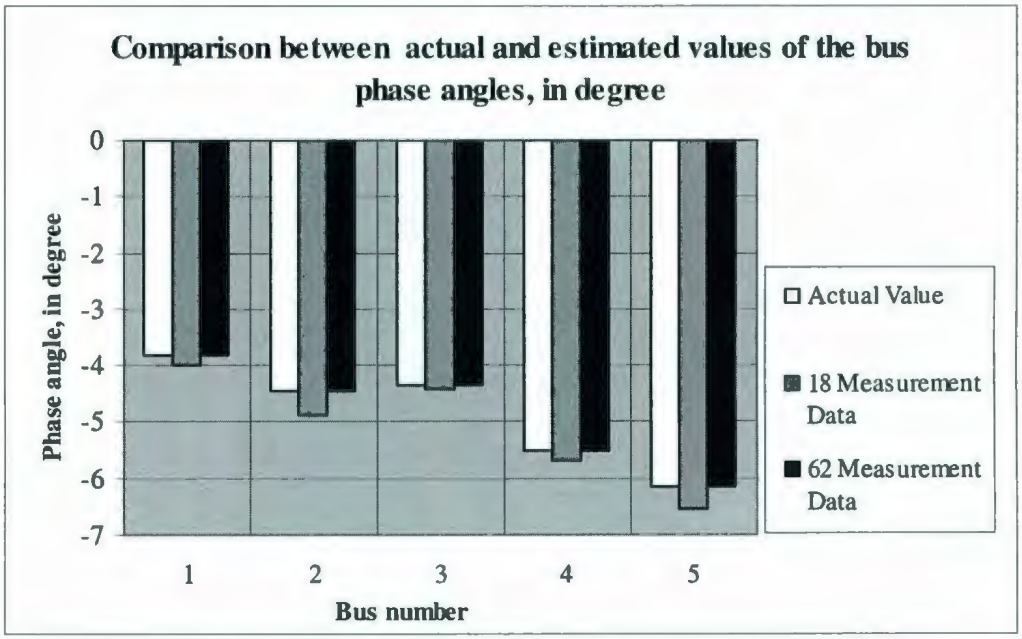

Figure 2.6: Comparison between actual and estimated values of the bus phase angle, in degree

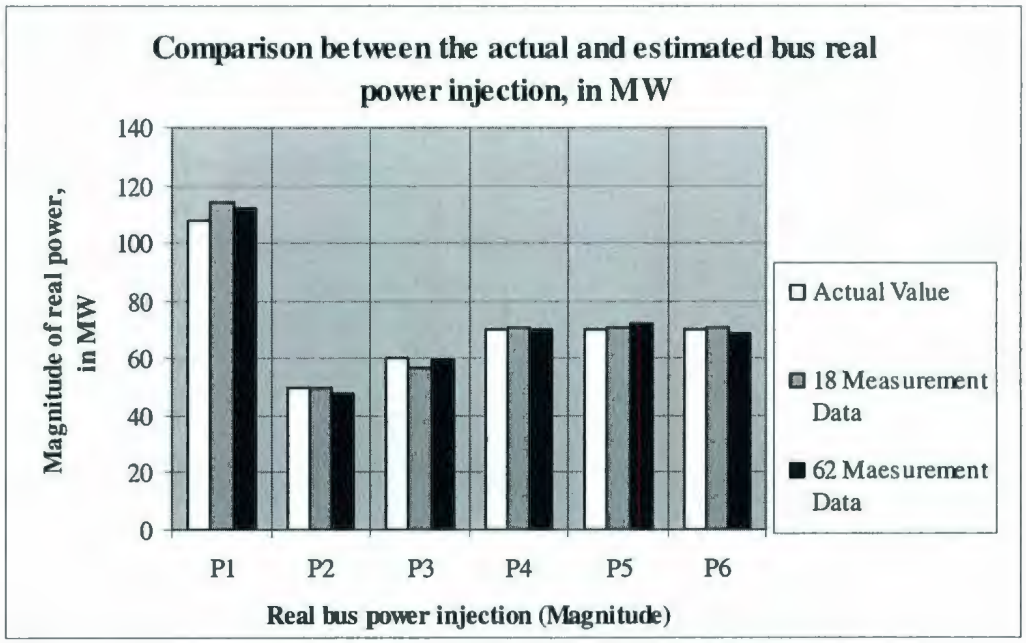

Figure 2.7: Comparison between actual and estimated bus real (P_i) power injection, in MW

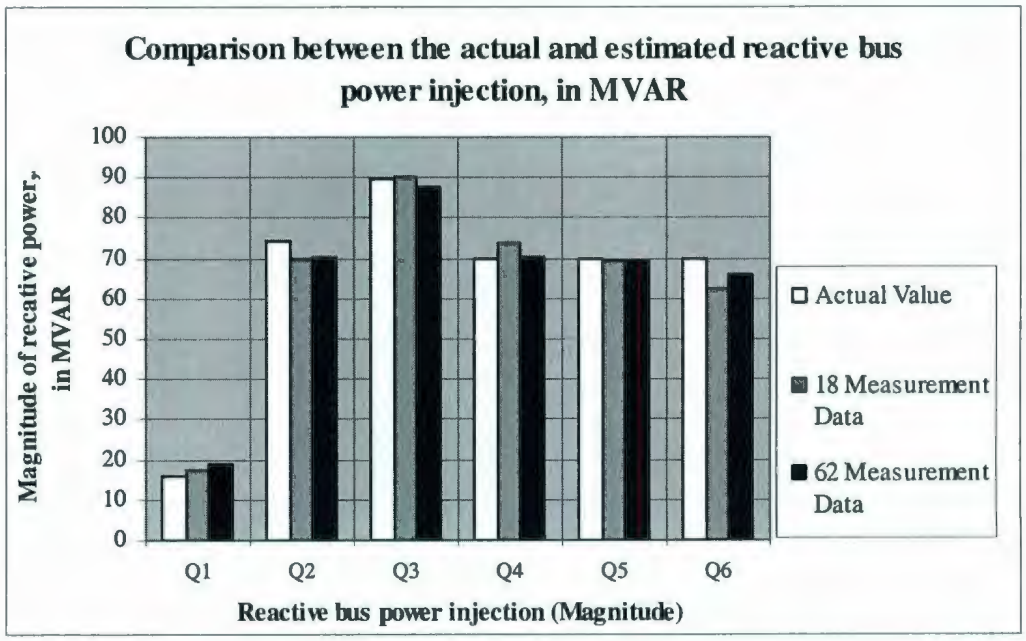

Figure 2.8: Comparison between actual and estimated bus reactive (Q_i) power injection, in MVAR

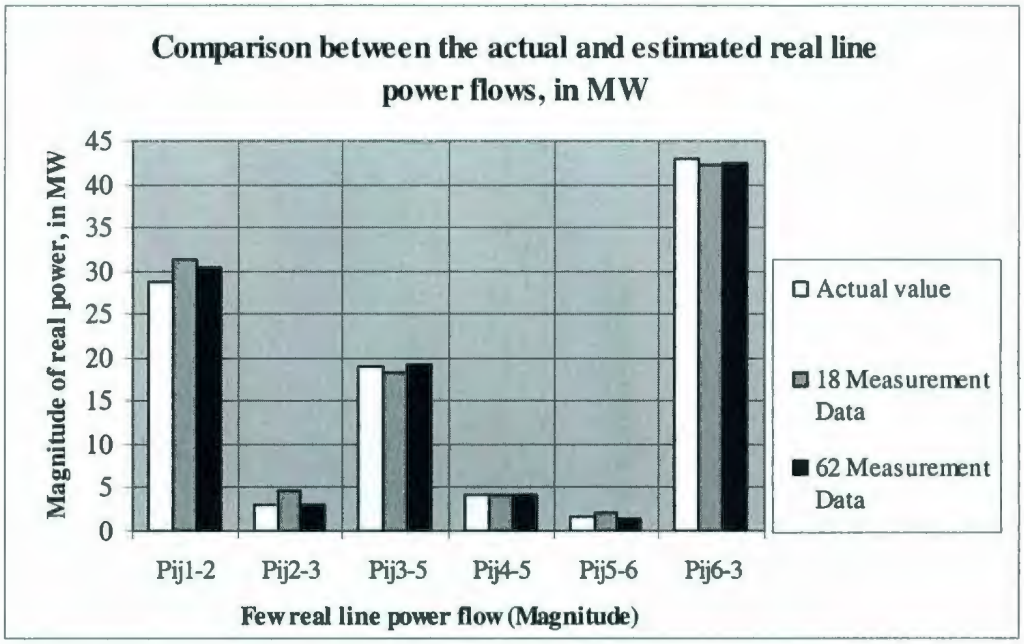

Figure 2.9: Comparison between actual and estimated real line power injection, in MW (Pij1-2 is the real line power flow from bus 1 to bus 2)

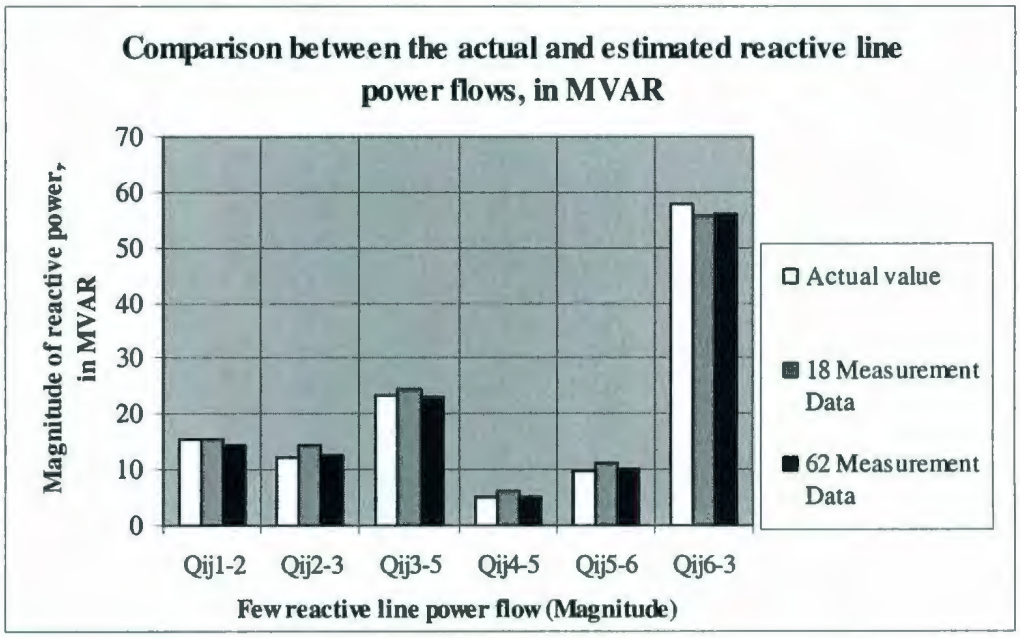

Figure 2.10: Comparison between actual and estimated reactive line power flow, in MVAR (Qij1-2 is the real line power flow from bus 1 to bus 2)

2.4.5 39-Bus System

The 10-unit 39 bus New England test ac network as shown in Figure 2.11 is the second system of this case study, which is used for the implementation of the state estimation using WLS. This system is chosen to check the performance of the state estimator with a larger power system. This system is also solved with two measurement data sets, 131 and 277. There are 39 buses in this system, i.e. N=39. Therefore, 2N-1=77 state variables to be estimated, which comprises N=39 bus voltage magnitudes and N-1=38 bus phase angles. Bus 31 is the slack bus (the bus phase angle is zero). The buses 31, 32, 33, 34, 35, 36, 37, 38 and 39 represent a bus connected to a generating station (PV buses). Buses 3, 4, 7, 8, 12, 15, 16, 18, 20, 21, 23, 24, 25, 26, 27, 28 and 29 represent a bus connected to the load centre (PQ buses). Details of the 39-bus system are given in Appendix B.

There are 34 transmission lines and 12 transformers with tap ratio one, hence there are 184 line power flows (46*2=92 real and 46*2=92 reactive). The 277 measurement data consists of 27 real and 27 reactive bus power injections, 92 real and 92 reactive line power flows and 39 bus voltage magnitudes. Voltage magnitudes, power injections and a few line power flows form the 131 measurement data. The voltage level for the generating station buses and the transmission line buses are 13.8KV and 345KV, respectively

Matlab is used to formulate the iterative algorithm for the WLS. Set $\varepsilon = 0.0001$ and $k = 0$. The matrices $h(x^k)$, the Jacobian matrix $H(x^k)$ and the gain matrix $G(x^k)$ are all calculated. The Jacobian H matrix for both measurement data are calculated using appropriate formulas. The order of the H matrix for 277 measurement data is 277X77 and 131X77 for 131 measurement data. The iteration continues until the maximum estimated values Δx^k are less than or equal to the chosen value of the ε, i.e. $|\Delta x^k| \leq \varepsilon$. If the value is greater than ε, then x^k is updated and the iteration continues until the inequality is met.

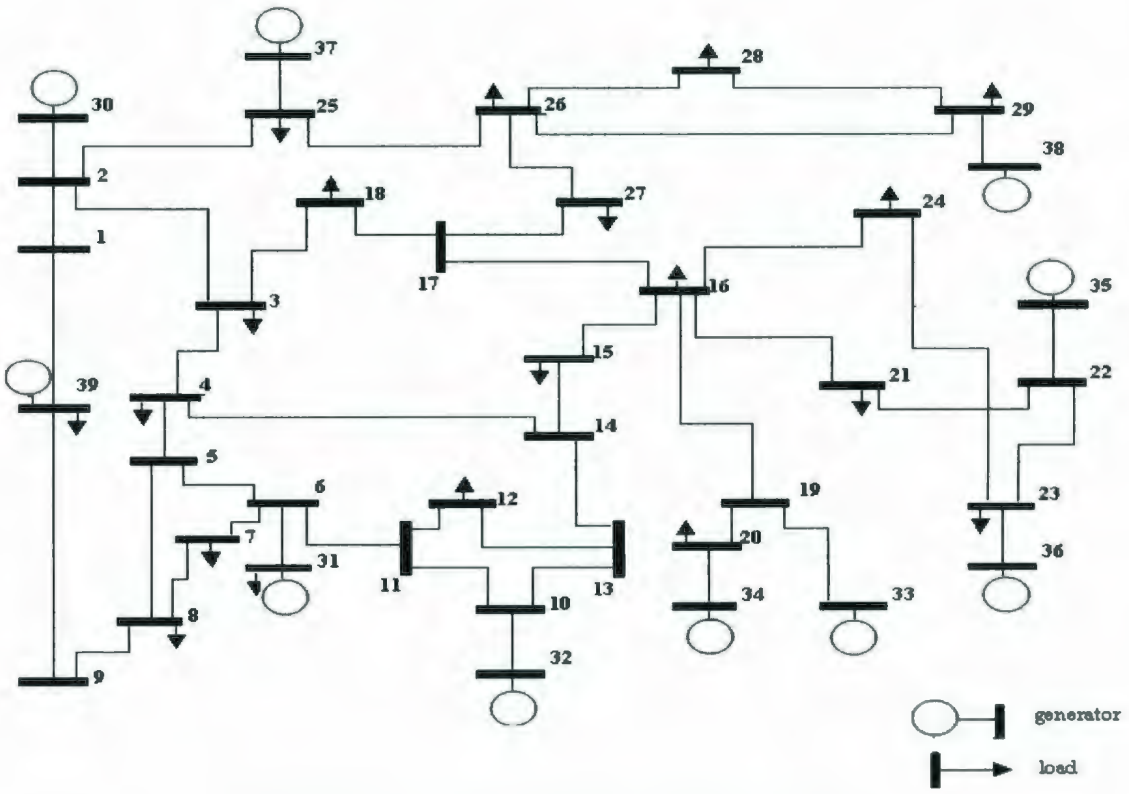

Figure 2.11: 10 unit 39-bus New England test system [8].

The algorithm converges at the fourth iteration, giving a reliable estimate to the system. Using the estimated state variables, the line power flows are calculated.

In order to evaluate the performance of the state estimator, a base case or a reference case of the system is required. Hence, the system is solved using the Power World Simulator and the power flow list from the simulator is assumed to be the actual or true power flow values of this system. The estimated values are compared against the actual values using a bar chart. Different shades are used in the bar chart to represent each case (blank - for actual case, slightly shaded - for 131 measurement data and dark - for 277 measurement data).

This system is quite large; hence only five randomly chosen values are used for comparison. The plot for the comparison between estimated state variables and the actual values are given in Figure 2.12 and Figure 2.13. The estimated (both real and reactive) bus power injection and line power flows values are also plotted against the actual values, as shown in Figure 2.14 through Figure 2.17. From Figure 2.12 and 2.13, it is clear that the estimated values are close to the actual values. The bus power injection plots and the line power flow plots also show that their values lie close to the actual case values. By summarizing the results of the estimated values in the entire figure, it can be seen that they lie close to the actual case values and differ by a slight degree, in only some cases. This shows that even with smaller measurement data, the state estimation is able to perform well and provide a reliable estimate of state variables.

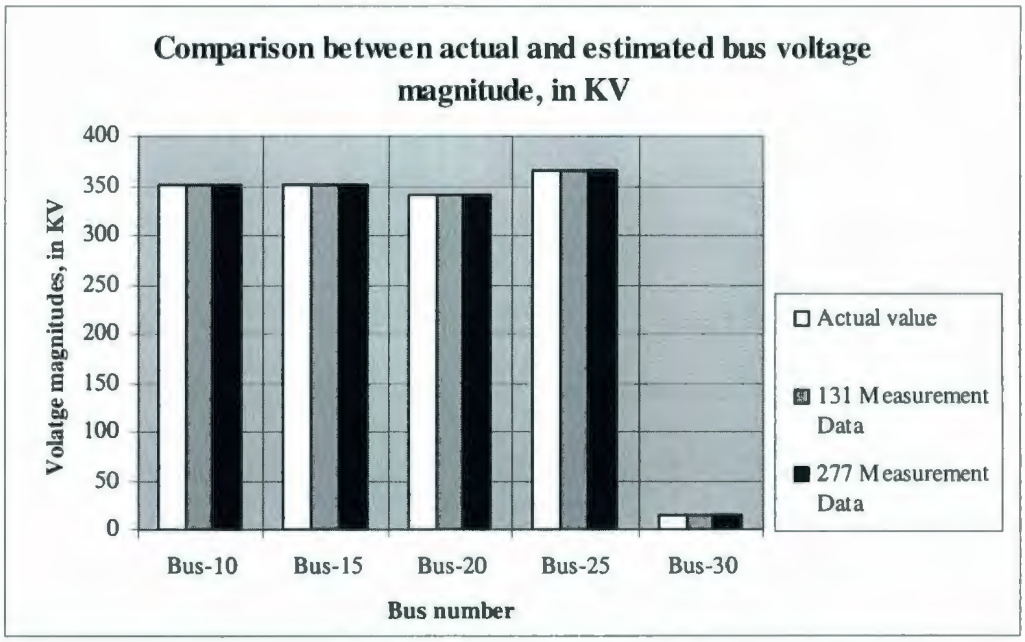

Figure 2.12: Comparison between a few actual and estimated bus voltage magnitudes, in KV

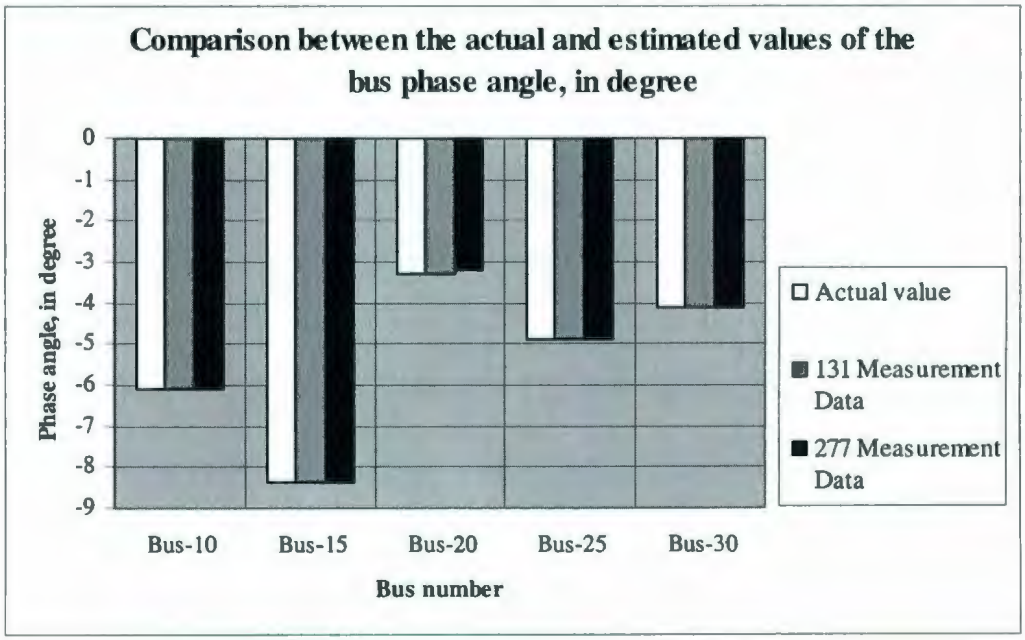

Figure 2.13: Comparison between a few actual and estimated bus phase angles, in degree

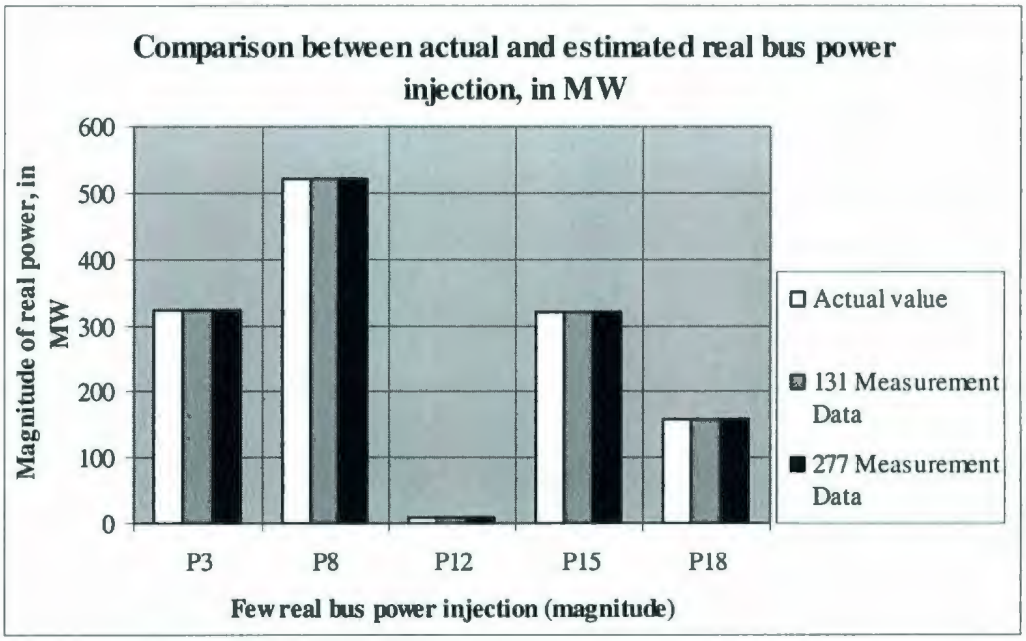

Figure 2.14: Comparison between a few actual and estimated (P_i) real bus power injections, in MW

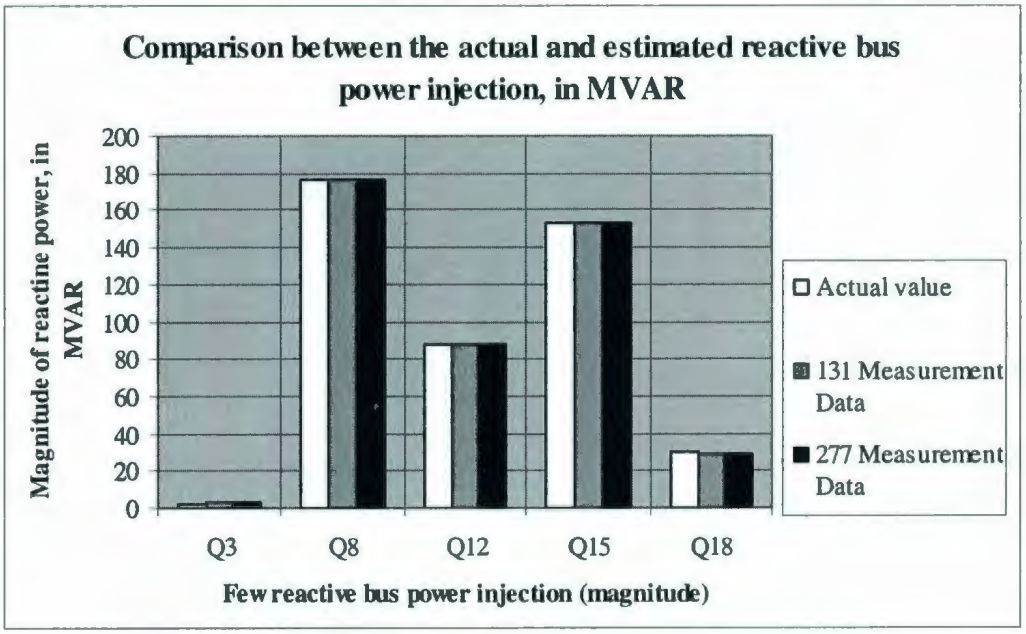

Figure 2.15: Comparison between a few actual and estimated (Q_i) reactive bus power injections, in MVAR

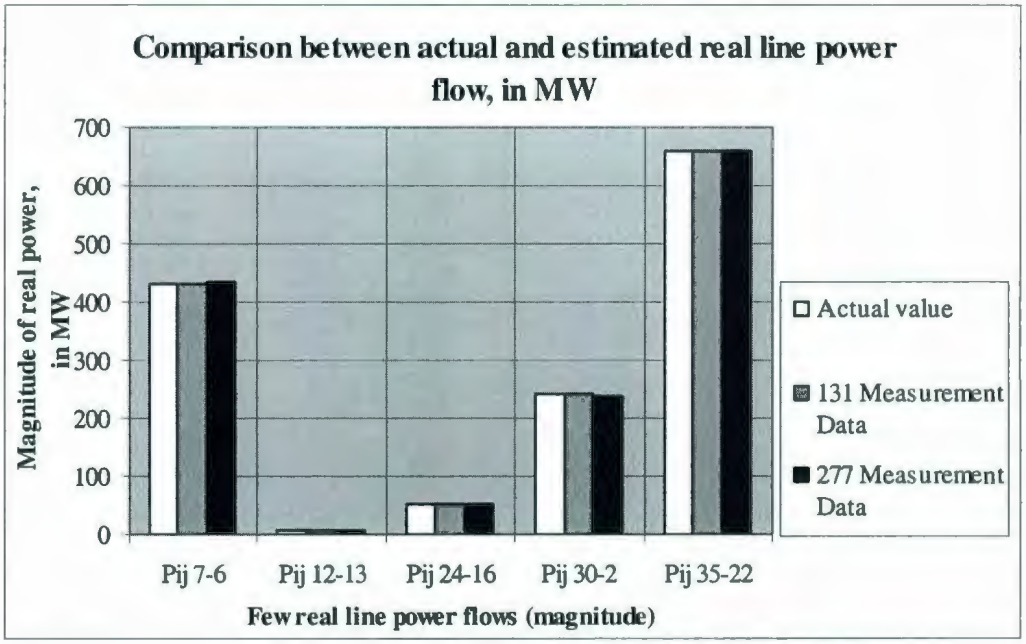

Figure 2.16: Comparison between a few actual and estimated real line power flows, in MW (Pij7-6 is the real line power flow from bus 7 to bus 6)

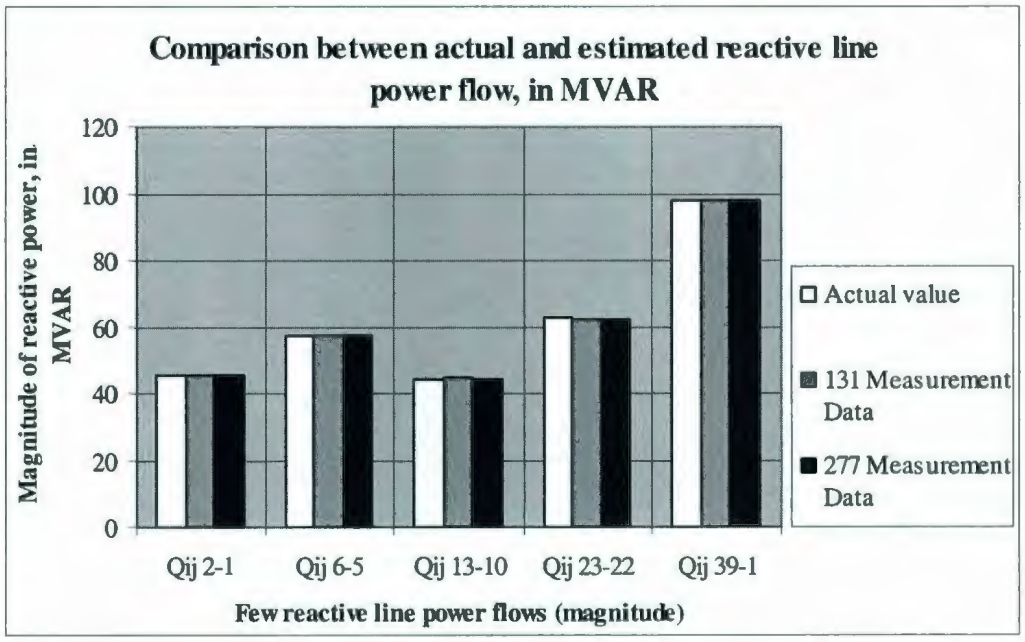

Figure 2.17: Comparison between a few actual and estimated reactive line power flows, in MVAR (Qij2-1 is the real line power flow from bus 2 to bus 1)

2.5 SUMMARY

State estimation is a unique approach estimating the unknown system state variable at any particular point of time, with only a few available measurements. The estimated variables are reliable and can be used to estimate the line power flows in a power system. These estimated line power flows are utilized to evaluate the system condition so as to make a decision or even to predict the faults before they occur. Only static state estimation was studied in this chapter.

In this chapter, a detailed study of the state estimation method is presented. The measurement and components were formulated and implemented. The implementation was done using the two ac systems, 6-bus and 39-bus system. Both systems were initially solved with fewer measurements and later with full measurement data. In both cases, the state estimator was able to provide a reliable estimate of the state variables. The results were compared with the actual case from the Power World Simulator.

Another important aspect of state estimation is the ability to identify, detect and, if possible, eliminate the bad data present in the measurement data. This application is examined in the next chapter.

CHAPTER 3

BAD DATA DETECTION, IDENTIFICATION AND ELIMINATION

3.1 INTRODUCTION

The power system measurements are acquired from the central computer in a power system. Figure 3.1 illustrates various measurements in a power system. The measured data are all gathered in the Remote Terminal Unit (RMU) in a substation. The RMU provides an interface for the measurements to be transferred to the central computer through telemetry. The analog measurements from the meters are converted to digital signals by the analog-to-digital converter in the RMU. In Figure 3.1, meters 1, 2

and 3 give the generation power, bus voltage and generation voltage, respectively. The meters 4, 5 and 6 give the line power flows.

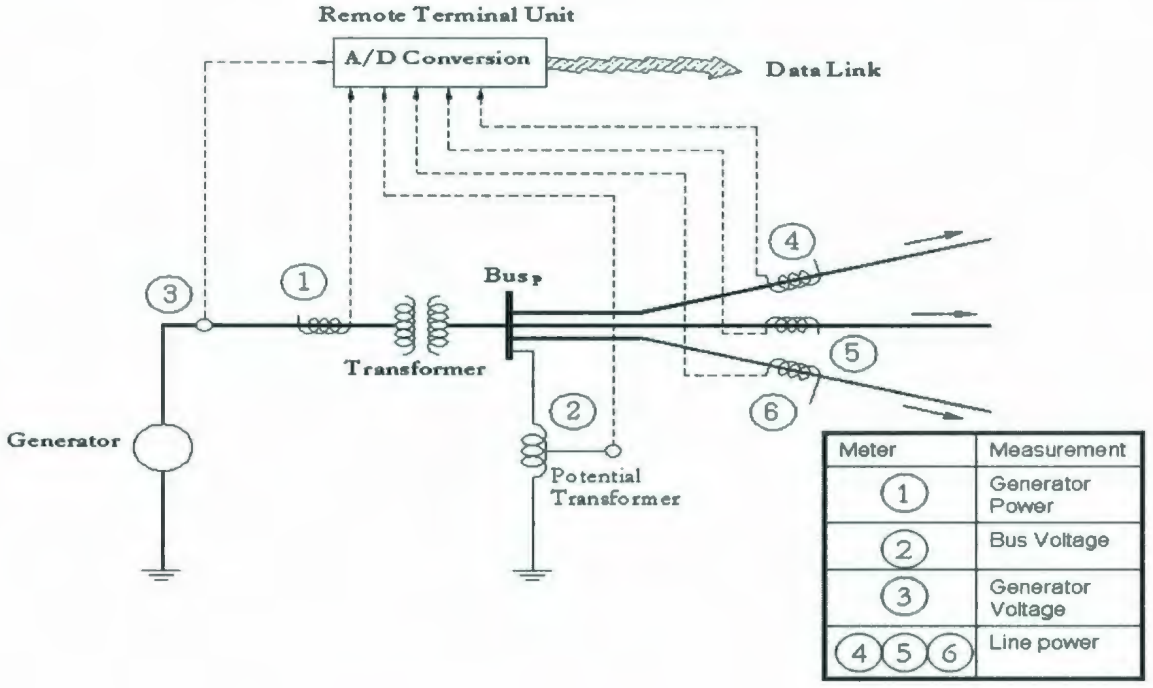

Figure 3.1: Measurements in a power system [9]

Power system state estimation is based on these measurements. Random error usually exists in these measurements due to inaccuracy in meters and the telecommunication medium. Hence, the true value of the quantity being measured is never available in a power system. The state estimator provides the best estimate of the unknown system states with these available data at any particular point of time. Hence, it should also be efficient enough to detect, identify and if possible eliminate measurement errors, apart from the estimation of the unknown state variables.

A few obvious bad data, for example, are negative voltage magnitude and very large measurements with higher order than the expected values, which can be easily detected and eliminated, but most of the bad data are unfortunately undetectable. Therefore the state estimator should be well equipped with advanced features to detect and identify any type of bad data. The bad data may appear due to the type, location and number of measurements that are in error.

The bad data can be broadly classified as single bad data and multiple bad data. In single bad data, only one of the measurements in the large system will have a large error and in multiple data more than one measurement will be in error. The multiple bad data is further classified as follows [5]:

- Multiple non-interacting bad data: They occur in measurements with weakly correlated measurement residuals.
- Multiple interacting but non-conforming bad data: Non-conforming bad data in measurements with strongly correlated residuals.
- Multiple interacting and conforming bad data: Consistent bad data in the measurements with strongly correlated measurement residuals.

In this chapter the bad data processing techniques are formulated and implemented to 6-bus and 39-bus systems.

3.2 BAD DATA DETECTION USING CHI-SQUARED METHOD

The procedure to find whether or not the measurement set contains any bad data is detection. The detection procedure is carried out by processing the measurement residuals only after the WLS algorithm converges. One of the most commonly used methods of detection of bad data is the chi-squared test. To determine whether the estimated values differ significantly from the measured values, a useful statistical measure is the χ^2 test of inequality. The chi-squared test allows testing for deviations of observed frequencies from expected frequencies. The quantity is a measure of the deviation of samples from the expected value as in equation (3.1) [10].

$$\chi^2 = \sum_{i=1}^{n} \frac{(O_i - E_i)^2}{E_i} \tag{3.1}$$

where: O_i and E_i are the observed and expected values respectively. This statistical measure is based on the chi-squared probability distribution, which differs in shape depending on its degrees of freedom, which is the difference between the number of measurements (m) and the number of state variables (n). By comparing the weighted sum of the error with the χ^2 value for a particular degree of freedom and significance

level, it is determined whether the errors exceed the bounds of what is expected by chance alone. The significance level is the upper bound on the probability that a type I error occurs upon conducting a hypothesis test. A type I error occurs when the null hypothesis is correct but is rejected. A significance level of 0.03 indicates that there is a 3% chance that a bad data exists, or a 97% level of confidence in the goodness of the data.

The steps involved in this method are summarized in a flowchart shown below in Figure 3.2. Initially, the WLS state estimation is used to solve the system to get the estimate of the unknown state variables $\hat{x}$. With estimated values, the weighted sum of errors or the objective function $J(\hat{x})$ is computed using the formula in equation (3.2):

$$J(\hat{x}) = \sum_{i=1}^{m} \frac{[z_i - h_i(\hat{x})]^2}{\sigma_i^2} \tag{3.2}$$

where: $\hat{x}$ is the estimated state vector.

$h_i(\hat{x})$ is the estimated measurement i.

z_i is the measured value of the measurement i.

$\sigma_i^2 = R_{ii}$ is the variance of the error in the measurement i.

m is the number of measurements.

The value of $J(\hat{x})$ is compared with the chi-squared value of a particular degree of freedom and significance level. If the value of $J(\hat{x})$ is greater than or equal to the χ^2

value then the measurement set consists of bad data, or, on the other hand if it is less than the χ^2 value, then the measurements are free of bad data with the chosen level of significance. Matlab command CHI2INV (p, m-n) is used to find the χ^2 of any desired value.

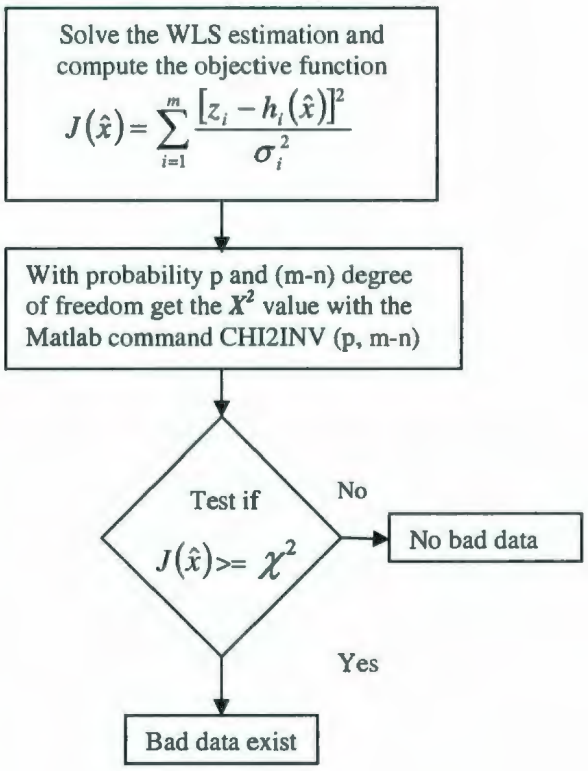

Figure 3.2: Flow chart showing the Chi-square method to detect bad data

The χ^2 method for the detection of bad data is applied to the 6-bus system with 62 measurement data and the 10-unit 39-bus New England test system with 131 measurement data, used in Chapter 2.

3.2.1 6-Bus System

In order to study the chi-squared method, four bad data were introduced in the measurement data. This system has 11 state variables (n) with 62 measurements (m). The real and reactive line power flow from bus 1 to bus 4 (measurement 20 and 23) and from bus 2 to bus 4 (measurement 31 and 33) were arbitrarily changed to represent the bad data (bad data is high lighted in bold fonts in Table 3.1). The WLS technique is executed to this system with bad data. A Matlab program is formulated to compute the weighted sum of the error $J(\hat{x})$ with the estimated state variables using the equation (3.2). The confidence level assumed for this system is 95% and the degree of freedom is 51, i.e. m-n = 62-11 = 51.

The $J(\hat{x})$ calculated is 266.7159. It is compared with the χ^2 distribution value found using the Matlab command CHI2INV (0.95, 51), which is 68.6693. The value of $J(\hat{x})$ is much greater than the χ^2 distribution value. Hence, the presence of bad data in the measurements is detected. Table 3.1 displays bad data introduced to the measurement set and the $J(\hat{x})$ value calculated for both (no bad and bad data) cases.

Table 3.1: The bad data introduced to the 6-bus system and $J(\hat{x})$ value

Measurement number i =1.....62	No Bad Data (pu)*	Four Bad Data (pu)*
1	1.1310	1.1310
2	0.4840	0.4840
15	1.0900	1.0900
16	0.9813	0.9813
17	0.9791	0.9791
18	0.9952	0.9952
19	0.3150	0.3150
20	0.3890	**0.9890**
21	0.3570	0.3570
22	0.0860	0.0860
23	0.3280	**0.7280**
24	0.1740	0.1740
30	-0.1320	-0.1320
31	0.2120	**0.6120**
32	0.0940	0.0940
33	-0.1190	-0.1190
34	0.3830	**0.7830**
55	0.1020	0.1020
56	-0.4430	-0.4430
57	-0.2220	-0.2220
58	-0.2230	-0.2230
59	-0.2990	-0.2990
60	-0.5110	-0.5110
61	-0.0150	-0.0150
62	0.0290	0.0290
	$J(\hat{x})$=41.1400	$J(\hat{x})$= 266.7159

* per unit (pu) 100MVA and 230KV base

3.2.2 39-Bus System

This 39-bus system is the second test system. There are four bad data introduced in the measurement data. This system has 77 state variables (n) with 131 measurements (m) (as in Chapter 2) used for state estimation. The measurements 86, 97, 106 and 122 were arbitrarily changed to represent bad data (bad data is high-lighted in bold fonts in Table 3.2). The weighted least-square technique is executed to the system with bad data.

A Matlab program is formulated to compute the weighted sum of the error $J(\hat{x})$ with the estimated state variables using equation (3.2). The confidence level assumed for this system is 95%.

The $J(\hat{x})$ calculated is 109.0551. It is compared with the χ^2 distribution value 72.1532. This value of $J(\hat{x})$ is much greater than the χ^2 distribution value. Hence, the presence of bad data is detected. Table 3.2 gives the bad data introduced to the measurement set and the $J(\hat{x})$ value calculated for both cases.

Table 3.2: The bad data introduced to the 39-bus system and $J(\hat{x})$ value

Measurement number i=1.....131	No Bad Data (pu)*	Four Bad Data (pu)*
1	0	1.7522
2	0	0.094
12	0	0.4647
65	0	0
86	**0**	**13.7188**
91	0	0.0921
92	0	0.1352
97	**0**	**23.6118**
100	0	0.2186
106	**0**	**13.1677**
120	0	0.0741
122	**0.0652**	**26.28**
131	0.0475	0.0234
	$J(\hat{x})$= 0.2532	$J(\hat{x})$= 109.0551

* per unit (pu) 100MVA and 345KV base

The χ^2 method only detects the presence of bad data, so the next step is identifying and eliminating it from the measurement set.

3.3 BAD DATA IDENTIFICATION AND ELIMINATION

The procedure to distinguish which specific measurement is the bad data is called identification of bad data. The identification of the bad data is facilitated by a largest normalized residual test. Considering the residual sensitivity and covariance matrices, measurement residuals may still be correlated even if errors are assumed to be independent with $E(e)=0, \text{cov}(e)=R$ and the WLS estimator of the linearized state vector will be given by:

$$\Delta\hat{x}=\left(H^T R^{-1} H\right)^{-1} H^T R^{-1}\Delta z = G^{-1} H^T R^{-1}\Delta z \tag{3.3}$$

Let $K = HG^{-1}H^T R^{-1}$, then the estimated value of Δz can be denoted by:

$$\Delta\hat{z} = H\Delta\hat{x} = K\Delta z \tag{3.4}$$

Now the measurement residual can be expressed as follows:

$$\begin{aligned} r &= \Delta z - \Delta\hat{z} = (I-K)\Delta z \\ &= (I-K)(H\Delta x + e) = (I-K)e \\ &= Se \end{aligned} \tag{3.5}$$

The matrix S, called the residual sensitivity matrix, represents the sensitivity of the measurement residuals to the measurement errors and I is the identity matrix. The normalized value of the residual for the measurement i can be obtained by simply dividing its absolute value by the corresponding diagonal entry in the residual covariance matrix as in equation (3.6):

$$r_i^N = \frac{|r_i|}{\sqrt{\Omega_{ii}}} = \frac{|r_i|}{\sqrt{R_{ii}S_{ii}}} \tag{3.6}$$

where Ω is the residual covariance matrix

$$\Omega = S * R$$

The normalized value of the residuals r^N is normally distributed with expectation 0 and variance 1, i.e. $r_i^N \sim N(0,1)$. Thus, the largest element in r^N can be computed against a statistical threshold to decide on the existence of bad data. This threshold value is decided based on the desired level of detection sensitivity. The flow chart in Figure 3.3 explains the steps involved in the test of identification and elimination.

After the WLS is solved, the measurement residual is calculated using the estimated values. Then, the normalized value for each measurement is calculated using the formula in equation (3.6). The largest value of the residual r_k^N is then compared with a certain threshold 'c' which is chosen based on the desired level of detection sensitivity. If the largest value of the residual is greater than the threshold value, then that particular measurement is identified as bad data and eliminated. Then, the state estimation is repeated with the measurement set without the bad data. The same procedure is followed from this step until all bad data are eliminated from the measurement set. The largest normalized residual technique is applied to the same systems.

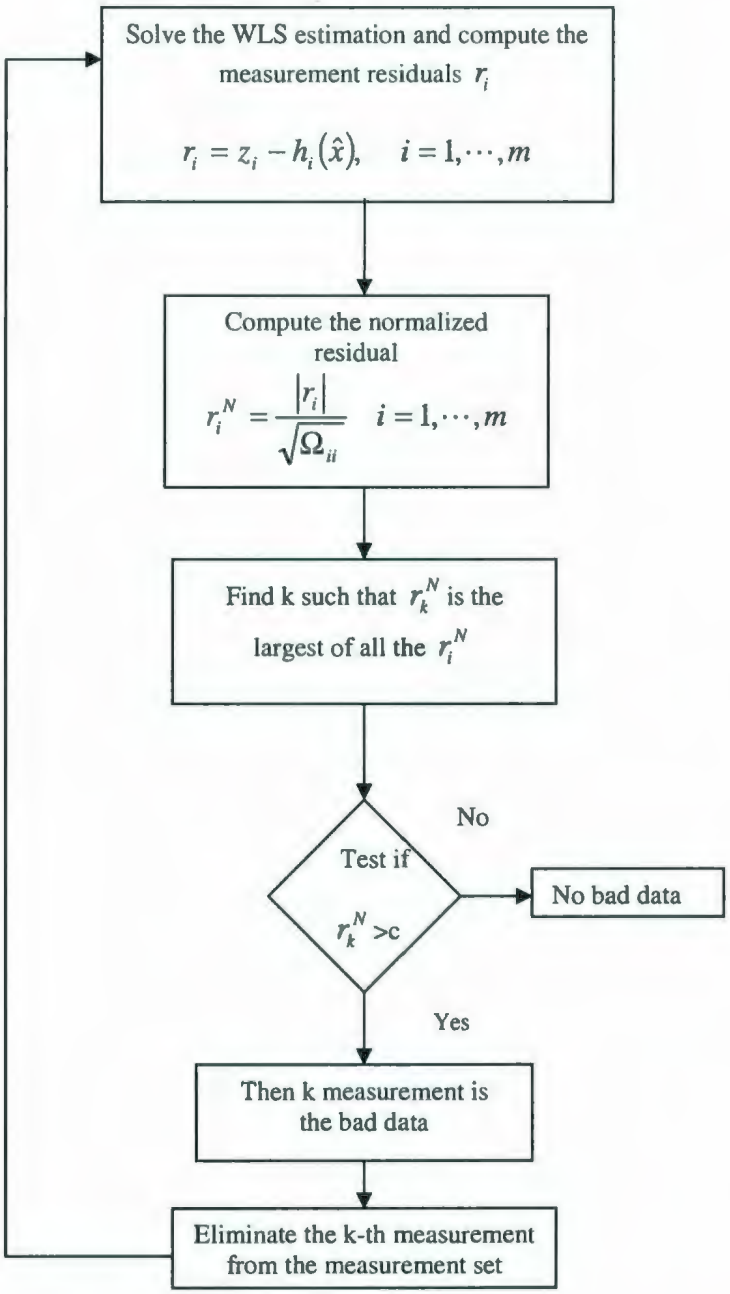

Figure 3.3: Flow chart showing the Largest Residual Test to identify and eliminate bad data

3.3.1 6-Bus System

By using the chi-squared method in the previous section, the 6 bus system is found to possess some bad data in the measurement. Now it has to be identified and eliminated using the largest normalized residual method. A Matlab program is formulated to calculate $r_i^N = \frac{|r_i|}{\sqrt{\Omega_{ii}}} \quad i = 1, \cdots, m$ for each measurement i. There are 62 measurements in this system and the sensitivity threshold 'c' chosen for this is 4 [5]. Table 3.3 gives the normalized residuals calculated for this system.

Table 3.3: The normalized residual for the 6-bus system

Measurement number i=1.....62	r_i^N Normalized Residuals
1	2.8798
2	1.4179
3	1.7514
17	0.0686
18	0.6221
19	0.3255
20	**9.8441**
21	0.4726
22	1.4023
23	**6.4339**
28	0.0817
29	0.6136
30	0.2358
31	**6.8846**
32	0.5406
33	0.3973
34	**5.2771**
35	1.507
36	1.1676
60	0.9902
61	0.2237
62	0.4515

From the table it can be seen that measurements 20, 23, 31 and 34 are identified as bad data, since their calculated residual value is greater than the threshold value 'c', i.e. 4. The next step is the elimination of these four bad data and WLS is carried out, this time with only 62-4 =58 measurements.

The chi-squared method is utilized again to check the presence of bad data. The χ^2 value for the 58 measurements is 64.0011. The calculated $J(\hat{x})$, after elimination, is tabulated in Table 3.4. The $J(\hat{x})$ value 37.3173 is less the χ^2 value. Thus, the bad data are identified and eliminated using the largest normalized residual.

Table 3.4: The value $J(\hat{x})$ calculated for the 6-bus system after elimination of bad data

Measurement number i =1.....58	$J(\hat{x})$ calculated after the elimination
1	0.0038
2	0.0823
15	0
16	0
18	0.0208
27	0.0895
30	2.0652
33	0.0010
57	0.1138
	$J(\hat{x})$=37.3173

A few of the calculated real power injection values estimated with four bad data and after the elimination of bad data are compared with the actual value of the real power injections, which is shown in Figure 3.4.

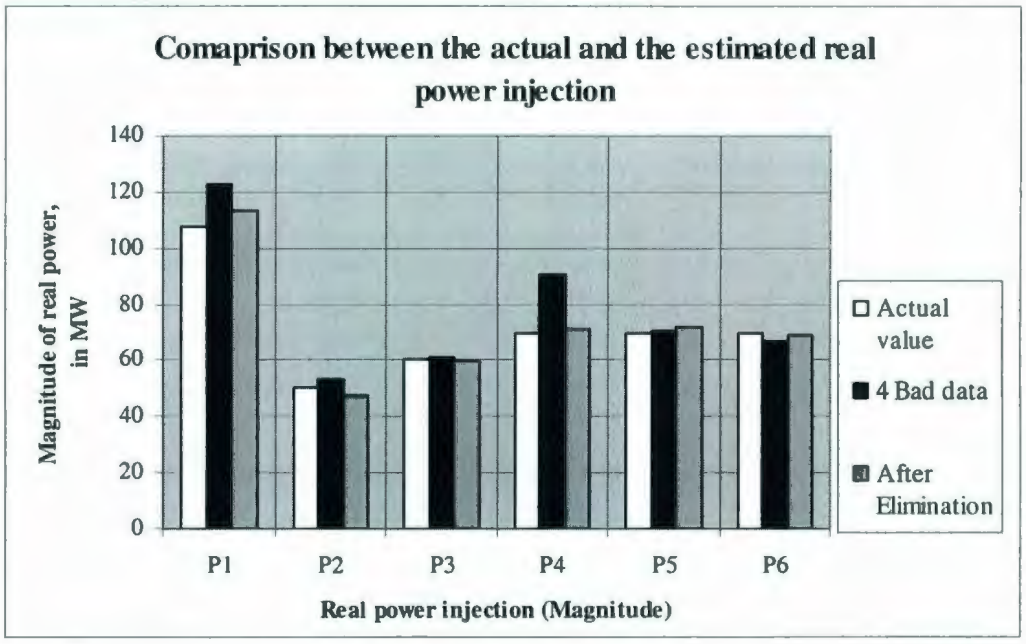

Figure 3.4: Comparison between few real power injections calculated with four bad data and after the elimination of bad data with the actual value, in MW

The results estimated after elimination are very close to the actual value and this also demonstrates that the bad data processing techniques efficiently detects, identifies and eliminates bad data.

3.3.2 39-Bus System

By using the chi-squared method in the previous section, the 39 bus system is found to possess some bad data in the measurement. Now it has to be identified and eliminated using the largest normalized residual method. A Matlab program is formulated

to calculate $r_i^N = \frac{|r_i|}{\sqrt{\Omega_{ii}}}$ $i = 1, \cdots, m$ for each measurement i. There are 131 measurements in this system and the sensitivity threshold 'c' chosen for this is 4. Table 3.5 gives the normalized residuals calculated for this system.

Table 3.5: The normalized residual for the 39-bus system

Measurement number i =1.....131	r_i^N **Normalized Residuals**
1	2.4218
2	0.6487
12	1.2844
22	0.6272
50	0
55	0
65	0
86	**4.0896**
91	0.3399
92	0.4094
97	**5.8061**
100	0.5137
106	**5.1113**
120	0.2008
122	**5.9746**
131	0.1874

From the table, it can be seen that measurements 86, 97, 106 and 122 are identified as bad data, since their calculated residual value is greater than the threshold value 'c', i.e. 4. The next step after identification is elimination. These four bad data are eliminated and WLS is carried out, this time with only 131-4 =127 measurements.

The chi-squared method is utilized again to check the presence of bad data. The χ^2 value for the 127 measurement is 67.5048. The calculated $J(\hat{x})$ is tabulated in Table 3.6. The $J(\hat{x})$ value 0.1246 is less than the χ^2 value. Thus, the bad data are identified and eliminated using the largest normalized residual.

Table 3.6: The $J(\hat{x})$ value calculated after the elimination of bad data for the 39-bus system

Measurement number i =1.....127	**$J(\hat{x})$ calculated after the elimination**
12	0.0001
22	0
25	0
30	0.0003
40	0
45	0.0083
50	0.0086
63	0.0048
70	0.0004
127	0.0163
	$J(\hat{x}) = 0.1246$

A few of the calculated real line power flow values estimated with four bad data and after elimination of bad data are compared with the actual value of the real line power flows, which is shown in Figure 3.5.

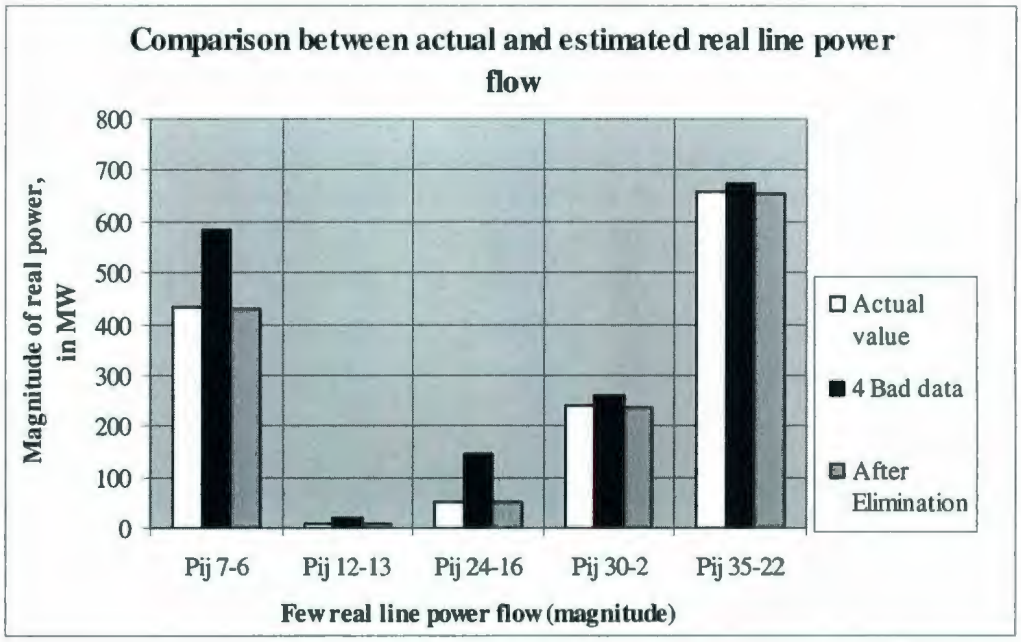

Figure 3.5: Comparison between few real line power flows calculated with four bad data and after the elimination of bad data with the actual value, in MW

The results estimated after elimination are very close to the actual value and this also demonstrates that the bad data processing techniques efficiently detects, identifies and eliminates bad data.

3.4 SUMMARY

Error detection and elimination of bad data are an additional aspect of state estimation, apart from the estimation of the unknown system state variable. The bad data is detected using a chi-squared test. Then, it is identified and eliminated using a largest normalized residual test. In this chapter, both methods were explored for 6-bus and 39-bus systems. The bad data were introduced to the system arbitrarily to demonstrate the error detection. In the next chapter, the network parameter error estimation will be studied and implemented.

CHAPTER 4

NETWORK PARAMETER ERROR ESTIMATION

4.1 INTRODUCTION

The network model is used in all Energy Management System (EMS) applications, such as economy-security functions. The economy-security function involves network monitoring, contingency analysis and optimal power flow. The EMS uses the real-time processes intended to sustain a designated security level at a minimum operational cost. The maintenance of the designated security level is designed to avoid emergency conditions and, if an emergency does occur, to guarantee the recovery of the network from the emergency conditions [11].

The electrical power system requires network parameters to build the network model used in EMS applications. State estimation is one of the EMS applications that play an important role in providing the network model [12]. Some of the network parameters are the transmission line resistance, line reactance, line charging capacitance, transformer reactance, transformer tap, shunt capacitor/reactor values, etc. The error in the network model is known as the network parameter error. The presence of error in the estimated state variables, using state estimation, may be due to bad data in the measurement, network parameter error and/or topology error. The topology errors occur when the open/close status of circuit breakers/switches is misread or when an out of service transmission line is considered to be in service during the state estimation. The parameter error identification and estimation are the additional features of the state estimation.

The influences of the parameter error on state estimation results are: a) correct measurements being identified as bad data due to their inconsistencies with the incorrect network parameters, b) severe impact on the quality of the state estimation solutions, c) this misleads other applications, such as security assessment, optimal power flow, and d) the operator loses confidence in the state estimation results [5]. Hence the state estimation should also be equipped to identify bad parameters and estimate the correct parameter value.

Compared to the significant amount of literature on state estimation, the number of publications devoted to the parameter estimation problem is very modest [5]. The following section reviews some papers that were used for the literature review and to select a method for parameter estimation. Reference [12] presents a new technique to identify the network parameter even in the presence of a bad analog measurement. The estimation is accomplished by formulating the parameter errors as zero equality constraint and then testing the significance of the associated Lagrange multipliers. Prior knowledge of the suspect parameter is not necessary for this method. Reference [13] proposes a two-step approach that consists of estimating the bias vectors (which combines the effects of parameter error and the state of the system) and estimating the parameter error from the sequence of the bias vector obtained due to several state estimation runs. The proposed method for estimation is based on the linearized decoupled state estimation.

Reference [14] presents parameter error identification using various methods, such as normalized residual, sensitivity analysis and suspicious branch selection algorithm. Parameter estimation (susceptance and tap ratio) is formulated and demonstrated using a real-time example. Reference [15] discusses various properties of parameter error and demonstrates them experimentally using 60 test cases. The experimental results in this paper suggest that: a) a single parameter error significantly affects the adjacent measurements, b) power flow measurements are more sensitive to

parameter error than the power injection measurements, and c) susceptance errors are more harmful than conductance errors.

Reference [16] suggests a classification of the existing methods for parameter estimation and their limitations. Reference [17] proposes a general method for the identification and correction of the real-time data, based on the sensitivity relationship between the measurement residuals and the parameter error, which is followed in this chapter. Real-time correction on erroneous transformer tap positions is demonstrated in this paper.

In this chapter, the measurements are assumed to have only line reactance error and to be free of bad measurement data. In general, there are various methods for identification of parameters (discussed in [14] and [17]). Parameter estimation is illustrated using two main methods. The first method is based on the residual sensitivity analysis that is performed at the end of state estimation, and the second method is state vector augmentation where the suspected parameters are included in the state vector. In the latter method the state vector and parameter are estimated simultaneously. The identification method used for parameter error is the normalized measurement residual method (chapter 3). The residual sensitivity analysis is used in this chapter for the estimation of the parameter error. The 6-bus and 39-bus systems used in chapter 3 will be used here as case studies for the network parameter error identification and estimation.

4.2 NETWORK PARAMETER IDENTIFICATION

A parameter error has the same effect as a set of correlated errors acting on all measurements involved in the erroneous branch, namely the power flow measurements and the power injection measurements located at the end nodes. This fact leads to a simple manipulation of the basic measurement model [13]:

$$z_s = h_s(x,p) + e_s = h_s(x,p_0) + \left[h_s(x,p) - h_s(x,p_0)\right] + e_s \tag{4.1}$$

where p and p_0 are respectively the true and erroneous value of the network parameter and the subscript s refers to the set of adjacent measurements. The term h_s is the nonlinear functions, relating measurement to state variables. The terms in brackets in equation (4.1) are equivalent to additional measurement error and if the parameter error is large enough, this term will lead to the identification of the bad data. When this happens, the adjacent measurements will most likely have the largest normalized residual [13]. The equivalent measurement error can be linearized as:

$$h_s(x,p) - h_s(x,p_0) \approx \left[\frac{\partial h_s}{\partial p}\right] e_p \tag{4.2}$$

where $\left(\partial h_s / \partial p\right)$ is a s-dimensional column vector of partial derivatives of h_s with respect to p, and $e_p = p - p_0$ is the parameter error. Those branches whose adjacent measurements have the largest normalized residual should be declared suspicious.

4.3 NETWORK PARAMETER ESTIMATION

The technique used in parameter estimation is based on the sensitivity relationship between residuals and measurement errors [13]. Equation (3.4), $r = S.e$ from Chapter 3 gives the measurement residuals. By combining the equation (4.1) and equation (3.4), a linear relationship can be established between the residual of the adjacent measurement r_s and the parameter error e_p:

$$r_s = \left(S_{ss} \frac{\partial h_s}{\partial p} \right) e_p + \bar{r}_s \tag{4.3}$$

where S_{ss} is the $s \times s$ submatrix of S corresponding to the s involved measurements and $\bar{r}_s$ is the residual vector that would be obtained when the parameter is correct. Equation (4.3) can be interpreted as a linear model linking some measurements r_s to an unknown

e_p in the presence of noise $\bar{r}_s$. This leads to the determination of e_p as an estimation problem [12]. The optimal linear estimate of e_p from r_s is given by:

$$\hat{e}_p = \left[\left(\frac{\partial h_s}{\partial p} \right)^T R_s^{-1} S_{ss} \left(\frac{\partial h_s}{\partial p} \right) \right]^{-1} \left(\frac{\partial h_s}{\partial p} \right)^T R_s^{-1} r_s \tag{4.4}$$

where R_s is the corresponding covariance matrix of the involved measurements. The parameter ($\hat{p}$) is estimated using the following relation:

$$\hat{p} = p_0 + \hat{e}_p \tag{4.5}$$

The state estimation using the WLS technique is rerun using the new estimated parameter and checked for parameter error using the largest normalized residual method. If the calculated largest normalized values are lower than the threshold value, the system is declared to be free of error and the estimated value is the accurate parameter value.

4.4 CASE STUDY

Two systems are used in this case study to demonstrate the identification of suspicious parameter and parameter estimation. These are the 6-bus and 39-bus systems from Chapter 2. The identification and estimation of the parameter is carried out considering that the error occurs in line characteristic data used for state estimation. The line reactance in the line characteristic data is subjected to random error manually. First, the systems are subjected to one parameter error, then two and finally four parameter error (for 39-bus system only). The parameter error is first identified and the correct parameter is estimated. The estimated parameter is updated to the system to check for any more bad parameters. An example from one parameter error case is illustrated below using the 6-bus system to show the procedure followed in this chapter.

4.4.1 6-Bus System

The 6-bus system shown in Figure 2.4, Chapter 2 is used in this case study. This system is utilized to illustrate one and two (transmission line reactance) parameter error identification and parameter estimation. The network parameter identification is facilitated using the normalized residual technique (chapter 3) and parameter estimation is performed using residual sensitivity analysis.

The parameter error is introduced to the system and the WLS technique is used to estimate the unknown system state variables. Using the estimated state variables, the normalized residual values are calculated for all the measurements. The values that exceed the threshold value of 3 [5] are considered to be the erroneous measurement of the system. The adjacent measurements to the parameter are also included in the estimation process of the parameter even though their value is less than 3.

The identification and estimation of one (single) parameter error is demonstrated by introducing a random error to the reactance of the transmission line, one at a time. There are 8 different cases used to illustrate single parameter identification and estimation. The method followed is illustrated with one case taken as an example (transmission line between buses 3 to 5). The line reactance between the line buses 3 to 5 is changed from 0.26 p.u to 2.26 p.u. Using the Matlab program, the normalized residual value is calculated.

Table 4.1: The normalized residuals for the 6-bus system with one parameter error (for the line 3-5)

Measurement number i=1.....62	r_i^N **Normalized residuals**
1	0.0348
3	0.9453
5	1.6673
9	**3.637**
26	**3.2055**
33	0.8737
37	**4.3548**
43	0.1244
48	**4.6927**
53	1.2409
59	**4.6192**

Table 4.1 gives some of the calculated normalized residual values for this particular case. From Table 4.1, measurements 9 (reactive power injection at bus 5), 26 (real power flow from bus 3 to bus 5), 37 (reactive power flow from bus 3 to bus 5), 48 (real power flow from bus 5 to bus 3) and 59 (reactive power flow from bus 5 to bus 3) are found to have normal residual values higher than the threshold value 3. These values are highlighted in the table. Since all the power flow measurements between bus 3 and bus 5 have high residual values and the reactance of the line is a more harmful parameter error than line resistance [16], the line reactance value from bus 3 to bus 5 is identified as the parameter error.

The next step after identification is the estimation of the correct parameter. The parameter estimation includes all the adjacent measurements of the suspicious line. These are power injection and line flow measurements between both the nodes (if available). From Table 4.1 it can be noted that the measurement 3 and 5 (real power injections of buses 3 and 5 respectively) are lower than the threshold value but are still included in the estimation. Figure 4.1 shows the measurements included in the estimation.

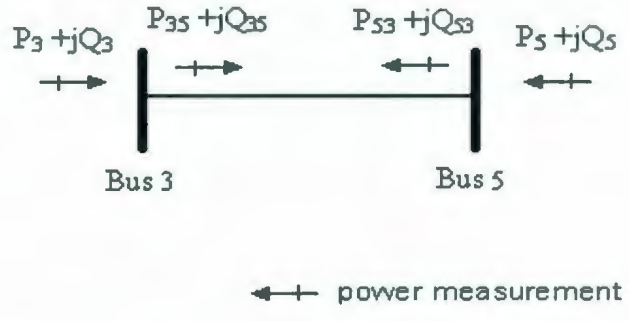

Figure 4.1: Shows the measurements included in the parameter estimation

Eight measurements are considered for parameter estimation. The derivatives $(\partial h_s / \partial p)$ of the measurements (dimension 8x1) with respect to the parameter are calculated for all the eight measurements. The S_{ss} matrix of dimension 8x8 is obtained from the S matrix for the corresponding measurements. r_s is calculated using equation (4.3) and then the parameter error is estimated using equation (4.4). From the estimated error, the parameter value is calculated using the relation in equation (4.5).

The value of the estimated parameter is 0.2602 p.u. The estimated parameter is updated in the network model and the WLS technique is used to estimate the state variables. The normalized residual values are calculated with the estimated state variable. The calculated values are well below the threshold value and therefore it is confirmed that the estimated values are an accurate value of the reactance of the line between buses 3 and 5. Table 4.2 gives some of the calculated normalized residual after parameter correction. The highlighted values are normalized residual values of identified suspicious measurements.

The same procedure is followed for all the eight different transmission lines shown in Table 4.3. The estimated parameter is compared to its actual parameter value as shown in Figure 4.2. The estimated parameter values are found to be close to the actual parameter values.

Table 4.2: The normalized residual values after parameter correction for the 6- bus system with one parameter error (for the line 3-5)

Measurement number i=1.....62	r_i^N **Normalized Residuals**
1	0.3513
3	1.8700
5	0.1461
9	**1.6192**
26	**0.4465**
33	0.5489
37	**0.1382**
43	0.1970
48	**1.4370**
53	1.3258
59	**0.5568**

Table 4.3: The estimated parameter values for 6-system with one parameter error

Serial Number	**Line number**	**Actual parameter value (p.u)**	**Erroneous parameter (p.u)**	**Estimated parameter (p.u)**
1	Line 1-2	0.2000	1.9000	0.2043
2	Line 1-4	0.2000	2.2000	0.2012
3	Line 1-5	0.3000	3.2000	0.2977
4	Line 2-4	0.1000	3.1000	0.1102
5	Line 2-5	0.3000	4.3000	0.3104
6	Line 2-6	0.2000	3.2000	0.2044
7	Line 3-5	0.2600	2.2600	0.2602
8	Line 3-6	0.1000	3.1000	0.1009

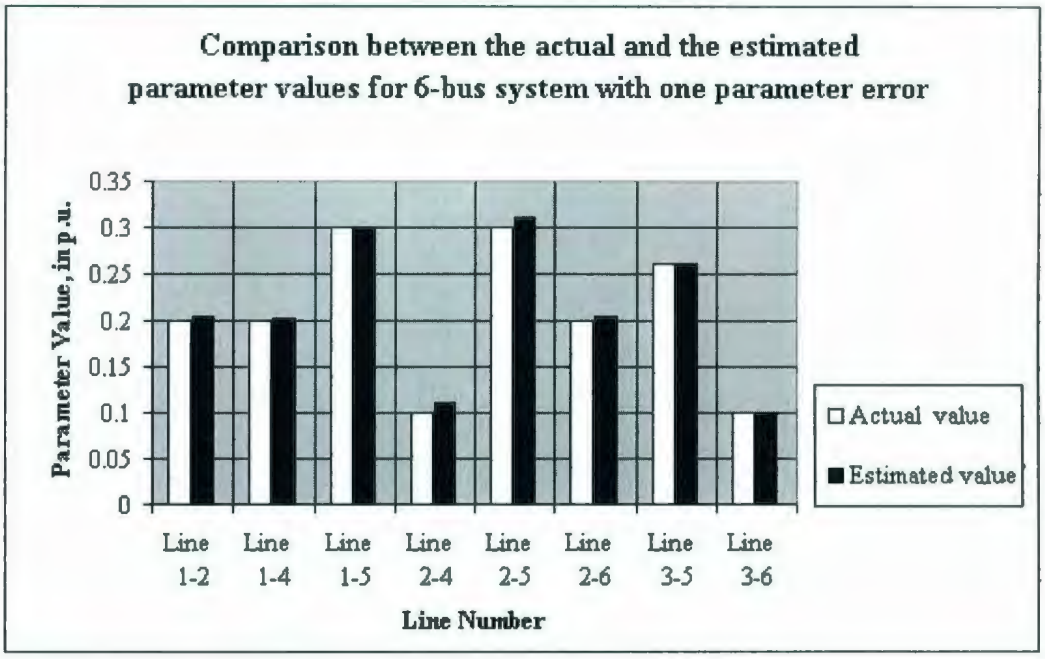

Figure 4.2 Comparison between actual and estimated parameter values for 6-bus system with one parameter error

Four different cases are used for two parameter line reactance error. The parameter error was introduced to two transmission lines at the same time. The identification and estimation of the parameter were performed using the procedure described above. The four different cases are shown in Table 4.4.

Table 4.4: The estimated parameter values for 6-bus system with two parameter errors

Case Number	Line number	Actual parameter value (p.u)	Erroneous parameter (p.u)	Estimated parameter (p.u)
1	Line 1-2	0.2000	3.2000	0.2004
	Line 1-4	0.2000	3.2000	0.2006
2	Line 3-5	0.2600	2.2600	0.2601
	Line 3-6	0.1000	3.1000	0.1005
3	Line 2-4	0.1000	3.1000	0.1006
	Line 2-6	0.2000	3.2000	0.2000
4	Line 1-2	0.2000	3.2000	0.2007
	Line 3-5	0.2600	3.2600	0.2601

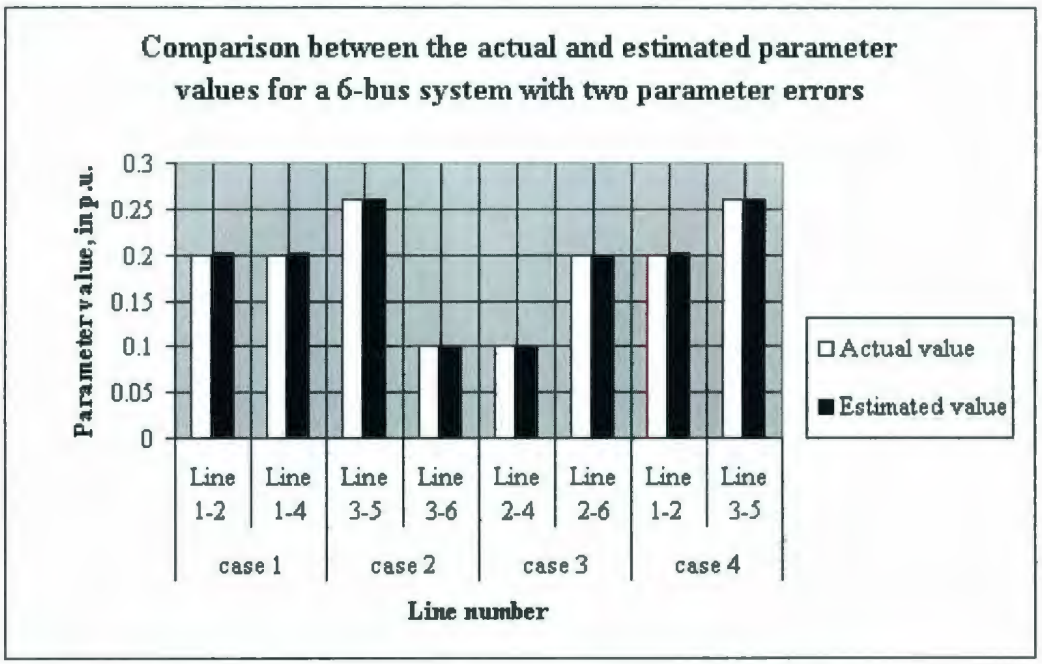

Figure 4.3 Comparison between actual and estimated parameter values for 6-bus system with two parameter errors

Figure 4.3 gives the comparison between the actual and estimated value for the 6-bus system with two parameter error. The estimated values are found to be close to the actual values.

4.4.2 39-Bus System

The 39-bus system shown in Figure 2.12, Chapter 2 is used in this case study. This system is utilized to illustrate one, two and four (transmission line reactance) parameter error identification and parameter estimation. For the one parameter error eight different cases exist. Then for two and four parameter error there are four and two cases respectively. Table 4.5 gives the estimated parameter for one parameter error and Figure

4.4 compares it to the actual parameter value. The estimated values are close to the actual parameter values.

Table 4.5: The estimated parameter values for the 39 bus system with one parameter error

Serial Number	Line number	Actual parameter value (p.u)	Erroneous parameter (p.u)	Estimated parameter (p.u)
1	Line 1-2	0.0411	1.0411	0.0413
2	Line 1-39	0.0025	2.0250	0.0251
3	Line 2-3	0.0151	3.0151	0.0152
4	Line 2-25	0.0086	1.0086	0.0086
5	Line 3-4	0.0213	2.0213	0.0212
6	Line 3-18	0.0133	3.0133	0.0133
7	Line 4-5	0.0128	1.0128	0.0128
8	Line 5-6	0.0026	2.0026	0.0026

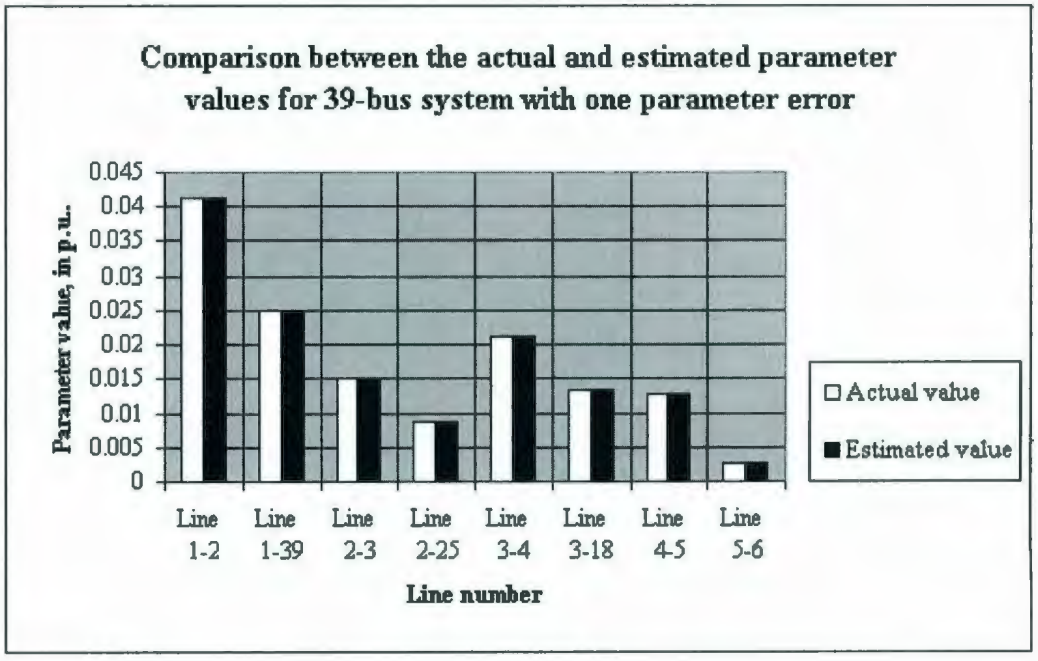

Figure 4.4 Comparison between actual and estimated parameter values for 39-bus system with one parameter error

Table 4.6 gives the estimated parameter value for two parameter error and Figure 4.5 compares it to the actual case. The figure shows that the estimated values are all close to the correct parameter values.

Table 4.6: The estimated parameter values for the 39-bus system with two parameter errors

Case Number	Line number	Actual parameter value (p.u)	Erroneous parameter (p.u)	Estimated parameter (p.u)
1	Line 1-2	0.0411	1.0411	0.0412
	Line 1-39	0.0250	2.0250	0.0250
2	Line 3-18	0.0133	3.0133	0.0133
	Line 5-6	0.0026	2.0026	0.0026
3	Line 3-4	0.0213	2.0213	0.0215
	Line 4-5	0.0128	1.0128	0.0126
4	Line 1-2	0.0411	1.0411	0.00410
	Line 5-6	0.0026	2.0026	0.0026

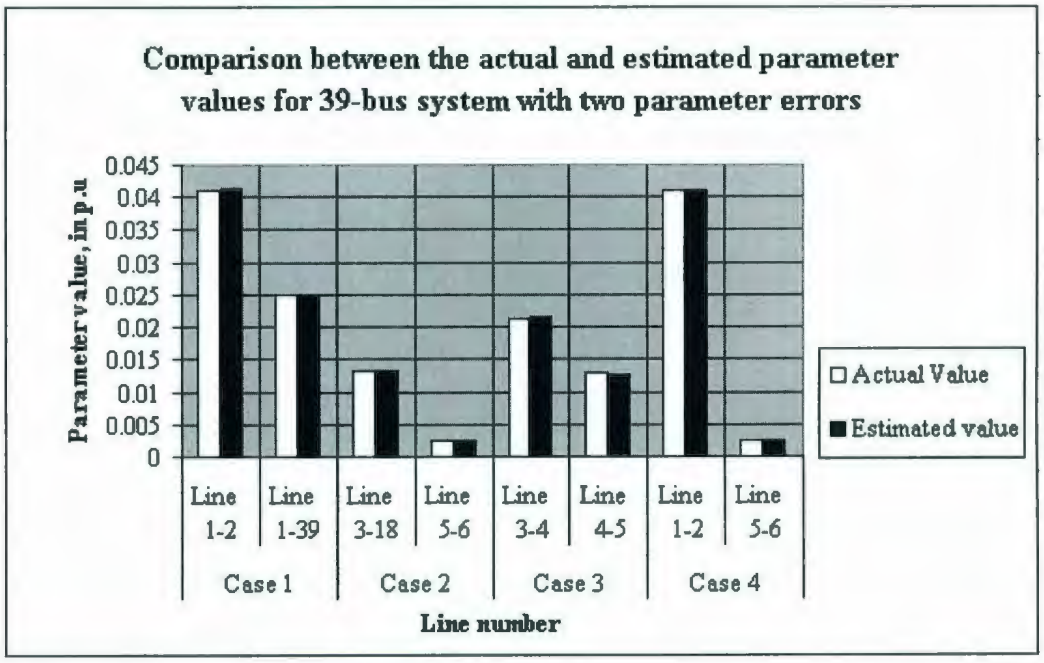

Figure 4.5: Comparison between actual and estimated values parameter values for 39-bus system with two parameter errors

Table 4.7 and Figure 4.6 give the estimated parameter value for four parameter error and its comparison with the actual parameter value respectively. The estimated values are all close to the actual values.

Table 4.7: The estimated parameter values for 39-bus system with four parameter errors

Case Number	Line number	Actual parameter value (p.u)	Erroneous parameter (p.u)	Estimated parameter (p.u)
1	Line 1-39	0.0250	1.0250	0.0252
	Line 2-25	0.0086	1.0086	0.0087
	Line 3-18	0.0133	1.0133	0.0134
	Line 5-6	0.0026	1.0026	0.0026
2	Line 1-2	0.0411	1.0411	0.0410
	Line 2-25	0.0086	1.0086	0.0086
	Line 3-4	0.0213	1.0213	0.0211
	Line 4-5	0.0128	1.0128	0.0126

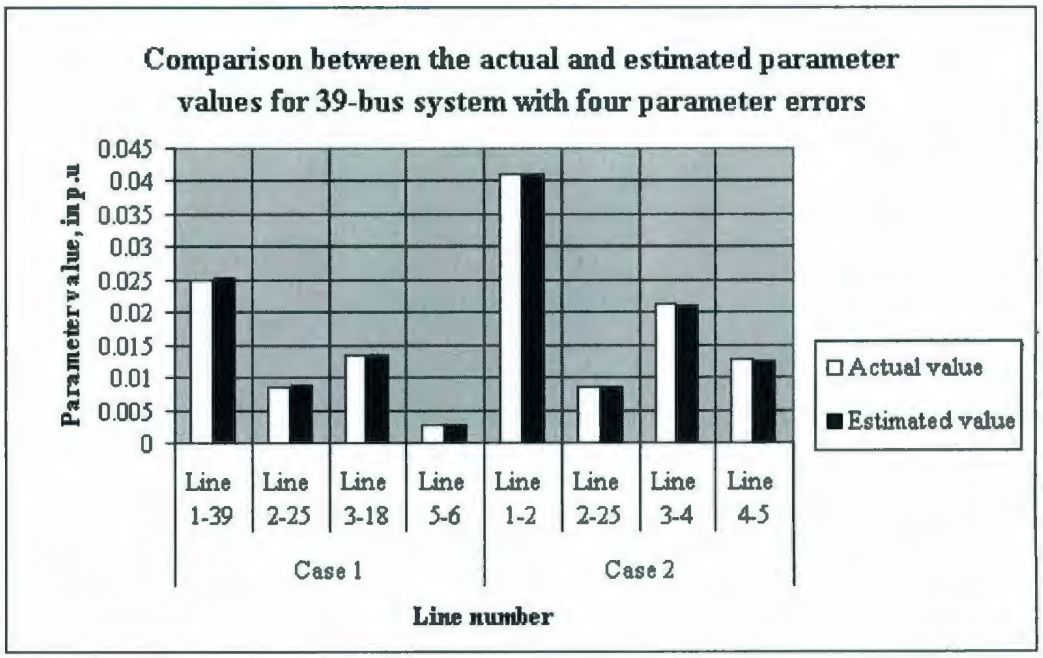

Figure 4.6: Comparison between actual and estimated parameter values for 39-bus system with four parameter errors

Thus network parameter estimation, which is another error detection property of the state estimation, is demonstrated using the residual sensitivity analysis. The estimated parameter values for all the case studies are found to be very close to the actual parameter values.

4.5 SUMMARY

The transmission line reactance parameter error estimation for 6-bus and 39-bus systems is formulated and implemented using the residual sensitivity analysis. The 6-bus is used for one and two parameter error estimation. The 39-bus system is used for one, two and four parameter error estimation. The estimation involves two steps: the error identification and estimation of the parameter. The identification of the parameter error is facilitated by the normalized residual technique. The suspicious measurement and its adjacent measurements are all included for the parameter error estimation, which is facilitated using the residual sensitivity analysis. A new parameter is designed with the estimated parameter error. The newly designed parameter value is included in the system model. The normalized values calculated, after updating the new parameter, are well below the threshold value. Parameter error estimation is an additional error detection feature of state estimation.

In the next chapter, some phasor measurements are assumed to be available with the conventional measurement data, in order to enhance the ability of the central state estimator to estimate the overall state of a very large power system.

CHAPTER 5

IMPLEMENTATION OF PHASOR MEASUREMENTS IN MULTI-AREA STATE ESTIMATION

5.1 INTRODUCTION

In Chapters 2-4, State Estimation and different aspects of SE were discussed using various case studies: bad data detection, identification, elimination and parameter estimation. In these chapters, the measurements considered to be available for SE were conventional measurements, such as power injection, line power flows and voltage magnitudes. In this chapter, a few synchronized phasor measurements are assumed to be available in addition to the conventional measurement data to enhance the performance of the state estimator for a very large power system. The phasor measurement, when present

in sufficient numbers with other measurements, improves the accuracy of SE [18-21] and the bad data detection at the area boundary buses, in a large power system with many control areas [22]. The 39-bus and IEEE 118-bus systems are used to demonstrate these aspects.

The next section is a general review of the synchronized Phasor Measurement Unit (PMU). The sections that follow it deal with the implementation of phasor measurement in SE, multi-area decomposition and formulation of two-level SE. In the final section, 39-bus and IEEE 118-bus systems case studies are used to illustrate the two-level SE.

5.2 SYNCHRONIZED PHASOR MEASUREMENT

Synchronized phasor measurement technology was developed near the end of the 1980s [23] and the first product appeared in the market in the early 1990s [24]. Reference [23] presents a historical review of the PMU development. Benefits of PMU applications in power systems, wide area monitoring protection and control are discussed in [24] and [25]. The impact of phasor technology on control centre advanced application is discussed in [26].

PMUs are the instruments that give the voltage and current measurements, time stamped with high precision [27]. These are equipment with Global Positioning Systems (GPS) receivers that allow the synchronization of several readings taken at distant points [28]. PMUs were developed from the invention of the symmetrical component distance relay (SCDR) [27]. Synchronization is made possible with GPS satellite system [29], which consists of 36 satellites, of which 24 are used at one time to produce time signals at the earth's surface. The GPS receivers resolve these signals into (x, y, t, z) coordinates, where t is time, by solving distance = rate* time [27]. Then the PMU time stamps the current and voltage reading with time obtained from the GPS receiver. The functional block diagram of PMU is displayed in Figure 5.1.

PMUs make it possible to measure the phase difference at different substations. The bus phase angles are one of the state variables that are estimated by the state estimator, and if PMUs are placed at the respective places, the phase angles can be directly measured. However, this is not always the case because it is very expensive to install PMUs and it is not feasible to install them in all parts of a power system.

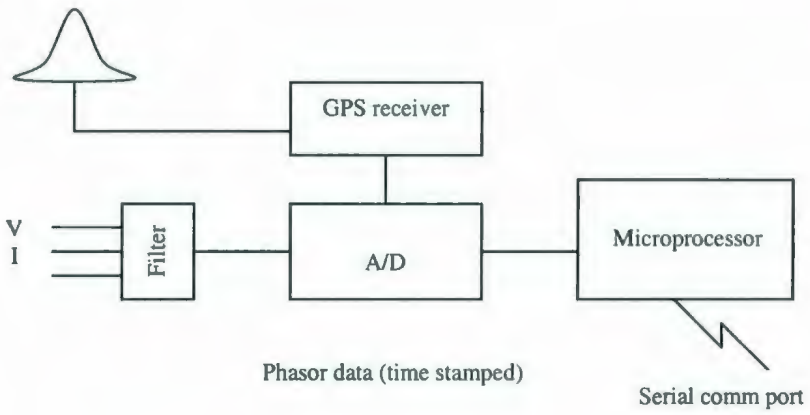

Figure 5.1: Phasor Measurement Unit [30]

5.3 PHASOR MEASUREMENTS IN STATE ESTIMATION

The inclusion of the phasor measurement changes the Jacobian matrix in the second level of the two-level SE which is demonstrated using the 6-bus system from chapter 2. Phasor measurements - 3.67 and -5.28 degrees were assumed to be available at buses 2 and 5 respectively. The standard deviation for the phasor measurements is 0.0001. The Jacobian function $H(s)=\left[\frac{\partial h(s)}{\partial s}\right]$ will be made to accommodate the phasor measurements. The phasor measurements are the bus phase angles. The new Jacobian matrix will be as in equation 5.1.

$$H(s)=\begin{bmatrix} \frac{\partial h(s)}{\partial \theta} & \frac{\partial h(s)}{\partial v} \\ \frac{\partial h(\theta)}{\partial \theta} & 0 \end{bmatrix} \tag{5.1}$$

where: $\frac{\partial h(s)}{\partial \theta}$ is the vector of the partial derivative of nonlinear functions, relating measurement to state variables, with respect to respective bus phase angles.

$\frac{\partial h(s)}{\partial v}$ is the vector of the partial derivative of nonlinear functions, relating measurement to state variables, with respect to respective bus voltage magnitudes.

$\frac{\partial h(\theta)}{\partial \theta}$ is the vector of the partial derivative of the phasor measurement with respect to the respective bus phase angles.

In chapter 2, section 2.5.4, for 62 measurement data, the dimension of the Jacobian matrix was 62X11. When two PMU measurements were added to the measurement data, its dimension changed to 64, as shown in Table 5.1. The dimension of the Jacobian matrix changed to 64X11 as in equation 5.2. A few expressions from the equation 5.2 are detailed below:

- $\frac{\partial h(PMU1)}{\partial v}=0$
- $\frac{\partial h(PMU1)}{\partial \theta_2}=1$

- $\frac{\partial h(Q_6)}{\partial \theta_2} = V_6 V_2 (-G_{62} \cos\theta_{62} - B_{62} \sin\theta_{62})$

- $\frac{\partial h(P_{12})}{\partial v_1} = V_1 V_2 (g_{12} \sin\theta_{12} - b_{12} \cos\theta_{12})$

where: V_1, V_2 & V_6 are the voltage magnitudes at buses 1, 2 & 6 respectively.

$\theta_{12} = \theta_1 - \theta_2$ difference between the bus phase angles at buses 1 & 2 respectively.

$\theta_{62} = \theta_6 - \theta_2$ difference between the bus phase angles at buses 6 & 2 respectively.

$G_{62} + jB_{62}$ are the 6th row and 2nd column element of the complex bus admittance matrix, and

$g_{12} + jb_{12}$ is the admittance of the series branch connecting buses 1 and 2.

SE was carried out with two PMU measurements. The estimated state variables and the line power flows for both SE and SE with PMU measurements are listed along with the actual value in Table 5.2 and 5.3 respectively. The estimated results were found to be close to the actual value.

Table 5.1: Measurements for the 6-bus system

Type of measurements	6-bus system	6-bus system with PMU measurements
Bus power injections	12	12
Line power flows	44	44
Bus voltage magnitudes	6	6
PMU measurement	0	2
Total measurements	62	64

$$H(s)=\begin{bmatrix}
\frac{\partial h(V_1)}{\partial \theta_2} & \cdots & \frac{\partial h(V_1)}{\partial \theta_6} & \frac{\partial h(V_1)}{\partial v_1} & \cdots & \frac{\partial h(V_1)}{\partial v_6} \\
\vdots & & \vdots & \vdots & & \vdots \\
\frac{\partial h(V_6)}{\partial \theta_2} & \cdots & \frac{\partial h(V_6)}{\partial \theta_6} & \frac{\partial h(V_6)}{\partial v_1} & \cdots & \frac{\partial h(V_6)}{\partial v_6} \\
\frac{\partial h(P_1)}{\partial \theta_2} & \cdots & \frac{\partial h(P_1)}{\partial \theta_6} & \frac{\partial h(P_1)}{\partial v_1} & \cdots & \frac{\partial h(P_1)}{\partial v_6} \\
\vdots & & \vdots & \vdots & & \vdots \\
\frac{\partial h(P_6)}{\partial \theta_2} & \cdots & \frac{\partial h(P_6)}{\partial \theta_6} & \frac{\partial h(P_6)}{\partial v_1} & \cdots & \frac{\partial h(P_6)}{\partial v_6} \\
\frac{\partial h(Q_1)}{\partial \theta_2} & \cdots & \frac{\partial h(Q_1)}{\partial \theta_6} & \frac{\partial h(Q_1)}{\partial v_1} & \cdots & \frac{\partial h(Q_1)}{\partial v_6} \\
\vdots & & \vdots & \vdots & & \vdots \\
\frac{\partial h(Q_6)}{\partial \theta_2} & \cdots & \frac{\partial h(Q_6)}{\partial \theta_6} & \frac{\partial h(Q_6)}{\partial v_1} & \cdots & \frac{\partial h(Q_6)}{\partial v_6} \\
\frac{\partial h(P_{ij})}{\partial \theta_2} & \cdots & \frac{\partial h(P_{ij})}{\partial \theta_6} & \frac{\partial h(P_{ij})}{\partial v_1} & \cdots & \frac{\partial h(P_{ij})}{\partial v_6} \\
\vdots & & \vdots & \vdots & & \vdots \\
\frac{\partial h(P_{ji})}{\partial \theta_2} & \cdots & \frac{\partial h(P_{ji})}{\partial \theta_6} & \frac{\partial h(P_{ji})}{\partial v_1} & \cdots & \frac{\partial h(P_{ji})}{\partial v_6} \\
\frac{\partial h(Q_{ij})}{\partial \theta_2} & \cdots & \frac{\partial h(Q_{ij})}{\partial \theta_6} & \frac{\partial h(Q_{ij})}{\partial v_1} & \cdots & \frac{\partial h(Q_{ij})}{\partial v_6} \\
\vdots & & \vdots & \vdots & & \vdots \\
\frac{\partial h(Q_{ji})}{\partial \theta_2} & \cdots & \frac{\partial h(Q_{ji})}{\partial \theta_6} & \frac{\partial h(Q_{ji})}{\partial v_1} & \cdots & \frac{\partial h(Q_{ji})}{\partial v_6} \\
\frac{\partial h(PMU_1)}{\partial \theta_2} & \cdots & \frac{\partial h(PMU_1)}{\partial \theta_6} & \frac{\partial h(PMU_1)}{\partial v_1} & \cdots & \frac{\partial h(PMU_1)}{\partial v_6} \\
\frac{\partial h(PMU_2)}{\partial \theta_2} & \cdots & \frac{\partial h(PMU_2)}{\partial \theta_6} & \frac{\partial h(PMU_2)}{\partial v_1} & \cdots & \frac{\partial h(PMU_2)}{\partial v_6}
\end{bmatrix} \tag{5.2}$$

Table 5.2: Estimated state variables for the 6-bus system

S. No	Actual value		Estimated state variables for 6-bus system		Estimated state variables for 6-bus system with PMU measurements	
	Voltage values at the buses (KV)*	Delta (δ) at the buses (degree)	Voltage values at the buses (KV)*	Delta (δ) at the buses (degree)	Voltage values at the buses (KV)*	Delta (δ) at the buses (degree)
1	241.5	0	240.5	0	241.0	0
2	241.5	-3.7	239.8	-3.8	240.2	-3.67
3	246.1	-4.3	244.6	-4.5	245.0	-4.24
4	227.6	-4.2	226.0	-4.3	226.4	-4.22
5	226.7	-5.3	225.2	-5.5	225.6	-5.28
6	231.0	-5.9	230.0	-6.1	230.3	-5.93

*(KV) Kilovolt

Table 5.3: Estimated line power flows for the 6-bus system

From Bus	To Bus	Actual value		6-bus system		6-bus system with PMU measurements	
		Real power flow, in (MW)*	Reactive power flow, in (MVAR)**	Estimated real power flow, in (MW)*	Estimated reactive power flow, in (MVAR)**	Estimated real Power flow, in (MW)*	Estimated reactive power flow, in (MVAR)**
1	2	28.86	-15.42	29.27	-15.21	29.22	-13.85
1	4	43.58	20.12	44.04	20.42	43.89	21.45
1	5	35.59	11.25	35.43	10.70	35.63	12.03
2	3	2.93	-12.27	3.12	-11.98	2.56	-12.49
2	4	33.10	46.06	32.89	45.95	32.94	45.04
2	5	15.51	15.35	14.89	14.63	15.30	14.92
2	6	26.25	12.40	26.91	13.15	25.44	11.12
3	5	19.12	23.17	18.08	22.21	19.20	22.91
3	6	43.78	60.73	44.44	61.69	43.39	58.50
4	5	4.08	-4.94	3.65	-5.34	3.93	-4.94
5	6	1.61	-9.00	2.65	-8.56	1.32	-10.04
2	1	-27.78	12.81	-28.34	12.65	-28.32	11.27

* Real power is measured in Megawatt (MW).

**Reactive power is measured in Megavar (MVAR)

5.4 MULTI-AREA DECOMPOSITION OF THE SYSTEM

Multi-area decomposition of a large power system is demonstrated in this section. Any large power system containing N buses is split into different areas and the buses that are assigned to any particular area basically fall into three categories: internal bus, boundary bus and external bus. Figure 5.2 illustrates the bus assignment for an area. In this figure, the bus assignment is given for Area 1, in which bus 1 is an internal bus (all of whose neighbors belong to Area 1), bus 2 is a boundary bus (whose neighbors are the Area 1 internal bus and at least one boundary bus from another area) and an external bus is bus 3 (which is the boundary bus of another area in connection with at least one boundary bus of Area 1).

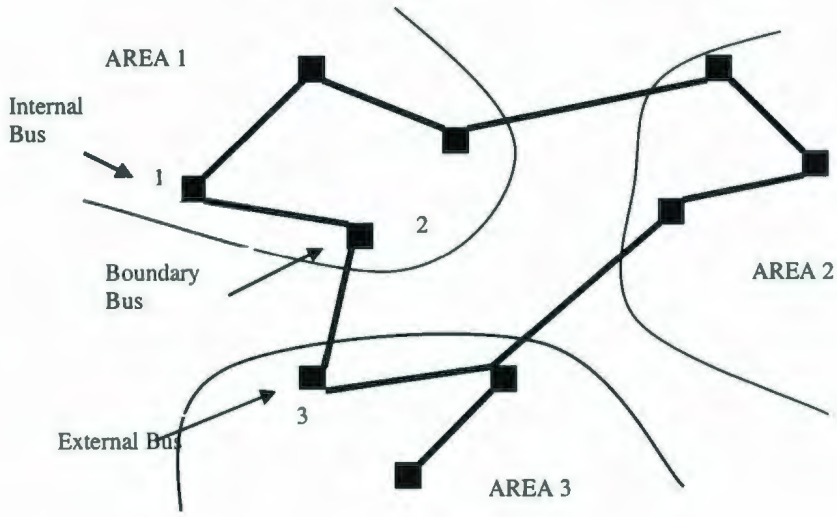

Figure 5.2: Bus assignment for areas [22]

The state variables associated with these buses can be defined for any area as in equation 5.3

$$x_i = \left[x_i^{b^T}, x_i^{\text{int}^T}, x_i^{ext^T} \right]^T \tag{5.3}$$

The vector x_i^b consists of the bus voltage magnitudes and phase angles at the boundary buses of area i; the vector x_i^{int} consists of the bus voltage magnitudes and phase angles of the internal buses of area i; the vector x_i^{ext} consists of the bus voltage magnitudes and phase angles of the external buses of area i.

5.5 FORMULATION OF TWO-LEVEL STATE ESTIMATION

In a very large power system, there are many control areas. Each control area has its own state estimator that processes the measurement received from its local substation, which is the first level SE. Generallly, the individual areas do not share their network data or estimated state variable data with their neighbors and they tend to operate independently. In order to schedule power transactions, which involve several control

areas, a system-wide state estimation solution is necessary [22]. The overall state of the system is a vital feature for load flow analysis, line power flow analysis and to distribute a reliable power supply between each area. The integrity of the overall system is also maintained with multi-area SE. This is accomplished by a Central State Estimator (CSE), which receives data from all the control areas and estimates the overall state of the power system (which is the second level SE). The method followed in Reference [22] is used in this chapter to illustrate the implementation of phasor measurement in multi-area state estimation.

The CSE receives only a few measurements from the individual areas to estimate the overall state of the system; hence, it requires a sufficient number of PMU measurements to enhance its performance. The CSE measurement data consist of the estimated state variables, boundary bus measurement, external bus measurements from all the areas and PMU measurements. Figure 5.3 shows the data and measurement exchange between the area and the CSE. Each area's state estimator will ensure that bad data are identified and corrected in that particular area. Bad measurement, which cannot be identified in first level of SE, is identified and eliminated in the CSE state estimation because the PMU provides the measurement redundancy around the boundary buses.

$$z_S = \left[z_u^{\,T}, z_{ps}^{\,T}, \hat{x}^{bT}, \hat{x}^{extT} \right]^T \tag{5.4}$$

Equation 5.4 represents the vector z_s, the measurement vector for the CSE. The vector z_u consists of the boundary measurement vector, which includes the line power flow and power injection at all boundary buses. The phasor measurement is represented as vector z_{ps}. The vectors $\hat{x}^b$ and $\hat{x}^{ext}$ consists of boundary and external state variables estimated by individual area SE respectively. The CSE has to minimize the $J_s = r_s^T R_s^{-1} r_s$ using the WLS technique explained in Chapter 2, where $z_s = h_s(x_s) + r_s$ and h_s is the measurement equation. The Jacobian matrix is modified to accommodate the phasor measurements as explained in the previous section.

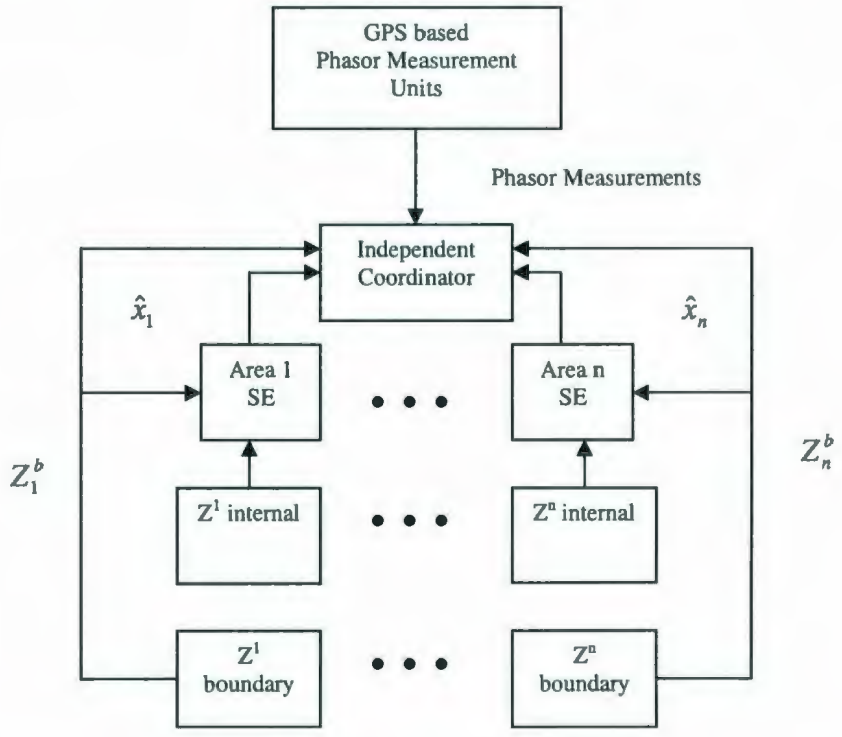

Figure 5.3: Data and measurement exchange [22]

5.6 CASE STUDIES

The case studies used to illustrate multi-area state estimation were the 39-bus (from Chapter 2) and the IEEE 118-bus system. Using these systems, two characteristics were studied; the first was the proficiency of PMU measurement in CSE and the second was its ability to detect the bad data in the boundary bus. Initially, the multi-area state estimation was carried out and then the bad data detection of boundary buses was performed. Each system was randomly divided into different areas and phasor measurements were assumed to be available for the CSE. The state estimation was carried out using the WLS technique (discussed in the previous chapters) for each area. The estimated state variables from all areas, along with boundary measurements and external measurements, were transmitted to the CSE. The CSE also used the WLS technique to calculate the overall state of the system. The overall estimated state variables and line power flows (estimated with two-level SE) were compared with the state variable estimated with Integrated SE (as in Chapter 2) and actual value from the Power World Simulator.

5.6.1 39-Bus System

The 39-bus system was divided into two areas (Area 1 and Area 2), as shown in Figure 5.4. The areas (Area 1 and Area 2) had three boundary and external buses. Table

C.1 in Appendix C presents the bus distribution for each area of this system. Various measurements such as real and reactive power injections, real and reactive line power flows, and voltage magnitudes (internal, boundary and external buses) were available to the corresponding areas as in Table C.2. There were four phasor measurements assumed to be available at bus 1, bus7, bus17 and bus 26 as indicated in Table C.3. The reference buses for the area were bus 31 and bus 33 respectively. The state estimation was carried out for both areas.

The measurements in equation 5.4 were available to the CSE, which also includes the five phasor measurements and estimated state variables from both areas. The standard deviation for the phasor measurements is 0.0001 and the slack bus of Area 1 was chosen as the slack bus for this estimation.

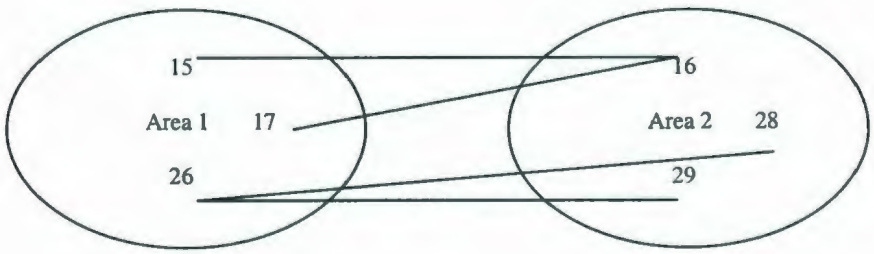

Figure 5.4: Control areas of 39-bus system

To determine the efficiency of the PMU measurements in the CSE, a few line power flows and voltage magnitudes were compared with actual values, as in Figures 5.5

-5.7. Different shades were used in the bar chart to represent each case (blank for actual value, dark for integrated SE data and slightly shaded for two-level SE data). The estimated values with PMU measurements were found to be very close to the actual value. The $J(x)$ objective function was also calculated for both integrated SE and two-level SE. They were found to agree with each other, which is shown in Table C.4 in the Appendix C.

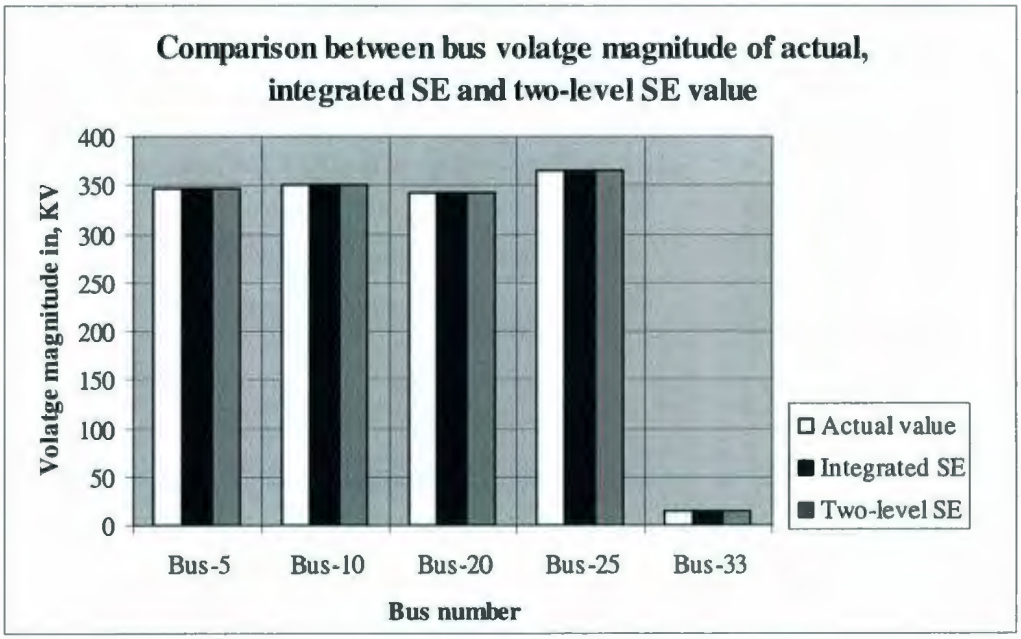

Figure 5.5: Comparison between the voltage magnitudes of actual, integrated SE & two-level SE value for the 39-bus system

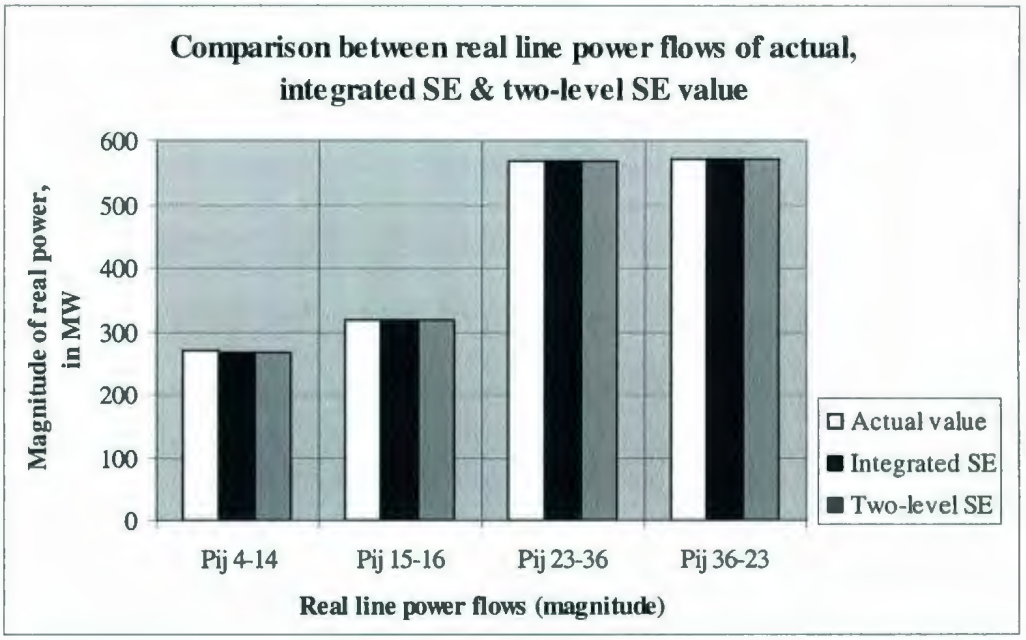

Figure 5.6: Comparison between the real line power flow of actual, integrated SE & two-level SE value for the 39-bus system

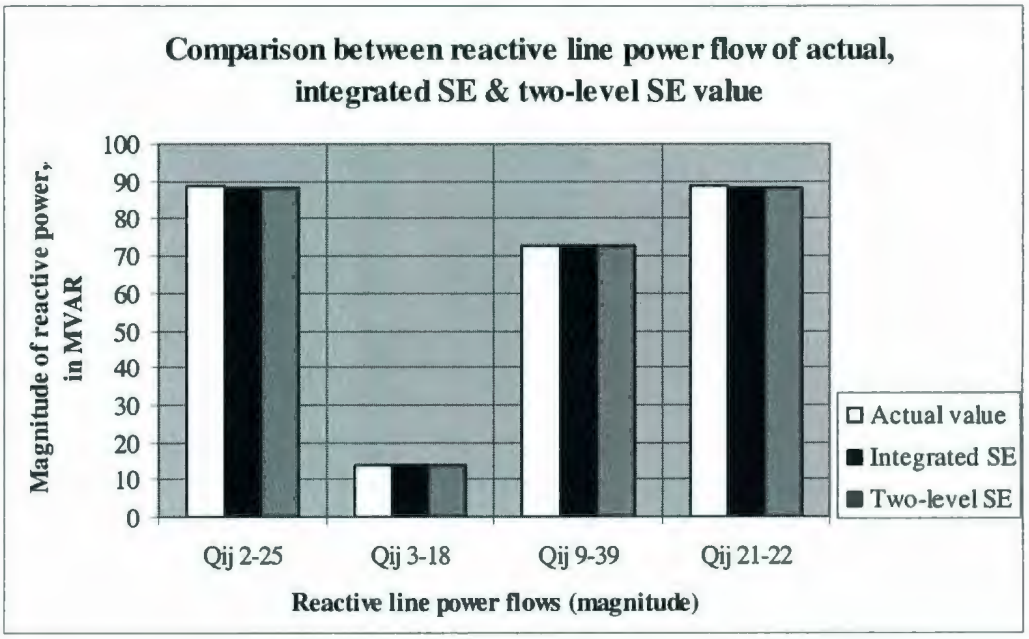

Figure 5.7: Comparison between the reactive line power flow of actual, integrated SE & two-level SE value for the 39-bus system

5.6.1.1 Bad Data Detection and Elimination

The CSE's ability to detect and identify single bad data even with low redundancy is verified in this section. The bad data that exist on the boundary bus, which becomes a critical measurement due to decomposition, is mostly not detected by the area state estimator when the measurement redundancy is low around the boundary bus [22]. The real power injection at bus 39 was changed from -1.518 p.u to 3.482 p.u in Area 1. State estimation was performed in that area and checked for bad data with the chi-squared test (Chapter 3) with 95% confidence interval and 135 degrees of freedom. The calculated value $J(\hat{x})$ was 148.2471, which was well below the chi-squared value 163.1161, as illustrated in Table 5.4, and the area state estimator failed to detect the bad data. The estimated state variables from all the areas were transmitted to the CSE, where the bad data detection test was carried out after the overall estimation of the state variables. The value of $J(\hat{x})$ was 260.9812, which was higher than the χ^2 value 244.8076. The normalized test was performed to detect the bad data and the value of the measurements associated with bus 39 was found to be close to or higher than 4 (chosen threshold value) as shown in Table 5.5. Hence the real power injection at bus 39 was eliminated and state estimation was performed again to check for more bad data. No more bad data were detected. Thus, the CSE in the presence of phasor measurement was able to detect the bad data when the measurement redundancy was low.

Table 5.4: $J(\hat{x})$ value calculated for Area 1 of the 39-bus system

Measurement Number i =1.....190	$J(\hat{x})$ value
5	0
12	0
15	1.333
30	71.0447
36	0
	$J(\hat{x})$=148.2471

Table 5.5: Normalized residual values calculated for the CSE of the 39-bus system

Type of measurement	Measurements i=1.....287	r_i^N Normalized Residuals
P- 39	27	**3.7106**
Q -7	30	0.9752
Q -39	54	**15.8243**
P_{ij} 3-18	60	0.0195
P_{ij} 9-39	69	**3.3207**
P_{ij} 17-18	79	0.01303
Pij 39-9	161	**3.4152**
P_{ij} 31-6	183	0.1496
Q_{ij} 39-1	194	**12.3507**

5.6.2 IEEE 118-Bus System

The main characteristics of the IEEE 118-bus system [31], as shown in Figure 5.8, are listed in Table C.5. The voltage level for the generating station buses and the transmission line buses are 13.8KV and 345KV respectively. This system was divided into nine control areas, as in [32], and the schematic is given in Figure 5.9. The bus distribution among the control areas is given briefly in Table C.6. These tables list the internal, boundary, external and slack buses for the respective areas. Various

measurements such as power injections (real and reactive), line power flows (real and reactive), and voltage magnitudes (internal, boundary and external buses) are available to the corresponding areas, as shown in Table C.7.

The state estimation was carried out at two different levels. In the first level, SE was carried out in the individual control areas, and in the second level the over all system states were estimated by CSE, which received the data from the first level of the SE. The CSE had access to boundary measurements, a few PMU measurements, and estimated state variables (boundary and external bus) of each area. The boundary measurement vectors included real and reactive bus power injections and real and reactive line power flows. Nine phasor measurements were assumed to be available, as shown in Table C.8. The PMU measurements enhance the performance of the CSE where the number of measurements was lower than in the integrated SE.

This system was solved considering three different loading conditions, i.e. 100%, 75% and 50%. The bad measurement was detected and eliminated in the respective control areas during the first-level SE. To compare the performance of CSE, the IEEE-118 bus system was also solved with the integrated state estimation or normal state estimation procedure, as discussed in Chapter 2. The $J(x)$ objective function was also calculated for both and they were found to agree with each other, which is shown in Table C.9.

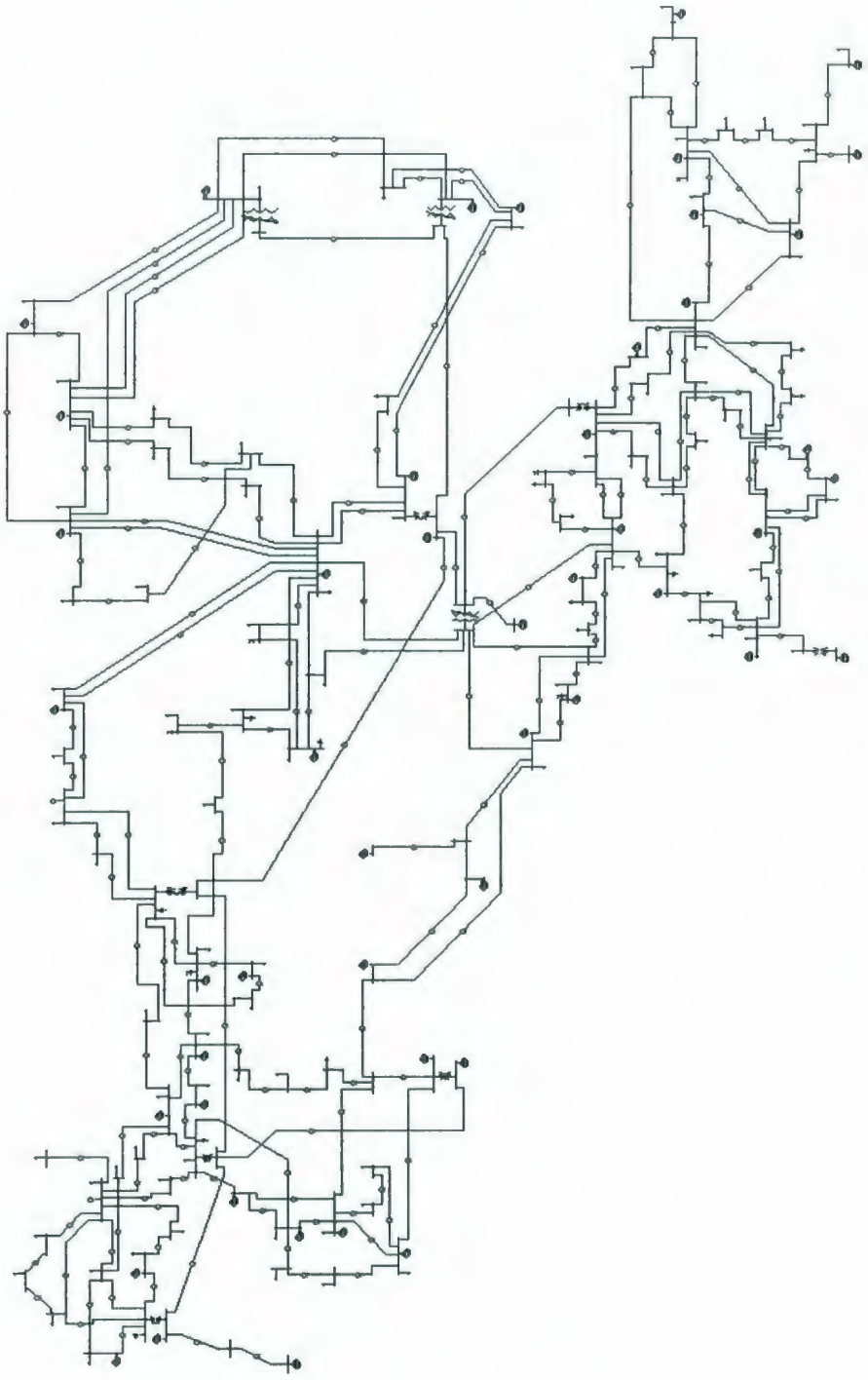

Figure 5.8: IEEE 118-bus system [31]

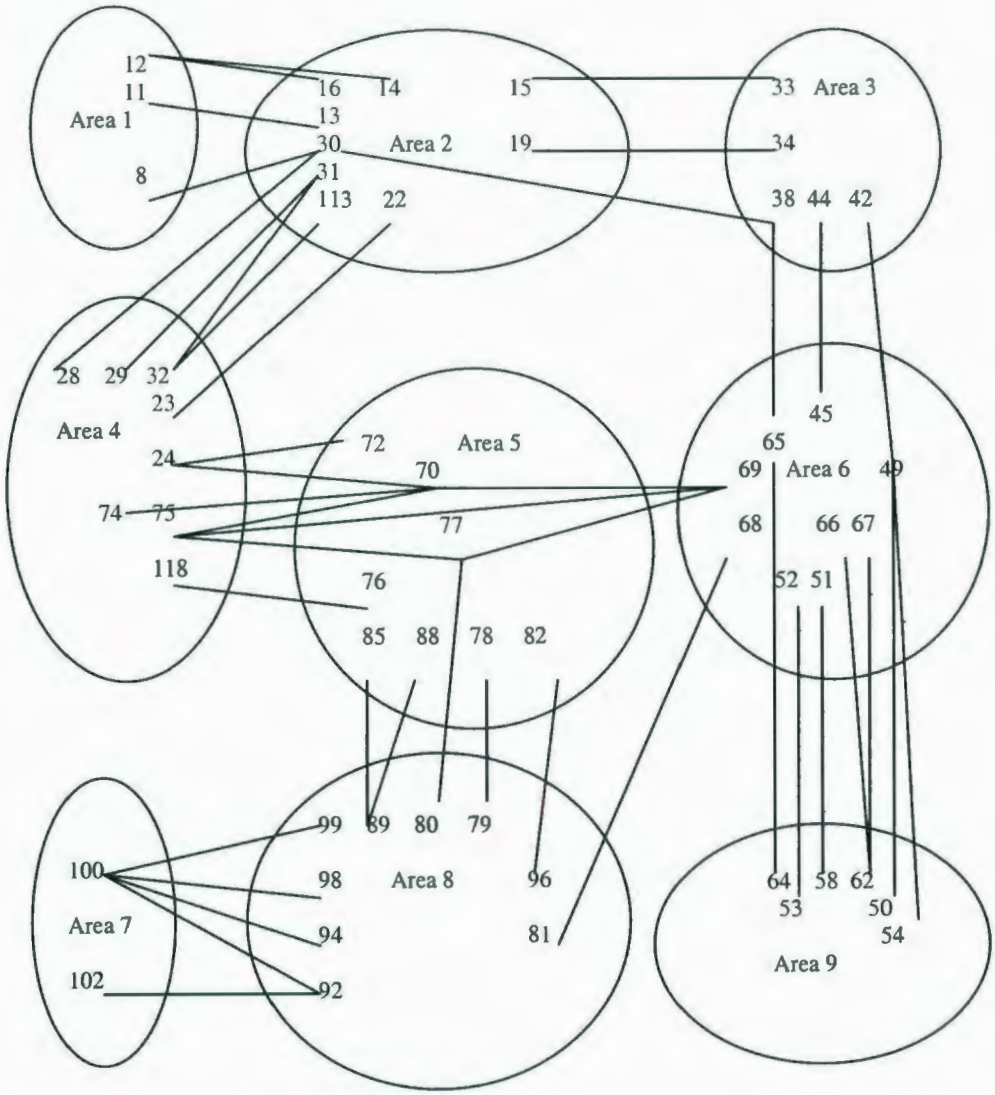

Figure 5.9: Control areas of the IEEE 118-bus system [32]

To assess the performance of the two-level SE, a base case or a reference case of the system was required. Hence, the system was solved using the Power World Simulator [7] with different loading conditions and the power flow list from the simulator was assumed to be the actual or true power flow values of this system. The estimated line

power flow values of integrated SE and two-level SE (Multi-area SE) were compared against the actual values using a bar chart. Different shades were used in the bar chart to represent each case (blank for actual value, dark for integrated SE data and slightly shaded for two-level SE data).

The comparison between actual values and a few estimated line power flows and voltage magnitudes is given in Figure 5.10 through Figure 5.18. In all the loading conditions, the estimated line power flows of the multi-area SE were found to be very close to the actual value in most cases, which proves that, even with a smaller number of measurements, the CSE was able to perform well with the presence of the synchronized PMU measurements. In summarizing the results of the estimated values, it can be concluded that they lie close to the actual case values and differ only by a slight degree in both cases.

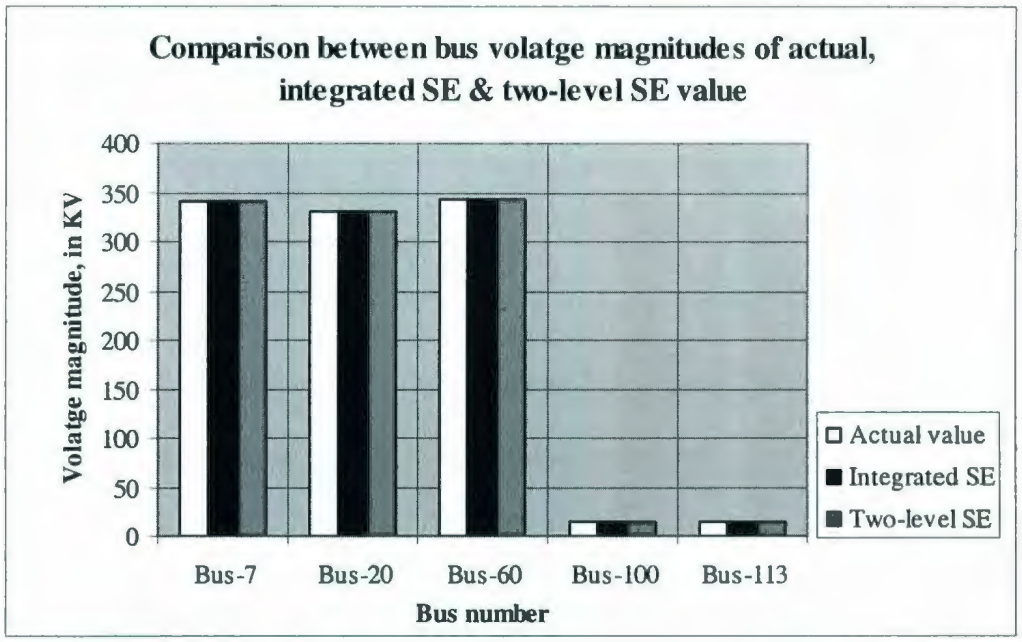

Figure 5.10: Comparison between the voltage magnitude of actual, integrated SE & two-level SE value for 100% loading condition of the 118-bus system

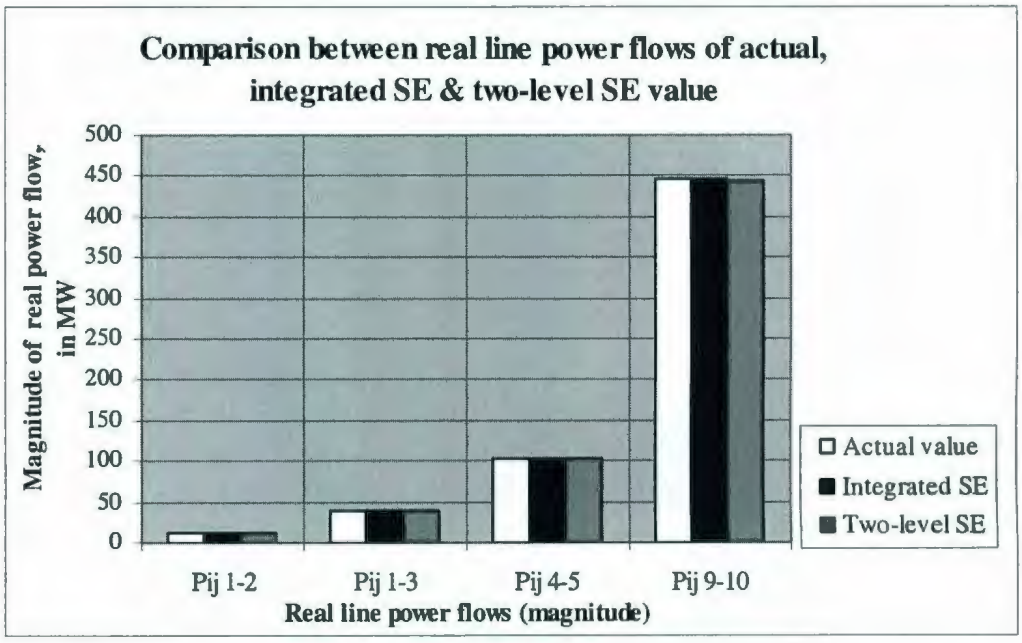

Figure 5.11: Comparison between the real line power flow of actual, integrated SE & two-level SE value for 100% loading condition of the 118-bus system

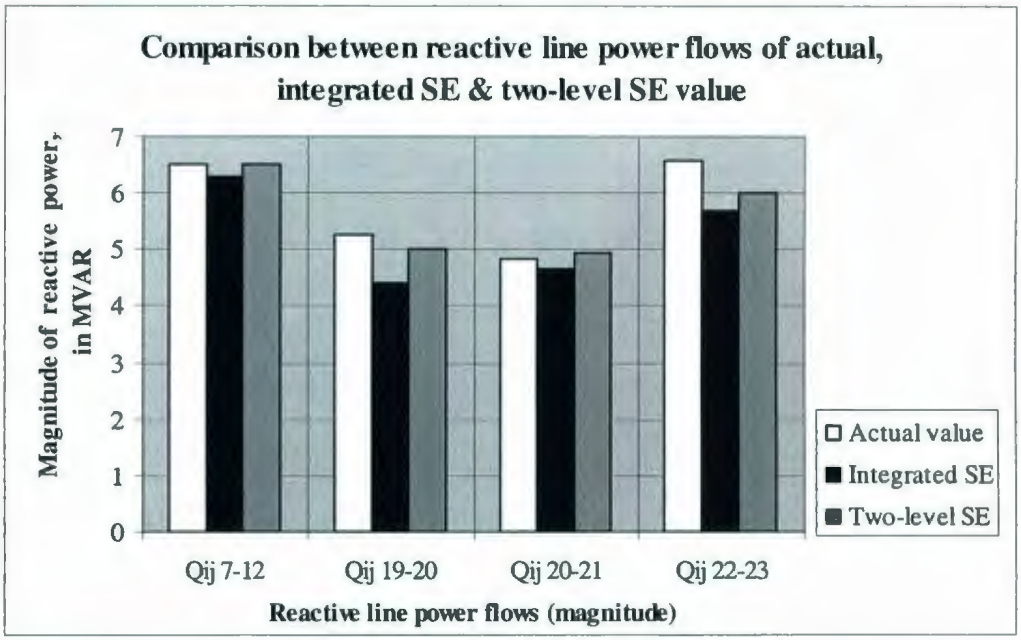

Figure 5.12: Comparison between the reactive line power flow of actual, integrated SE & two-level SE value for 100% loading condition of the 118-bus system

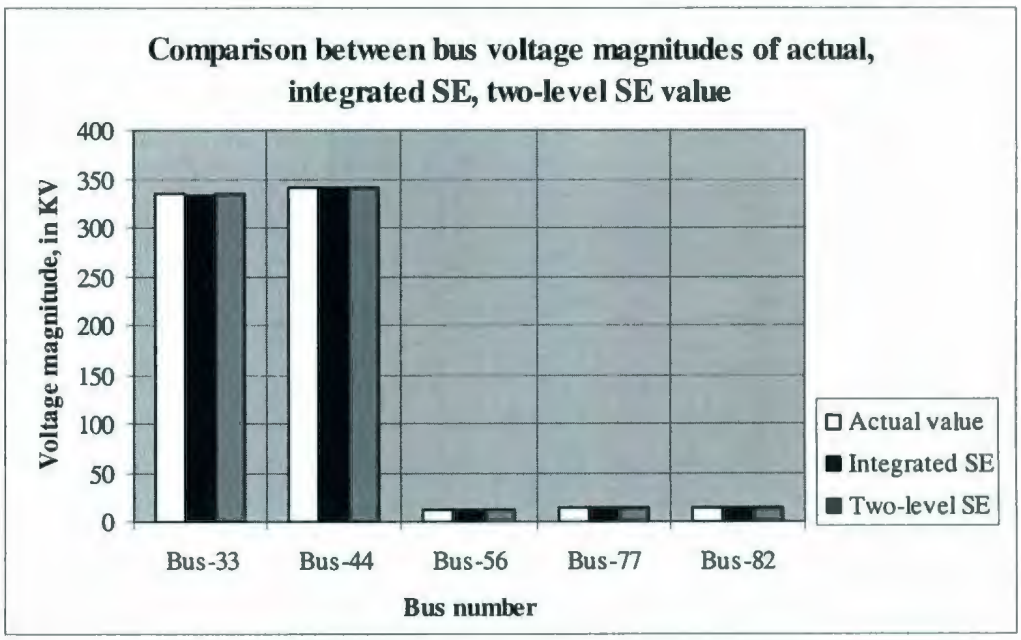

Figure 5.13: Comparison between the voltage magnitude of actual, integrated SE & two-level SE value for 75% loading condition of the 118-bus system

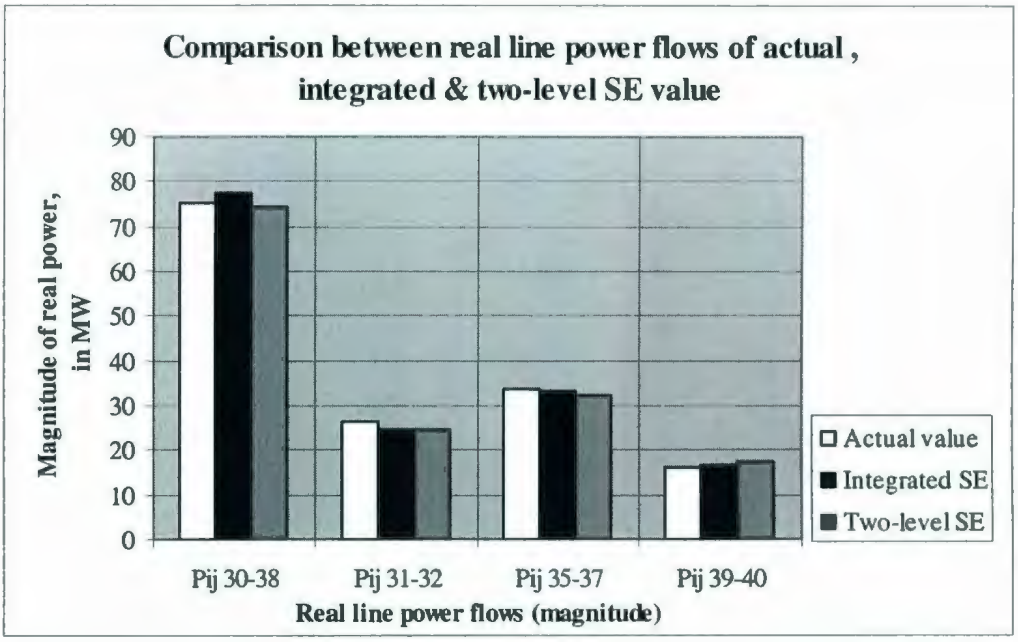

Figure 5.14: Comparison between the real line power flow of actual, integrated SE & two-level SE value for 75% loading condition of the 118-bus system

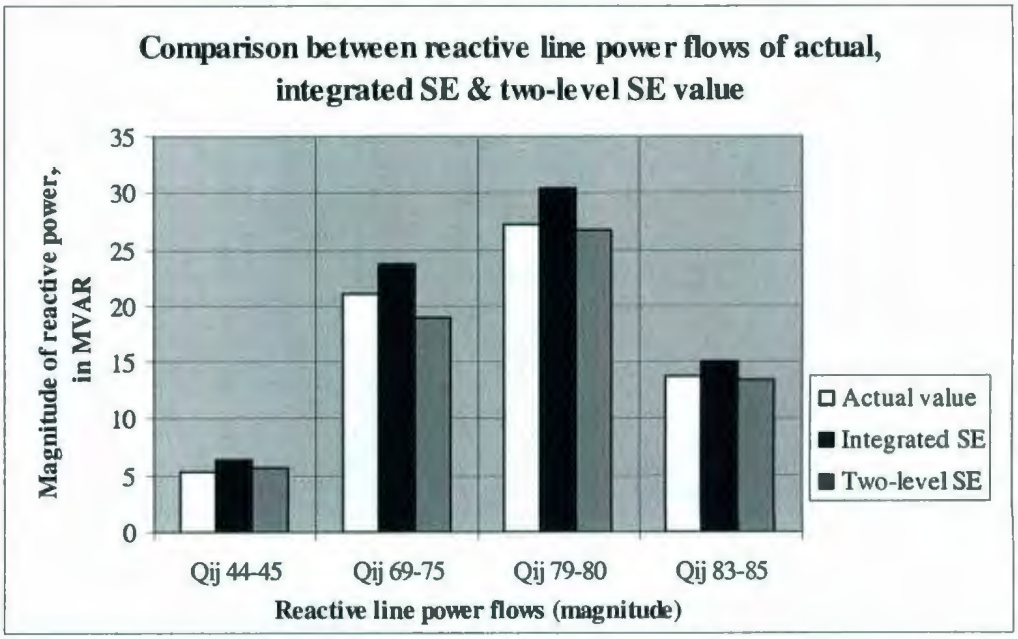

Figure 5.15: Comparison between the reactive line power flow of actual, integrated SE & two-level SE value for 75% loading condition of the 118-bus system

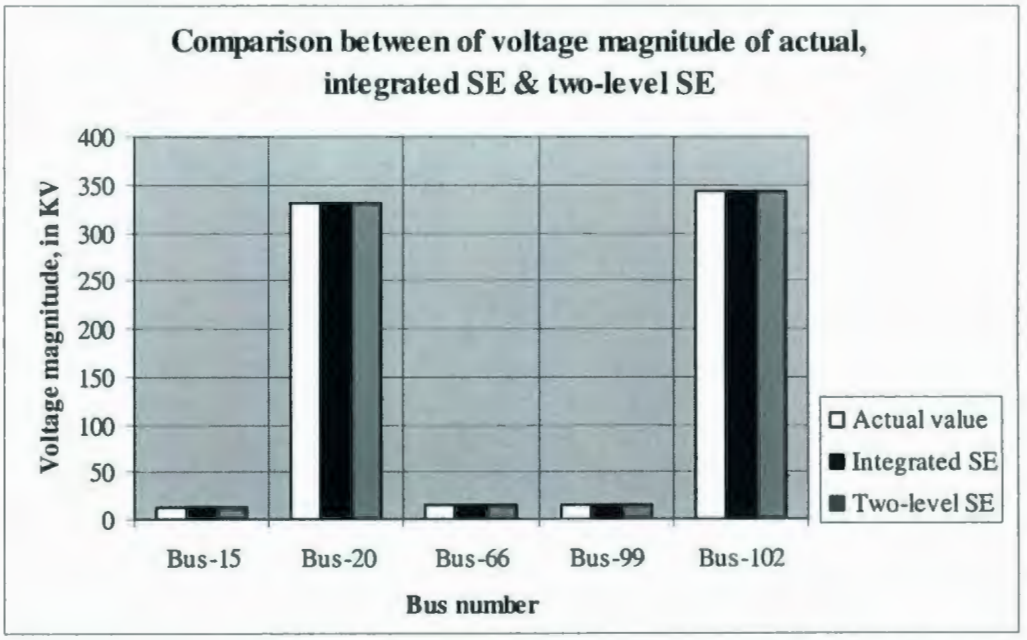

Figure 5.16: Comparison between the voltage magnitude of actual, integrated SE & two-level SE value for 50% loading condition of the 118-bus system

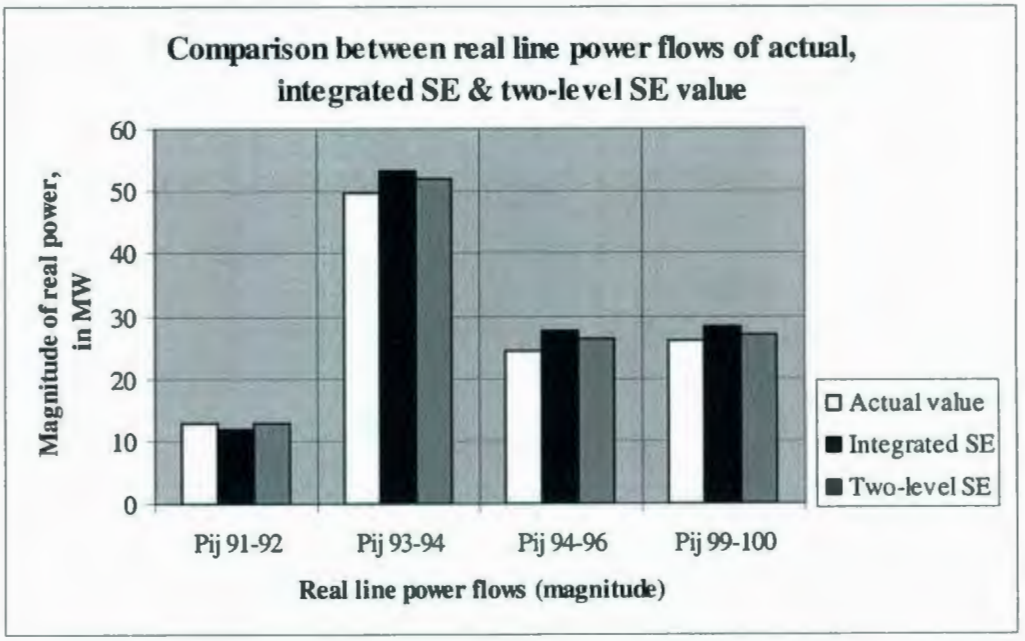

Figure 5.17: Comparison between the real line power flow of actual, integrated SE & two-level SE value for 50% loading condition of the 118-bus system

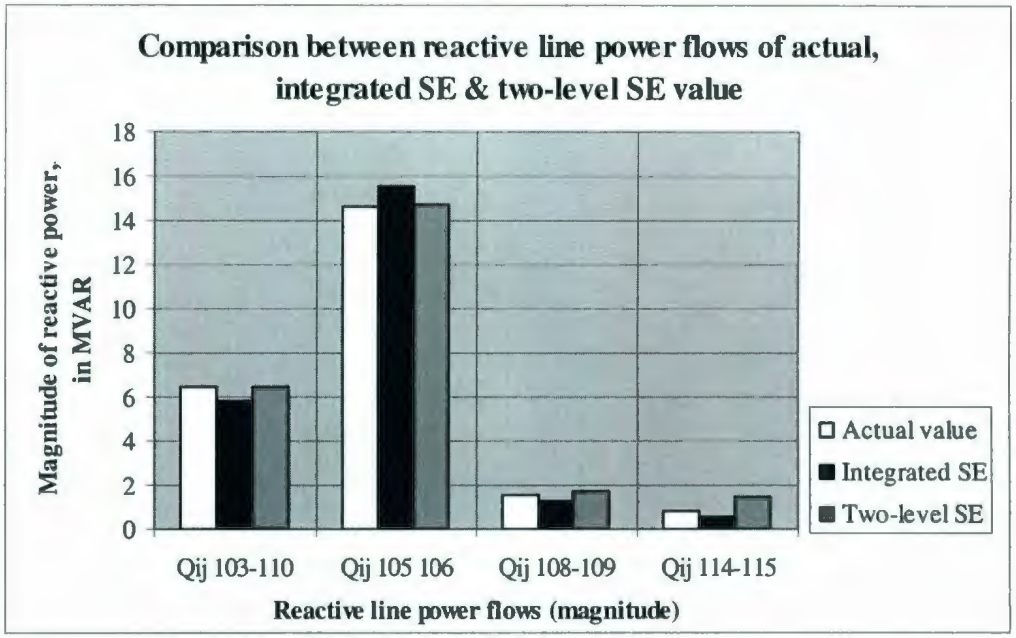

Figure 5.18: Comparison between the reactive line power flow of actual, integrated SE & two-level SE value for 50% loading condition of the 118-bus system

5.6.2.1 Bad Data Detection and Elimination

To study the bad data detection ability of the CSE, the real power injection at bus 68 was changed from 0 p.u to 2 p.u in Area 6. SE was performed in that area and checked for bad data with the chi-squared test (Chapter 3) with 95% confidence interval and (154-53) 101 degree of freedom. The calculated value $J(\hat{x})$ was 109.0314, which was well below the Chi-squared value 125.4584, as illustrated in Table 5.6, and the area state estimator failed to detect the bad data. The estimated state variables from all the areas were transmitted to the CSE, where the bad data detection test was carried out after the overall estimation of the state variables. The value of $J(\hat{x})$ was 491.3992, which was

higher than the χ^2 value 445.5159. The normalized test was performed to detect the bad data and the value of the measurements associated with bus 68 was found to be higher than 4 (chosen threshold value), as shown in Table 5.7. Hence, the real power injection at bus 68 was eliminated and state estimation was performed again to check for more bad data. No more bad data were detected. Thus, the CSE in the presence of phasor measurement was able to detect the bad data when the measurement redundancy was low.

Table 5.6: $J(\hat{x})$ value calculated for Area 6 of the 118-bus system

Measurement Number i=1.....154	$J(\hat{x})$ value
1	0.0158
12	00032
15	3.8667
30	0.0026
36	0.0007
	$J(\hat{x})$=109.0314

Table 5.7: Normalized residual values calculated for the CSE of the 118-bus system

Type of measurement	Measurements i=1.....633	r_i^N Normalized Residuals
P- 68	35	**18.4979**
P_{ij} 3-12	241	0.0035
P_{ij} 32-114	290	0.045
P_{ij} 68-116	357	**19.33**
Q_{ij} 68-116	551	**6.58**

5.7 SUMMARY

State estimation for a very large system was investigated with 39 and 118-bus systems. Initially, the systems were separated into smaller areas with internal, boundary and external buses. Each separate area had its own state estimator to estimate its states, detect and eliminate bad data. Phasor measurements were assumed to be available for the CSE. The estimated state variables and phasor measurements were transmitted to the CSE, which determined the overall state of the power system. The results of the CSE were found to be very close to the actual value. The CSE also detected the bad data that existed in measurements, which became a critical measurement due to decomposition, when the measurement redundancy was low. This was verified by introducing a bad measurement to the measurement data which was detected and eliminated by the CSE with the aid of phasor measurements. The phasor measurement improved the efficiency of the CSE by aiding in the overall estimation of the state variables of the system even when the measurement redundancy was low.

CHAPTER 6

CONCLUSIONS AND FUTURE WORK

6.1 CONCLUSIONS

The main focus of any power utility is the reliable and secure operation of its power system, so it can deliver an uninterrupted power supply to its customers. A reliable estimate of any power system is essential for its smooth operation. The technique that estimates the state of any power system is state estimation. Estimated state variables are then used in estimating the line power flows, which are then used in system control centers in the implementation of the security-constrained dispatch and control of the power system.

The works presented in this thesis are state estimation implemented with the WLS technique, the bad data processing technique, network parameter estimation and phasor measurements implementation to the conventional measurement data. Various power system models, such as 6-bus, 39-bus and 118-bus systems were used in this thesis. The 6-bus and 39-bus systems were used to implement state estimation with the WLS technique. Two measurement data for each system were utilized and the results were compared with the actual value (from the Power World Simulator). The estimated state variables, power injections and line power flows lie very close to the actual value. This shows that even with smaller measurement data, the state estimation is able to perform well and provide a reliable estimate of state variables.

In the bad data processing technique, the 6-bus and 39-bus systems were utilized. First, a few bad data were introduced into the measurement data of the system and a chi-squared test was used to detect bad data and then, the normalized residual technique was used to identify the detected bad data. The detected bad data was eliminated and state estimation was performed. The chi-squared method revealed no bad data when tested again for the systems. A few real power injections for the 6-bus system and real line power flows for the 39-bus system, estimated with bad data and after elimination, were compared with actual values using the bar charts. The results estimated after elimination lie very close to the actual value and this proves that the bad data processing techniques can efficiently detect, identify and eliminate bad data.

Network parameter estimation was also studied using the 6-bus and 39-bus systems. One, two and four errors were introduced to the line reactances of the systems. The parameter estimation of the true estimate involved two steps: the error identification and the estimation of the parameter. The identification of the parameter error was facilitated by the normalized residual technique and parameter error estimation was facilitated by residual sensitivity analysis. The estimated parameter was updated into the system and state estimation was performed and checked for the bad parameter. No parameter error was detected after the update. The estimated parameters were compared to the actual value in bar charts with different shades. The estimated values lie very close to the actual value and this shows that the normalized residual technique provides the best estimate of the network parameter.

In the final part of the thesis, phasor measurements were implemented to the conventional measurement data. State estimation for a very large system was investigated with 39-bus and 118-bus systems. A two-level state estimation method was devised for a large power system. The first-level state estimation was implemented with individual areas of the power system and, in the second level, the over-all state of the system was estimated by the CSE with phasor measurements. The systems were also solved with integrated state estimation to compare it with the performance of the two-level state estimation. The estimated state variables and line power flows for both cases were compared to the actual value and the results of the two-level estimation lie very close to the actual value. Undetected bad data, which became critical due to decomposition in the

first-level state estimation, was also identified by the CSE. This also demonstrated that the phasor measurements, when present in sufficient numbers, enhanced the performance of the state estimation.

6.2 FUTURE WORK

This section summarizes some investigations and research that may be performed as an extension to the work presented in this thesis.

- Except for the second level of the two-level state estimation in the previous chapter, the measurement data were conventional data, such as real and reactive bus injections, line power flows and voltage magnitudes. The current measurement may be included in the measurement data.

- For network parameter estimation, only line reactance was focused on. Transmission line resistance, line charging capacitance and transformer tap values may also be estimated for network parameter estimation.

- Parameter estimation based on state vector augmentation may also be implemented for network parameter estimation. In state vector augmentation the suspected parameter is included in the state vector and simultaneously estimated with the state variables.

- In this thesis the power system models used were 6-bus, 39-bus and 118-bus systems. A more complex and larger system with more areas can be used for multi-area state estimation.

- Topology errors, such as branch status errors and substation configuration errors [5], can also be studied and implemented for various power system models. This information is significant, since the breaker/switches status in any substation can cause the network topology to change. The estimated state variables and power values with flawed network topology will also be in error.

REFERENCE

[1] E. Iwata, *"Report faults Ohio utility"*, *USA Today*, pp. 1A, November 20, 2003.

[2] A. J. Wood, B. F. Wollenberg, *"Power generation operation and control"*, John Wiley & Sons, Inc., Singapore, 1984.

[3] F. Schweppe, J. Wildes, D. Rom, *"Power system static state estimation: parts II, III, and I"*, Power Industry Computer Conference, June 1969.

[4] J. J. Grainger, W. D. Stevenson Jr, *"Power system analysis"*, McGraw Hill, Inc., Toronto, 1994.

[5] A. Abur, A. G. Expósito, *"Power system state estimation theory and implementation"*, Marcel Dekker, Inc., 2004.

[6] Matlab version 7.0, Math Works Inc., USA, 2005.

[7] Power World Simulator, Version 11.0, Power World Corporation, Urbana, IL, USA, 1996-2005.

[8] M. A. Pai, *"Energy function analysis for power system stability"*, Kluwer Academic Publishers, 1989.

[9] G. L. Kusic, *"Computer-aided power systems analysis"*, Prentice-Hall, Englewood Cliffs, New Jersey 07632, 1986.

[10] Chi-squared illustrated at http://en.wikipedia.org/wiki/Pearson's_chi-square_test, June 2007

[11] A. Monticelli, *"State estimation in electric power systems: A generalized approach"*, Kluwer Academic Publishers, 1999.

[12] J. Zhu, A. Abur, *"Identification of network parameter errors"*, IEEE Trans. Power systems, Vol. 21, No. 2, May 2006, pp. 586-592.

[13] W. -H. E. Liu, F. F. Wu, S. -M. Lun, *"Estimation of parameter errors from measurement residuals in state estimation"*, IEEE Trans. Power system, Vol. 7, No. 1, February 1992, pp. 81-89.

[14] W. -H. E. Liu, S. -L. Lim, *"Parameter error identification and estimation in power system state estimation"*, IEEE Trans. Power system, Vol. 10, No. 1, February 1995, pp. 200-209.

[15] P. Z. Periñán, A. G. Expósito, *"Off-line determination of network parameter in state estimation"*, 12th Power System Computation Conference, Dresden, August 19-23, 1996, pp. 1207-1213.

[16] P. Z. Periñán, A. G. Expósito, *"Power system parameter estimation: A survey"*, IEEE Trans. Power system, Vol. 15, No. 1, February 2000, pp. 216-222.

[17] T. V. Cutsem, V. H. Quintana, *"Network parameter estimation using online data with application to transformer tap position"*, IEE Proceeding, Vol. 135, Pt. C, No. 1, January 1988, pp. 31-40.

[18] M. Zhou, V. A. Centeno, J. S. Thorp, A. G. Phadke, *"An alternate for including phasor measurements in state estimation"*, IEEE Trans. Power systems, Vol. 21, November 2006, pp. 1930-1937.

[19] J. S. Throp, A. G. Phadke, K. J. Karimi, *"Real time voltage-phasor measurement for static state estimation"*, IEEE Trans. Power apparatus and syst., Vol. PAS-104, No. 11, November 1985, pp. 3098-3106.

[20] A. G. Phadke, J. S. Throp, K. J. Karimi, *"State estimation with phasor measurements"*, IEEE Trans. Power systems, Vol. 1, No. 1, February 1986, pp. 233-241.

[21] R. Zivanovic, C. Cairns, *"Implementation of PMU technology in state estimation: An overview"*, in Proc. IEEE 4th AFRICON, September 24-27, 1996, Vol. 2, pp. 1006-1011.

[22] L. Zhao, A. Abur, *"Multiarea state estimation using synchronized phasor measurements"*, IEEE Trans. Power systems, Vol. 20, No. 2, May 2005, pp. 611-617.

[23] A. G. Phadke, *"Synchronized phasor measurements: A historical overview"*, in Proc. IEEE Power Eng. Soc. Asia Pacific Transmission Distribution Conf. Exhib., Oct 6-10, 2002, Vol. 1, pp. 476-479

[24] D. Novosel, V. Madani, B. Bhargava, K. Vu, J. Cole, *"Dawn of the grid synchronization"*, IEEE Power & Energy magazine, January/February 2008, pp. 49-60

[25] A. G. Phadke, J. S. Thorp, *"History and application of phasor measurement"*, IEEE conf. Proceeding, Power syst conf. and exposition, Atlanta, GA , October 29 – November 1, 2006, pp. 331-335.

[26] D. Atanackovic, H. Clapauch, G. Dwernychuk, J. Gurney, *"First steps to wide area control"*, IEEE Power & Energy magazine, January/February 2008, pp. 61-68.

[27] M. Rice, G. T. Heydt, *"Phasor measurement unit data in power system state estimation: intermediate project report for the PSERC project, "Enhanced state estimator"*, Power Systems Engineering Research Center, Univ. of Wisconsin, January 2005.

[28] K. Chow, J. Shin, S. Hyun, *"Optimal placement of phasor measurement units with GPS receiver"*, Proc. IEEE Power Engineering Society Winter Meeting, Vol. 1, January 2001, pp. 258-262.

[29] W. Lewandowski, J. Asoubib, W. J. Klepczynski, *"GPS: Primary tool for time transfer"*, Proceedings of the IEEE, Vol. 87, No. 1. January 1999, pp. 163-172.

[30] A. G. Phadke, *"Synchronized phasor measurement"*, IEEE Computer Application in Power, April 1993, pp. 11-15.

[31] IEEE 118-bus system, available at http://powerworld.com/cases.asp, December 2007.

[32] A. Abur, M. K. Celik, *"Multi-area linear programming state estimator using Dantzig-Wolfe decomposition"*, in Proc. Tenth power syst. Computer conf., Graz, Austria, August 19-24, 1990, pp. 1038-1044.

APPENDIX A

DATA FOR THE 6-BUS SYSTEM AND STATE ESTIMATION RESULTS

Appendix A contains the data for the 6-bus system discussed in the thesis and the state estimation results for the system. The main characteristics of the system are given in Table A.1. Table A.2 gives the transmission line characteristics for the system. The estimated state variable for 18 and 62 measurement data are tabulated with the actual value in Table A.3. In the Table A.4 the actual value of bus power injection and estimated bus power injection for both 18 and 62 measurement data are tabulated. Table A.5 gives the actual value of line power flows, tabulated together with the estimated line power flows for both 18 and 62 measurement data.

Table A.1: Main characteristic of the 6-bus system

Number of buses	6
Number of Lines	11
Number of generators	3

Table A.2: Line characteristics of the 6-bus system [2]

From Bus	To Bus	Resistance (pu)*	Reactance (pu)*	Line Charging (pu)*
1	2	0.1000	0.2000	0.0400
1	4	0.0500	0.2000	0.0400
1	5	0.0800	0.3000	0.0600
2	3	0.0500	0.2500	0.0600
2	4	0.0500	0.1000	0.0200
2	5	0.1000	0.3000	0.0400
2	6	0.0700	0.2000	0.0500
3	5	0.1200	0.2600	0.0500
3	6	0.0200	0.1000	0.0200
4	5	0.2000	0.4000	0.0800
5	6	0.1000	0.3000	0.0600

*per unit (pu) values are based on 100 MVA and 230 KV base

Table A.3: Actual and estimated state variables for the 18 and 62 measurement data

The Actual Value		The result for 18-data		The result for 62-data	
Voltage values at the buses (KV)*	Delta (δ) at the buses (degree)	Voltage values at the buses (KV)*	Delta (δ) at the buses (degree)	Voltage values at the buses (KV)*	Delta (δ) at the buses (degree)
241.5	0	240.1	0	240.5	0
241.5	-3.7	239.6	-3.99	239.8	-3.8
246.1	-4.3	245.2	-4.88	244.6	-4.5
227.6	-4.2	225.2	-4.4	226.0	-4.3
226.7	-5.3	225.3	-5.7	225.2	-5.5
231.0	-5.9	230.6	-6.5	230.0	-6.1

*(KV) Kilovolt

Table A.4: Actual and estimated power injections for the 18 and 62 measurement data

Bus name	Actual value real power injection, in (MW)*	Actual value reactive power flows, in (MVAR)**	18-data estimated real power injection, in (MW)*	18-data estimated reactive power injection, in (MVAR)**	62-data estimated real power injection, in (MW)*	62-data estimated reactive power injection, in (MW)**
Bus 1	107.9	16	114.4	17.5	111.9	18.6
Bus 2	50	74.4	49.5	69.8	47.5	70.1
Bus 3	60	89.6	56.9	90.3	59.5	87.8
Bus 4	70	70	70.6	74	70.1	70.1
Bus 5	70	70	70.7	69.5	71.8	69.5
Bus 6	70	70	71.0	62.3	68.9	65.9

* Real power is measured in Megawatt (MW)

**Reactive power is measured in Megavar (MVAR)

Table A.5: Actual and estimated power flows for the 18 and 62 measurement data

From Bus	To Bus	Actual value real power flows, in (MW)*	Actual value reactive power flows, in (MVAR)**	18-data estimated real power flow, in (MW)*	18-data estimated reactive power flow, in (MVAR)**	62-data estimated real power flow, in (MW)*	62-data estimated reactive power flow, in (MW)**
1	2	28.86	-15.42	29.73	-15.00	29.27	-15.21
1	4	43.58	20.12	44.33	20.55	44.04	20.42
1	5	35.59	11.25	35.53	10.65	35.43	10.70
2	3	02.93	-12.27	03.35	-11.73	03.12	-11.98
2	4	33.10	46.06	32.52	45.16	32.89	45.95
2	5	15.51	15.35	14.71	14.37	14.89	14.63
2	6	26.25	12.40	27.47	13.65	26.91	13.15
3	5	19.12	23.17	17.59	21.76	18.08	22.21
3	6	43.78	60.73	44.91	62.02	44.44	61.69
4	5	04.08	-04.94	03.59	-05.41	03.65	-05.34
5	6	01.61	-09.00	-03.20	-08.02	02.65	-08.56
2	1	-27.78	12.81	-28.78	12.47	-28.34	12.65
4	1	-42.49	-19.94	-43.21	-20.24	-42.93	-20.16
5	1	-34.50	-13.45	-12.95	-34.38	-34.38	-13.01
3	2	-02.89	05.73	-03.31	05.17	-03.08	05.43
4	2	-31.59	-45.13	-31.05	-44.76	-31.40	-45.05
5	2	-15.02	-18.01	-14.26	-17.20	-14.43	-17.42
6	2	-25.67	-16.01	-26.82	-17.07	-26.29	-16.66
5	3	-18.02	-26.09	-16.63	-24.98	-17.08	-25.35
6	3	-42.77	-57.86	-43.85	-59.08	-43.40	-58.67
5	4	-04.05	-02.78	-03.56	-02.37	-03.62	-02.43
6	5	-01.56	03.87	-03.16	02.18	-02.61	02.73

* Real power is measured in Megawatt (MW).

**Reactive power is measured in Megavar (MVAR)

APPENDIX B

DATA FOR THE 10-UNIT 39-BUS NEW ENGLAND TEST SYSTEM AND STATE ESTIMATION RESULTS

Appendix B contains the data for the 10-unit 39-bus New England test system discussed in the thesis. The main characteristics of the system are given in Table B.1. Table B.2 gives the transmission line characteristics for the system. The estimated state variables are tabulated with the actual value in Table B.3. In the Table B.4, the actual value of bus power injection and estimated bus power injection are tabulated. Table B.5 gives the actual value of line power flows tabulated together with the estimated line power flows for few values.

Table B.1: Main characteristic of the 39-bus system

Number of buses	39
Number of Lines	46
Number of generators	10
Voltage levels	Generating station bus 13.8KV
	Transmission line bus 345KV

Table B.2: Line characteristics of the 10-unit 39-bus New England test system

From Bus	To Bus	Line resistance (pu)*	Line Inductance (pu)*	Line charging (pu)*
1	2	0.0035	0.0411	0.6987
1	39	0.001	0.025	0.75
2	3	0.0013	0.0151	0.2572
2	25	0.007	0.0086	0.146
3	4	0.0013	0.0213	0.2214
3	18	0.0011	0.0133	0.2138
4	5	0.0008	0.0128	0.1342
4	14	0.0008	0.0129	0.1382
5	6	0.0002	0.0026	0.0434
5	8	0.0008	0.0112	0.1476
6	7	0.0006	0.0092	0.113
6	11	0.0007	0.0082	0.1389
7	8	0.0004	0.0046	0.078
8	9	0.0023	0.0363	0.3804
9	39	0.001	0.025	1.2
10	11	0.0004	0.0043	0.0729
10	13	0.0004	0.0043	0.0729
13	14	0.0009	0.0101	0.1723
14	15	0.0018	0.0217	0.366
15	16	0.0009	0.0094	0.171
16	17	0.0007	0.0089	0.1342
16	19	0.0016	0.0195	0.304
16	21	0.0008	0.0135	0.2548
16	24	0.0003	0.0059	0.068
17	18	0.0007	0.0082	0.1319
17	27	0.0013	0.0173	0.3216
21	22	0.0008	0.014	0.2565
22	23	0.0006	0.0096	0.1846
23	24	0.0022	0.035	0.361
25	26	0.0032	0.0323	0.513
26	27	0.0014	0.0147	0.2396
26	28	0.0043	0.0474	0.7802
26	29	0.0057	0.0625	1.029
28	29	0.0014	0.0151	0.249
12	11	0.0016	0.0435	0
12	13	0.0016	0.0435	0
6	31	0	0.025	0
10	32	0	0.02	0
19	33	0.0007	0.0142	0
20	34	0.0009	0.018	0
22	35	0	0.0143	0
23	36	0.0005	0.0272	0
25	37	0.0006	0.0232	0
2	30	0	0.0181	0
29	38	0.0008	0.0156	0
19	20	0.0007	0.0138	0

* per unit (pu) are based on 100 MVA , 345 KV base.

Table B.3: Actual and estimated state variables for the 131 and 277 measurement data

Bus Number	Actual Value of bus phase angle (degree)	Estimated bus Phase angle for 131 measurement data, in (degree	Estimated bus Phase angle for 277 measurement data, in (degree)	Actual value of bus voltage magnitude (KV)*	Estimated bus Voltage magnitudes for 277 measurement data (KV)*	Estimated bus Voltage magnitudes for 277 measurement data (KV)*
1	-9.64	-9.6397	-9.64	360.939	360.9277	360.9358
2	-6.43	-6.4251	-6.42	361.146	361.1494	361.1392
3	-9.223	-9.2312	-9.23	354.936	354.9436	354.9344
4	-10.25	-10.2451	-10.24	346.035	346.0192	346.0218
5	-9.23	-9.2344	-9.23	346.5525	346.5529	346.5593
6	-8.55	-8.5507	-8.55	347.3805	347.3812	347.3882
7	-10.79	-10.7929	-10.79	343.689	343.6866	343.6915
8	-11.3	-11.318	-11.31	343.344	343.3483	343.3521
9	-11.52	-11.5169	-11.51	354.591	354.591	354.5908
10	-6.11	-6.1071	-6.10	350.727	350.727	350.7483
11	-6.94	-6.9385	-6.94	349.1745	349.176	349.184
12	-6.92	-6.9191	-6.92	344.862	344.862	344.8496
13	-6.77	-6.7694	-6.77	349.7265	349.7265	349.7448
14	-8.31	-8.3082	-8.30	348.795	348.8013	348.8072
15	-8.37	-8.3689	-8.37	350.0715	350.0715	350.062
16	-6.81	-6.8101	-6.81	355.7295	355.7295	355.7219
17	-7.86	-7.8579	-7.85	356.2125	356.2125	356.218
18	-8.81	-8.8105	-8.81	355.281	355.2794	355.264
19	-1.98	-1.9751	-1.97	362.043	362.043	362.0568
20	-3.29	-3.2924	-3.29	341.757	341.757	341.8158
21	-4.32	-4.3157	-4.31	355.7295	355.7295	355.7233
22	0.22	0.2243	0.23	362.0085	362.0085	362.0233
23	0.03	0.0343	0.04	360.2835	360.2835	360.2771
24	-6.66	-6.6643	-6.66	357.627	357.627	357.6237
25	-4.89	-4.887	-4.88	364.6995	364.6994	364.6985
26	-5.73	-5.7318	-5.73	362.457	362.457	362.4474
27	-7.86	-7.8642	-7.86	357.558	357.558	357.5413
28	-1.72	-1.7191	-1.72	361.698	361.698	361.7191
29	1.21	1.2047	1.20	361.7325	361.7325	361.7677
30	-4.09	-4.0935	-4.09	14.4279	14.4279	14.4283
31	0	0	0	13.5516	13.5516	13.5532
32	1.71	1.7124	1.71	13.56678	13.5668	13.5684
33	3.31	3.3101	3.31	13.76136	13.7614	13.7627
34	2.02	2.0233	2.02	13.96974	13.9697	13.9739
35	5.27	5.265	5.27	14.48034	14.4803	14.4809
36	8.03	8.0318	8.03	14.6763	14.6763	14.6767
37	2.03	2.0259	2.03	14.18364	14.1836	14.1839
38	8.62	8.6182	8.62	14.1657	14.1657	14.1677
39	-11.58	-11.575	-11.57	14.214	14.2143	14.2141

* (KV)Kilovolt

Table B.4: Actual and estimated power injections for the 131 and 277 measurement data

Bus name	Actual value real power injection, in (MW)*	Estimated real power injection for 131measurement data , in (MW)*	Estimated real power injection for 277 measurement data , in (MW)*	Actual value reactive power flows, in (MVAR)**	Estimated reactive power injection for 131measurement data, in (MVAR)**	Estimated reactive power injection for 277 measurement data, in (MVAR)**
Bus 3	322.00	321.85	321.85	2.40	3.02	3.02
Bus 4	500.00	499.60	499.60	184.00	182.86	182.86
Bus 7	233.80	235.86	235.86	84.00	83.31	83.31
Bus 8	522.00	520.00	520.00	176.00	176.64	176.64
Bus 12	8.50	8.79	8.56	88.00	87.66	87.67
Bus 15	320.00	320.10	320.10	153.00	152.65	152.65
Bus 16	329.00	331.72	330.53	32.30	31.16	31.23
Bus 18	158.00	159.28	157.99	30.00	28.72	28.849
Bus 20	680.00	680.18	680.18	103.00	102.48	102.48
Bus 21	274.00	273.18	273.18	115.00	114.63	114.63
Bus 23	247.50	247.42	247.42	84.60	-83.74	83.74
Bus 24	308.60	307.55	307.55	-92.20	91.90	-91.90
Bus 25	224.00	224.68	223.89	47.20	-47.15	47.25
Bus 26	139.00	138.03	139.50	17.00	-16.74	16.59
Bus 27	281.000	282.17	280.83	75.5	-74.85	74.10
Bus 28	206.00	205.86	205.63	27.60	-27.54	27.55
Bus 29	283.50	283.90	283.73	26.90	-27.06	27.05
Bus 30	240.00	240.027	239.44	144.90	144.85	144.82
Bus 31	549.60	549.46	549.46	202.00	202.00	202.00
Bus 32	635.40	635.51	635.51	205.47	205.68	205.68
Bus 33	640.00	640.38	640.38	112.96	113.28	113.28
Bus 34	520.00	520.12	520.13	169.56	169.48	169.48
Bus 35	660.00	660.18	660.18	216.75	216.85	216.85
Bus 36	570.00	570.07	570.07	104.48	104.31	104.31
Bus 37	550.00	550.22	549.77	3.31	3.43	3.39
Bus 38	870.30	870.37	870.37	35.18	35.14	35.14
Bus 39	152	151.85	151.85	152.51	-152.58	152.58

* Real power is measured in Megawatt (MW)

**Reactive power is measured in Megavar (MVAR)

Table B.5: Actual and estimated line power flows for the 131 and 277 measurement data

From Bus	To Bus	Actual real line power flow (MW)*	Estimated real line power flow for 131 measurement data (MW)*	Estimated real line power flow for 277 measurement data (MW)*	Actual reactive Line Power flow (MVAR)**	Estimated reactive line power flow for 131 measurement data (MVAR)**	Estimated reactive line power flow for 277 measurement data (MVAR)**
1	2	-148.15	-148.11	-148.11	-23.12	-22.96	-22.96
1	39	148.15	148.23	148.23	23.12	23.28	23.28
2	3	357.99	358.16	358.16	88.45	88.42	88.42
2	25	-266.84	-266.51	-266.51	88.51	88.18	88.18
3	4	93.05	93.05	93.05	108.28	107.98	107.98
3	18	-58.71	-58.37	-58.37	-13.64	-14.01	-14.01
4	5	-138.97	-138.64	-138.64	-8.94	-8.62	-8.62
4	14	-268.26	-268.19	-268.19	-48.57	-48.03	-48.03
5	6	-468.35	-470.93	-470.93	-56.15	-55.89	-55.89
5	8	329.22	328.63	328.63	58.28	58.37	58.37
6	7	432.92	433.63	433.63	91.61	91.47	91.47
6	11	-352.11	-351.65	-351.65	-35.99	-35.97	-35.97
7	8	197.95	196.60	196.60	1.08	1.58	1.58
8	9	4.13	4.18	4.18	-108.48	-108.46	-108.46
9	39	3.94	3.87	3.87	-72.50	-72.58	-72.58
10	11	354.28	354.01	354.01	72.95	72.21	72.21
10	13	281.13	279.70	282.08	40.23	40.36	40.17
13	14	273.06	273.49	272.48	-2.30	-2.45	-2.39
14	15	3.56	3.74	3.74	-35.98	-36.25	-36.25
15	16	-316.44	-316.36	-316.36	-151.50	-151.43	-151.43
16	17	216.28	215.24	216.43	-39.05	-38.30	-38.37
16	19	470.85	-470.92	-470.92	-54.88	-54.53	-54.53
16	21	-341.10	-341.61	-341.61	14.24	14.18	14.18
16	24	-50.82	-51.85	-51.85	-97.23	-97.04	-97.04
17	18	217.06	218.00	216.71	11.04	10.16	10.25
17	27	-1.09	-0.51	-1.12	-39.81	-40.38	-40.33
21	22	-615.98	-615.69	-615.69	-88.54	-88.27	-88.27
22	23	41.12	40.93	40.93	42.59	41.99	41.99
23	24	362.11	362.08	362.08	1.54	1.64	1.64
25	26	52.30	52.17	52.51	-11.98	-12.19	-12.22
26	27	283.19	283.80	283.07	66.41	66.39	66.43
26	28	-160.35	-160.25	-160.48	-17.98	-17.95	-17.92
26	29	-209.63	-209.50	-209.67	-21.30	-21.26	-21.23
28	29	-367.38	-367.14	-367.17	29.03	29.13	29.13
12	11	-0.77	-0.36	-0.36	-42.27	-28.54	-28.54
12	13	-7.73	-7.43	-7.19	-45.73	-31.93	-31.93
6	31	-549.60	-549.45	-549.45	-113.11	134.79	134.79
10	32	-635.42	-635.50	-635.50	-113.18	202.58	202.58

* Real power is measured in Megawatt (MW)

**Reactive power is measured in Megavar (MVAR)

APPENDIX C

DATA FOR THE IEEE 118-BUS SYSTEM AND MULTI-AREA STATE ESTIMATION RESULTS

Appendix C contains the bus distribution for each area, measurement data for each area and number of phasor measurements available for CSE of the 10-unit 39-bus New England test system and IEEE 118-bus system in the thesis. The bus distribution among two areas for 39-bus system is illustrated in Table C.1. Table C.2 shows the measurement data available for each area and Table C.3 shows the PMU measurement available in the overall system. Table C.4 provides the calculated objective function $J(x)$ for the 39-bus system. The main characteristics of the 118-bus system are shown in Table C.5. Table C.6 tabulates the bus distribution among the control areas of the 118-bus system. Table C.7 illustrates the measurement distribution of all the areas. Table C.8 provides the phasor measurements assumed to be available for the CSE. Table C.9

tabulates the calculated objective function $J(x)$ for both integrated and two-level SE for three different loading conditions.

Table C.1: Bus distribution for 39-bus system

Area	Internal Buses	Boundary buses	External Buses	Slack bus
Area 1	1, 2, 3, 4, 5, 6, 7, 8, 9, 10, 11, 12, 13, 14, 18, 25, 27, 30, 31, 32, 37, 39	15, 17, 26	16, 28, 29	31
Area 2	16, 19, 20, 21, 22, 23, 24, 28, 29, 33, 34, 35, 36, 38	16, 28, 29	15, 17, 26	20

Table C.2: Measurements available for the areas 1 & 2 of 39-bus system

Area	Type of measurements			
	Bus power injections	Line power flows	Bus voltage magnitudes	Total measurements
1	30	132	28	190
2	26	68	17	111

Table C.3: Synchronized phasor measurements

Phasor measurement	Bus Number	Area Number
1	1	1
2	7	1
3	17	1
4	26	1

Table C.4: Result of integrated and multi-area SE Solution

$J(x)$: Objective Function	
Integrated	Two-level
119.44	113.62

Table C.5: Main characteristic of the 118-Bus system

Number of buses	118
Number of Lines	194
Number of generators	54
Voltage levels	Generating station bus 13.8KV
	Transmission line bus 345KV

Table C.6: Bus distribution for 118 bus system

Area	Internal Buses	Boundary buses	External Buses	Slack bus
Area 1	1, 2, 3, 4, 5, 6, 7, 9, 10, 117	8, 11, 12	13, 14, 16, 30	12
Area 2	17, 18, 20,21	13, 14, 15, 16, 19, 22, 30, 31, 113	8, 11, 12, 23, 26, 29, 32, 33, 34, 38	113
Area 3	35, 36, 37,38, 39, 40,41, 43	33, 34, 38, 42, 44	15, 19, 30, 45, 49, 65	65
Area 4	25, 26, 27,114, 115	23, 24, 28, 29, 32, 74, 75, 118	22, 30, 31, 69, 70, 72, 76, 77, 113	113
Area 5	71,73, 83,84, 86, 87	70, 72, 76, 77, 78, 82, 85, 88	24, 69, 74, 75, 80, 89, 96, 118	87
Area 6	46, 47, 48,116	45, 49, 51, 52, 65, 66, 67, 68, 69	38, 42, 44, 50, 53, 54, 58, 62, 64, 70, 75, 77, 81, 118	69
Area 7	101, 103,104, 105,106, 107,108, 109,110, 111,112	100, 102	92, 94, 98, 99	100
Area 8	90, 91, 93,95, 97	79, 80, 81, 89, 92, 94, 96, 98, 99	68, 77, 78, 82, 85, 88, 100, 102	100
Area 9	55, 56, 57,59, 60, 61, 63	50, 53, 54, 58, 62, 64	49, 51, 52, 65, 66, 67	67

Table C.7: Measurements available for the areas 1-9 of 118-bus system

Area	Type of measurements			
	Bus power injections	Line power flows	Bus voltage magnitudes	Total measurements
1	29	40	17	86
2	42	56	23	121
3	31	48	18	97
4	42	58	22	122
5	44	66	23	133
6	46	80	27	153
7	34	46	17	97
8	40	74	22	136
9	34	72	19	125

Table C.8: Synchronized phasor measurements

Phasor measurement	Bus Number	Area Number
1	10	1
2	12	1
3	15	2
4	23	4
5	33	3
6	45	6
7	51	6
8	59	9
9	65	6

Table C.9: Result of integrated and multi-area SE solution

Loading Condition	$J(x)$: Objective Function	
	Integrated	Two-level
100% loading	18.94	18.84
75% loading	18.61	18.11
50% loading	18.31	18.19